NOTICE

The quality of this microfiche is heavily dependent upon the quality of the original thesis submitted for microfilming. Every effort has been made to ensure the highest quality of reproduction possible.

If pages are missing, contact the university which granted the degree.

Some pages may have indistinct print especially if the original pages were typed with a poor typewriter ribbon or if the university sent us a poor photocopy.

Previously copyrighted materials (journal articles, published tests, etc.) are not filmed.

Reproduction in full or in part of this film is governed by the Canadian Copyright Act, R.S.C. 1970, c. C-30. Please read the authorization forms which accompany this thesis.

THIS DISSERTATION
HAS BEEN MICROFILMED
EXACTLY AS RECEIVED

AVIS

La qualité de cette microfiche dépend grandement de la qualité de la thèse soumise au microfilmage. Nous avons tout fait pour assurer une qualité supérieure de reproduction.

S'il manque des pages, veuillez communiquer avec l'université qui a conféré le grade.

La qualité d'impression de certaines pages peut laisser à désirer, surtout si les pages originales ont été dactylographiées à l'aide d'un ruban usé ou si l'université nous a fait parvenir une photocopie de mauvaise qualité.

Les documents qui font déjà l'objet d'un droit d'auteur (articles de revue, examens publiés, etc.) ne sont pas microfilmés.

La reproduction, même partielle, de ce microfilm est soumise à la Loi canadienne sur le droit d'auteur, SRC 1970, c. C-30. Veuillez prendre connaissance des formules d'autorisation qui accompagnent cette thèse.

LA THÈSE A ÉTÉ
MICROFILMÉE TELLE QUE
NOUS L'AVONS REÇUE

GENERATION OF CONSTANT ENVELOPE BANDLIMITED BPSK SIGNAL

BY

HOOSHMAND YAZDANI

THESIS SUBMITTED TO THE SCHOOL OF GRADUATE STUDIES, UNIVERSITY OF OTTAWA, IN PARTIAL FULFILMENT OF THE REQUIREMENTS FOR THE DEGREE OF MASTER OF APPLIED SCIENCE

DEPARTMENT OF ELECTRICAL ENGINEERING
UNIVERSITY OF OTTAWA
OTTAWA, ONTARIO

JUNE, 1981

ABSTRACT

After examining the effects of channel non-linearities on the power spectrum density of several bandlimited PSK signals, a modified BPSK modulation technique using pre-modulation filtering is described. The modified BPSK modulator achieves a smooth phase transition from 0° to 180° by going through an intermediate value of 90°. The resultant PSK signal has a very low AM component, particularly suitable for data transmission through non-linear channels.

The design and implementation of the modified BPSK system is presented. Experimental tests performed in a channel having a high degree of AM non-linearity (AM/AM conversion) have shown that the modified BPSK signal, when passed through a hardlimiter, has a spectrum with greatly reduced spectral sidelobes compared to the conventional BPSK signal.

The measured probability of error (P_e) performance of the modified BPSK system in an additive white Gaussian noise environment indicates that, for the same P_e in a linear channel, the modified BPSK system requires about 0.6 dB more E_b/N_o than the conventional BPSK system.

The modified BPSK signal has spectral lines at the carrier frequency plus multiples of the signalling frequency, which in some cases might be useful for timing recovery in the demodulation process.

ACKNOWLEDGEMENTS

The author wishes to express his sincere appreciation to his supervisors, Professor Willem Steenaart and Professor Kamilo Feher for their constructive criticisms, guidance and encouragement during the entire programme. In particular, the author is greatly indebted to Professor Feher who proposed the topic for the research.

Special thanks are also extended to Mr. Rawle Scott, and to the many people who helped him directly or indirectly, in making this work a success.

The author is also greatly indebted to his wife, Louise, for her patience and encouragement during the programme.

TABLE OF CONTENTS

LIST OF FIGURES

LIST OF SYMBOLS AND ABBREVIATIONS

A	Amplitude
$\{a_k\}$	Binary Sequence
AM	Amplitude Modulation
AM/AM	Amplitude Modulation to Amplitude Modulation Conversion
AMP	Amplifier
AM/PM	Amplitude Modulation to Phase Modulation Conversion
$\{b_k\}$	Binary Sequence
BA	Buffer Amplifier
BER	Bit Error Rate
bps, b/s	Bit Per Second
B.P.F.	Band-pass Filter
BPSK	Binary Phase-Shift Keying
BR	Bit Rate Bandwidth
C	Carrier
C/N	Carrier-to-noise Ratio in dB
dB	Decibel
dBm	Decibel Relative to One Milliwatt
Demod	Demodulator
DOC	Department of Communications
E_b/N_o	Energy per Bit-to-noise Density Ratio
erf(x)	Error Function $\frac{2}{\sqrt{\pi}} \int_0^x e^{-t^2} dt \leq 1$

erfc(x)	Complementary error function $\frac{2}{\sqrt{\pi}} \int_x^\infty e^{-t^2} dt \leq 2$
f	Frequency in Hertz
f_c	Carrier Frequency in Hz
f_s	Signalling Frequency in Hz
FCC	Federal Communications Commission
FM	Frequency Modulation
GEN	Generator
h(t)	Impulse Response
H(f)	Network Transfer Function
Hz	Hertz
IF	Intermediate Frequency
ISI	Intersymbol Interference
j	$\sqrt{-1}$ Imaginary Number
LPF	Low-pass Filter
m	Integer
MBPSK	Modified BPSK
MOD	Modulator
Modem	Modulator—Demodulator
N	Noise Power
NB	Noise Bandwidth
NRZ	Non-return-to-zero
O-QPSK	Offset QPSK
OSC	Oscillator
PAM	Pulse Amplitude Modulation

P(e)	Probability of Error
PRBS	Pseudo-random Binary Sequence
PM	Phase Modulation
QPSK	Quaternary Phase Shift-Keying
QUAD-HYBD	Quadrature Hybrid
RF	Radio Frequency
R_e	Real Part
$S_m(f)$	Power Spectrum Density of m(t) Signal
t	Time Variable
T_s	Symbol Interval
TWT	Travelling Wave Tube
UP/P CONV	Unipolar to Bipolar Converter
W/Hz	Watt per Hertz
$\{\phi_k\}$	Sequence of Phases
$\delta(t)$	Dirac Delta Function or Unit Impulse Function
ω	Angular Frequency in Radian = $2\pi f$
ω_c	Carrier (Angular) Frequency
π	Ratio of the Circumference of a Circle to its diameter, x 22/7
$\otimes$	Multiplier or Mixer
$\sum_i$	Summation over i
$\lvert(.)\rvert$	Absolute Value of (.)
⊠	Power Splitter
Σ	Power Combiner or Linear Adder

CHAPTER ONE

INTRODUCTION

The growing demand for communications, particularly between widely separated areas, has resulted in an ever increasing proliferation of communication circuits. This growth has been most dramatic in the area of digital transmission systems.

In modern digital communication systems, however, one of the problems is that of determining the most effective way of using the available transmission power and channel bandwidth for a given data rate and an acceptable system performance, e.g., certain prescribed error probability or error rate.

To solve the above problem, attention has been directed towards modulation techniques, a fundamental process in communications.

One of the modulation techniques which efficiently employs bandwidth and power is Phase-Shift Keying (PSK) modulation. As a result it has been extensively used in digital communication systems.

The power spectra of PSK signals, however, have sidelobes (see Figure 1.1) that may interfere with other communication systems. To suppress the sidelobes and hence reduce the out-of-band interference to the specified level imposed

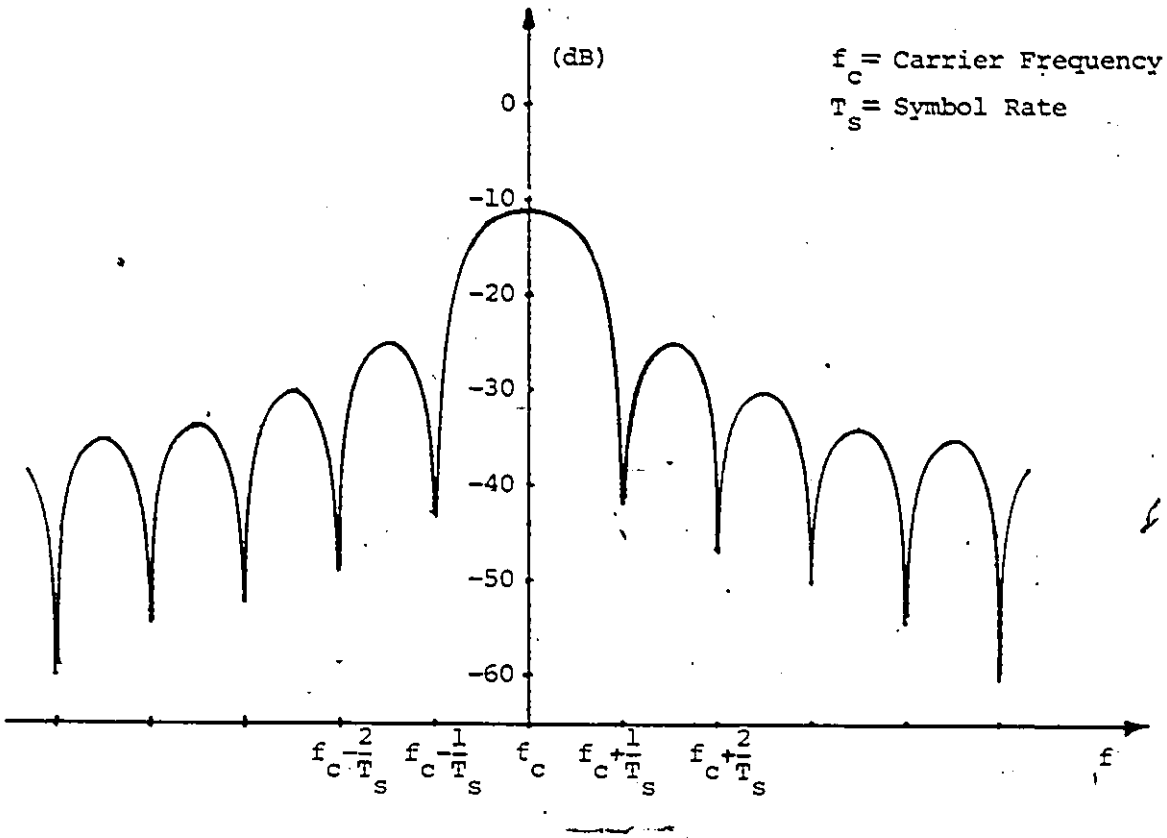

Figure 1.1 The Power Spectrum Density of a PSK Signal

by regulatory agencies such as DOC, FCC, etc., a certain amount of filtering is necessary at the PSK transmitter.

Filtering of PSK signals, however, produces great amounts of envelope fluctuations [1, 2, 3, 4]. In particular the envelope of the filtered PSK signal goes through zero during 180° phase transitions. When such a filtered signal is passed through nonlinear devices, usually employed in radio communication systems, such as limiters, up-converters, Travelling-Wave-Tube (TWT) amplifiers, etc., operating for economic reasons close to saturation, nonlinear distortion arises. The undesirable consequences of such distortions are increased bit error rate and spectrum spreading of the signal. The latter effect is known to be a critical point in PSK transmitter design, because it is likely to produce harmful interference and hence impairments into the neighbouring channels.

A typical example where such considerations are appropriate is in satellite communication channels, where the Travelling Wave Tube Amplifiers, TWTA, are used in both the satellite transponder and the ground station transmitter. Figure 1.2 shows a block diagram of a simplified satellite communication channel. A carrier phase-modulated by the input digital data streams, which consists of rectangular pulses, is assumed to access the appropriate satellite

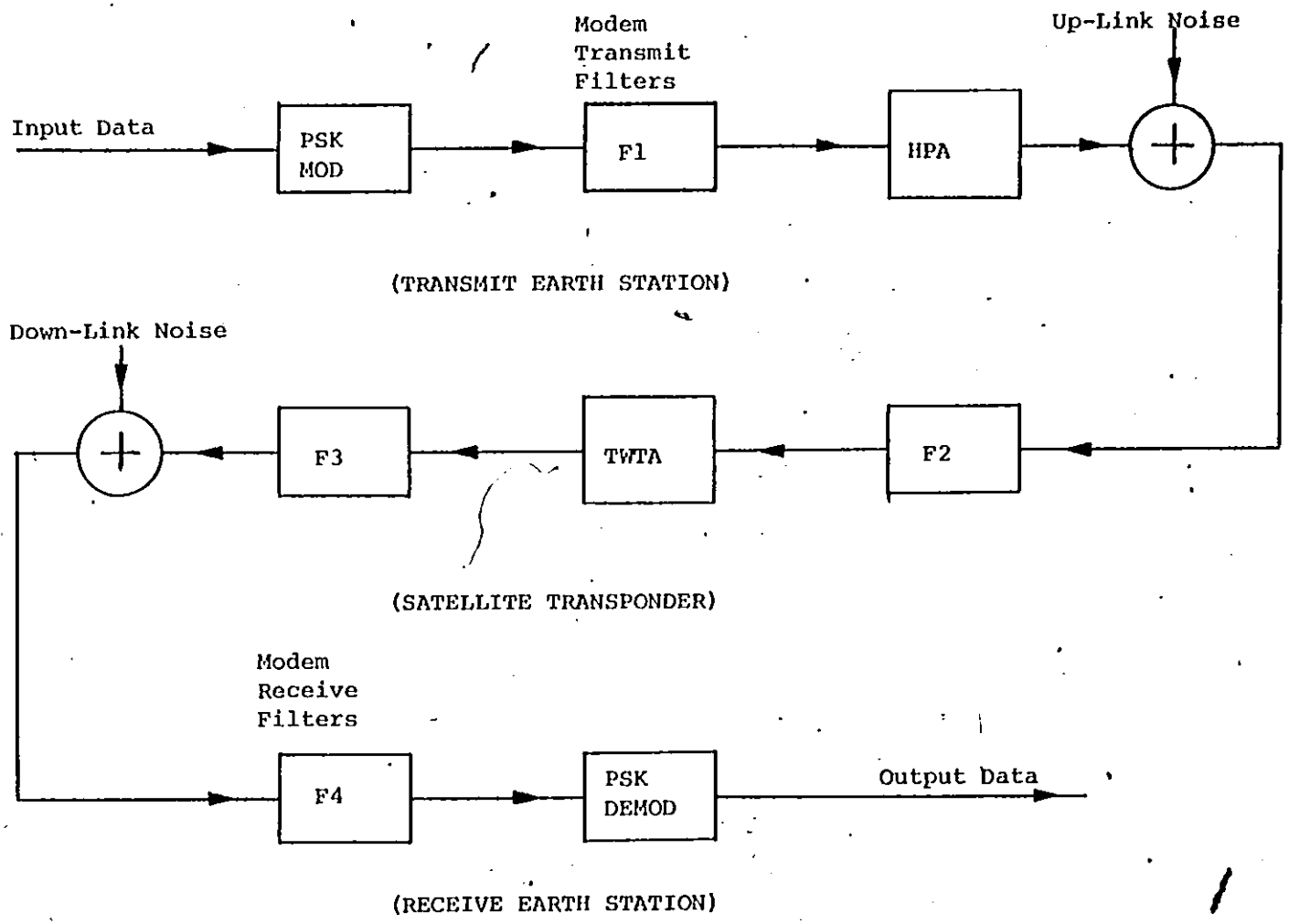

Figure 1.2 Block Diagram of a Simplified Satellite Communication Channel

transponder. Modem transmit filter F1 provides the desired waveform shaping before amplification by the earth station High Power Amplifier, HPA (usually a TWTA). At the satellite transponder, filter F2 rejects adjacent channels and out-of-band noise. Amplification is provided by the satellite TWTA, and filter F3 reduces the energy falling into the adjacent channels. Modem receive filter F4 provides additional waveform shaping and reduces the noise and interference at the input of the coherent PSK demodulator.

The most common source of nonlinearity in such a channel is the TWTA. This device is typically modelled by two memoryless characteristics: a function that defines output amplitude (or power) as a function of input amplitude, and a function that defines output phase shift as a function of input envelope level. These two functions are commonly referred to as the nonlinear AM/AM and AM/PM conversion characteristics of the TWTA, respectively. The zero memory assumption is valid since the satellite transponders are usually narrow compared to the TWTA bandwidth. Typical AM/AM and AM/PM characteristics of a TWTA is shown in Figure 1.3.

The impairments originating from the interaction of the spurious envelope fluctuations of filtered PSK signal with the TWTA nonlinearities can be divided into two classes: dynamic phase errors, which reduce the immunity to noise and ultimately require more transmit power, and spectrum spreading which

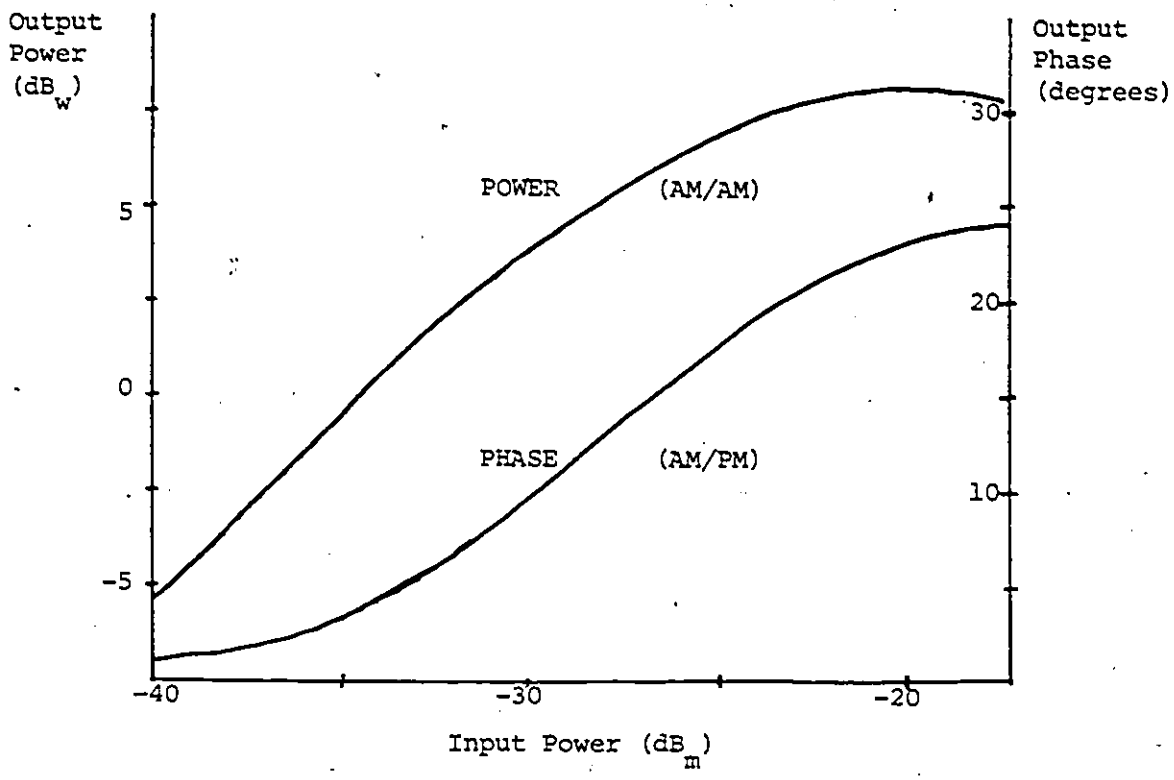

Figure 1.3 Typical AM/AM and AM/PM Characteristics of a TWTA

causes interference to other communication channels. Moreover, since the reference carrier and timing (clock) signals in a coherent PSK demodulator are derived from the received PSK modulated signal spectrum, the recovered carrier and clock are subjected to phase jitter due to spectrum distortion, in addition to the phase jitter associated with the thermal noise.

As a precaution against phase errors, the ground station TWTA is operated below saturation in a zone of less pronounced nonlinearity, with the obvious penalty that a TWTA designed for a larger power has to be used, with consequent technological and cost problems. The same precaution can be taken only to a limited extent at the satellite TWTA, due to primary power limitations, and the only possibility left for optimization is control of filter shaping in such a way as to minimize phase errors.

Post-TWTA filtering is effective in controlling spectrum spreading and is used at the satellite where the RF power involved is moderate. At ground stations, by contrast, high power filtering may become impractical and in some cases, where the transmit frequency agility is of particular interest, it is totally dismissed. Therefore, one way of controlling spectrum spreading, and hence the interference to other systems, is again to use TWTA's with higher saturation powers and to back off the operation point in order to achieve

sufficient linearity.

Because of the above considerations, reduction of the spurious envelope fluctuations of filtered (bandlimited) PSK signal can result in a more economical design for ground transmitters, and can allow more efficient use of the satellite power.

A first objective in achieving a small envelope fluctuations of filtered PSK signals is to avoid the envelope nulls corresponding to the instantaneous 180° phase transitions of the conventional PSK signals. Hence modified PSK signals, exhibiting smooth phase transitions and therefore constant envelope,are called for.

In this thesis a general method for generation of constant envelope bandlimited PSK signals, using premodulation filtering, is introduced. In particular, a new Binary PSK (BPSK) modulation scheme, which hereafter is called the MBPSK (Modified BPSK) modulation scheme, is designed, analyzed, and implemented.

The experimental tests performed have shown that the MBPSK signal,having a very low envelope fluctuations when passed through a channel with a high degree of AM/AM nonlinearity (hard-limiter-channel), has a greatly reduced spectral spreading compared to the conventional BPSK signal.

There are of course other modified PSK schemes such as Offset Quaternary PSK, O-QPSK [2], L-PSK [5], etc., that are better than the MBPSK system in terms of bandwidth efficiency and have

very low envelope fluctuations after filtering. However, the simplicity and the accompanying cost effectiveness of the MBPSK system in some cases might justify the bandwidth inefficiency, and hence become the over-riding reason for its application in data communication systems.

In Chapter Two, some of the basic principles of PSK modulation systems are reviewed. As the emphasis in this thesis will be on the generation of constant envelope bandlimited PSK signals for transmission over nonlinear channels, it is essential to review the conventional PSK systems, which are usually prone to nonlinear distortion and spectral spreading.

In Chapter Three, an intuitive analysis of the effects of channel nonlinearities on the power spectrum density of bandlimited PSK signals is presented. A new approach to the generation of a constant envelope bandlimited BPSK signal is introduced in Chapter Four. The hardware implementation of the new BPSK (modified BPSK) system is presented in Chapter Five. Measurement techniques and the results obtained are also presented. Finally, in Chapter Six, future research points and possible extension of this work are suggested.

CHAPTER TWO

PHASE-SHIFT KEYING (PSK) MODULATION

2.1 Introduction

Phase-Shift Keying (PSK) is a digital phase modulation technique in which the information of the digital signal is transmitted in the phase of the modulated carrier. This technique combines some attractive features of Amplitude Modulation (AM) and Frequency Modulation (FM). It requires less peak power than AM and may in some applications have a reduced bandwidth as compared to FM; hence it has been extensively used in digital communication systems.

In this chapter, some of the important properties of Binary PSK (BPSK) and Quaternary PSK (QPSK) systems will be described. As the emphasis in this thesis will be on the generation of constant envelope bandlimited PSK signal for transmission over nonlinear channels, it is essential to review these systems, which are usually prone to nonlinear distortion and spectral spreading.

After a brief and general discussion on the representation, generation, and detection of a PSK signal, BPSK and QPSK systems, their functional diagram, required bandwidth, and performance in an ideal channel will be reviewed. The problems of bandlimitation of PSK signals are also briefly discussed. No attempt is made to discuss the operation of

carrier recovery and bit timing (clock) recovery circuits, since these are beyond the scope of this thesis.

2.2 General Representation, Generation, and Detection of PSK Signals

A functional block diagram of a very general PSK system is shown in Figure 2.1 The basic PSK modulator may, without loss of generality, be assumed to have two inputs; a binary sequence of digital information and an RF carrier. Each input is processed; the data by a coder which produces a discrete message sequence in which each message is a member of a M-ary alphabet, and one message is sent every T_s seconds, which is the symbol period (M is usually a power of two since most digital systems start as binary systems, but a PSK system is not generally limited to these alphabet sizes); the carrier by the required phase shift networks. The processed signals are then combined in the modulator such that the information is contained in the phase of the RF carrier in accordance with the chosen encoding algorithm. The PSK modulator generates a signal given by:

$$m(t) = \mathrm{Re} \sum_{k=-\infty}^{+\infty} A\, e^{j\phi_k} e^{j\omega_c t} w(t-kT_s) \qquad (2.1)$$

where $w(t)$ is a T_s second rectangular pulse, $\{\phi_k\}$ is the sequences of the phases which contain the digital information and takes on discrete values over the interval $[0, 2\pi]$, ω_c and A are the frequency and the amplitude of the carrier

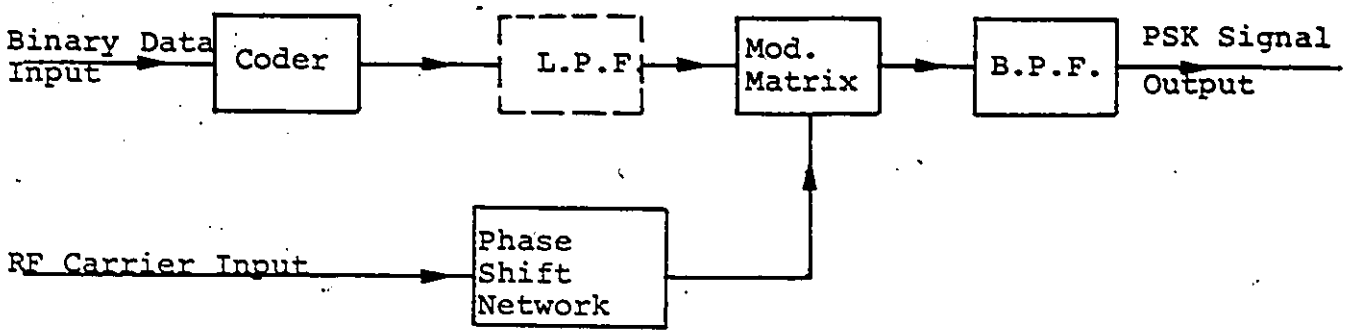

(a)

PSK Modulator Block Diagram

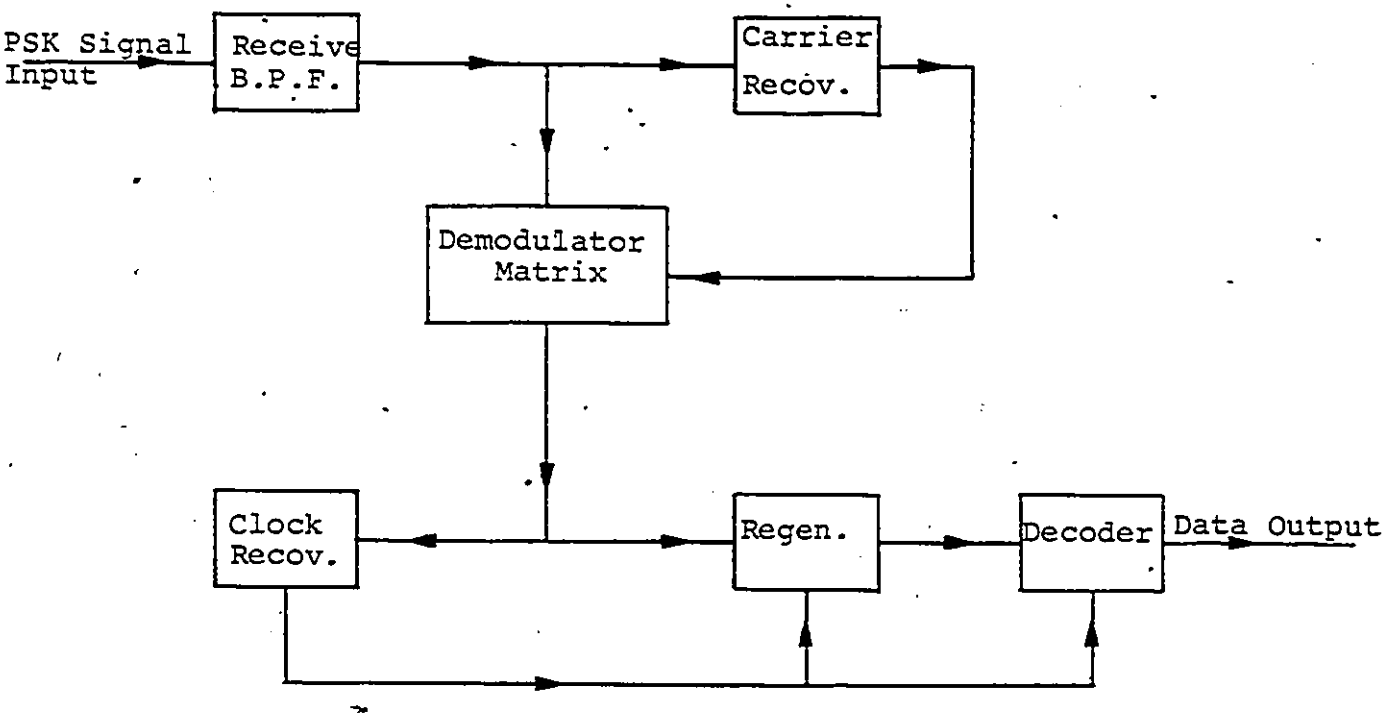

(b)

PSK Demodulator Block diagram

Figure 2.1 Functional Block Diagram of a PSK Modem

respectively.

m(t) represents a form of constant envelope signal which is a desirable property of PSK systems. The essentially linear structure of PSK signals as shown in (2.1), simplifies the analysis of spectral properties and response behaviour to linear systems.

Bandlimiting of the transmitted PSK signal may be accomplished by low-pass filtering of the data before modulation, or by bandpass filtering afterwards. When passed through a filter of the form $H(j\omega)$, the PSK signal takes the form:

$$m'(t) = \mathrm{Re} \sum_{k=-\infty}^{+\infty} A\, e^{j\phi_k} e^{j\omega_c t}\, p(t-kT_s) \qquad (2.2)$$

where p(t) is the complex function of time which represents the amplitude and phase response of the network $H(j\omega)$. To analyze the bandlimited PSK signal, m'(t), only the properties of the signal p(t) need to be considered [1].

This method of PSK signal representation is frequently used for satellite links, since it is the most efficient and easiest to analyze.

The basic coherent PSK demodulator is preceded by a receive bandpass filter which passes the signal and rejects the out-of-band noise and interference. The bandlimited PSK signal is then multiplied by a locally regenerated carrier reference. This carrier reference is generated by nonlinear operation of the carrier recovery circuit on the incoming bandlimited

PSK signal, which removes the phase and frequency variation effects of the modulation. The bandlimited baseband signals produced by the coherent demodulation are then regenerated and decoded. The timing signal for the regenerator and decoder is provided by the clock recovery circuit, which extracts a local clock from the bandlimited baseband signal.

2.3 BPSK System

If the sequences of phase $\{\phi_k\}$ in (2.1) take only two values, i.e., $\phi_k = 0^o$ or 180^o, a BPSK signal is obtained, that is:

$$m(t) = AV(t)\cos\omega_c t \qquad (2.3)$$

where

$$V(t) = \sum_{k=-\infty}^{+\infty} a_k w(t-kT_s), \text{ and } a_k = \cos\phi_k = \pm 1$$

The baseband (modulating) signal V(t), in (2.3) can be viewed as the output of the coder in Fig. 2.1, which in this case will be a random polar Non Return-to-Zero (NRZ) signal.

The resulting BPSK signal in (2.3) has the form of a sequence of plus-minus rectangular pulses of a continuously generated sinusoidal carrier as shown in Figure 2.2. Such a signal can be generated by a balanced modulator (mixer), as well as by direct phase modulation of a carrier [6].

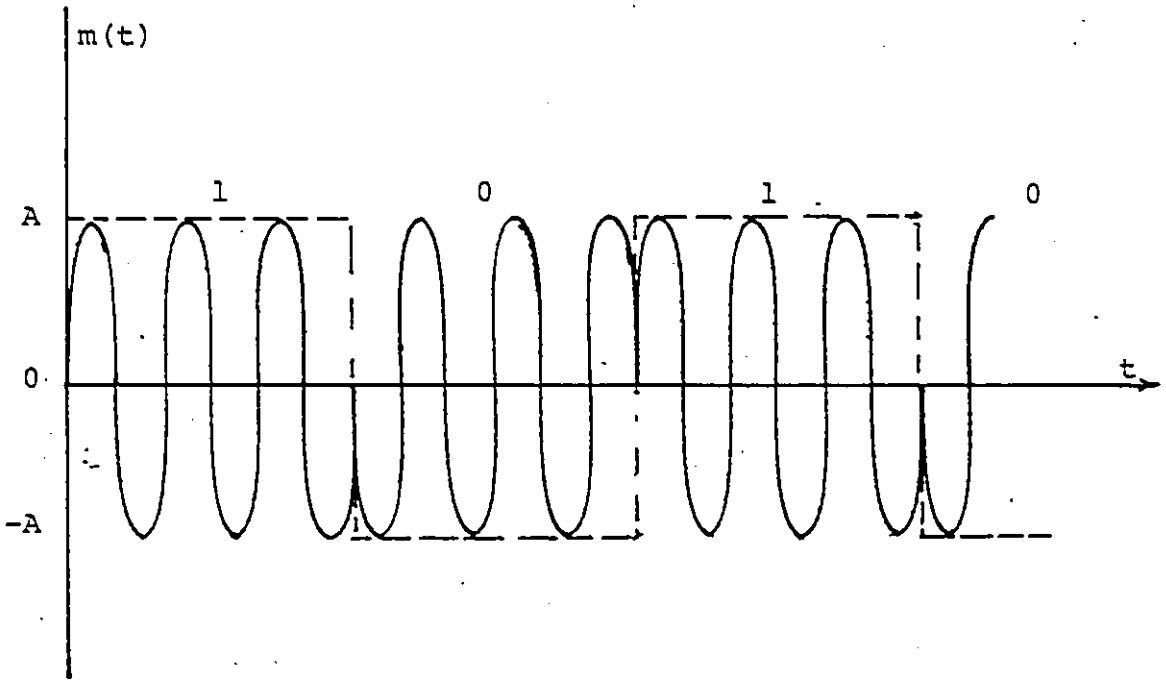

Figure 2.2 A BPSK Signal

The block diagram of a coherent BPSK system is shown in Figure 2.3, which is the simplest form of Figure 1.1. In Figure 2.4 the time domain representation of the signals at various points of this system (modem) is illustrated.

The power spectral density of a randomly modulated BPSK signal is given by [7].

$$S_m(f) = \frac{A^2 T_s}{2}\left[\frac{\mathrm{Sin}\pi(f-f_c)}{\pi(f-f_c)}\right]^2 \qquad f_c = \frac{\omega_c}{2\pi} \tag{2.4}$$

which is shown in Figure 2.5. From (2.4) and Figure 2.5, it can be seen that the BPSK signal has its highest power spectrum density around the carrier frequency and theoretically has an infinite bandwidth. In most applications, it is required to bandlimit the BPSK signal spectrum, and thus minimize the out-of-band interference which is a frequent cause of impairment into adjacent radio channels. Based on the equivalent performance of linearly modulated systems (of which PSK is one) with that of baseband systems, it can be shown [8] that the minimum required bandwidth for distortionless transmission of a BPSK signal is equal to the bit rate of the baseband modulating signal. For example, if it is required to transmit at the data rate of 40 kb/s, then the minimum theoretical transmission bandwidth necessary for a BPSK system is 40 kHz.

The probability-of-error performance, P_e, of a coherent BPSK system in an ideal channel is given by [9]:

$$P_e = 1/2\ \mathrm{erfc}\sqrt{\frac{E_b}{N_o}} \tag{2.5}$$

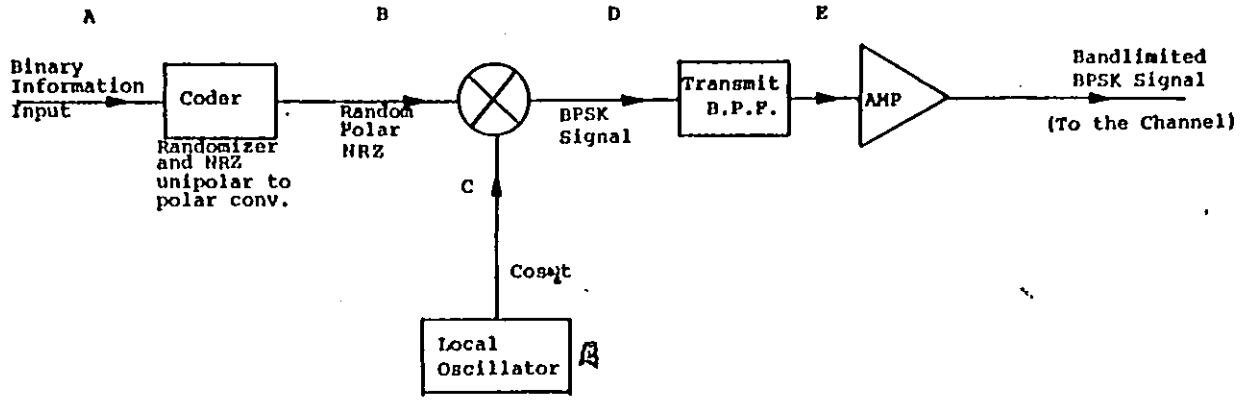

a) BPSK Modulator

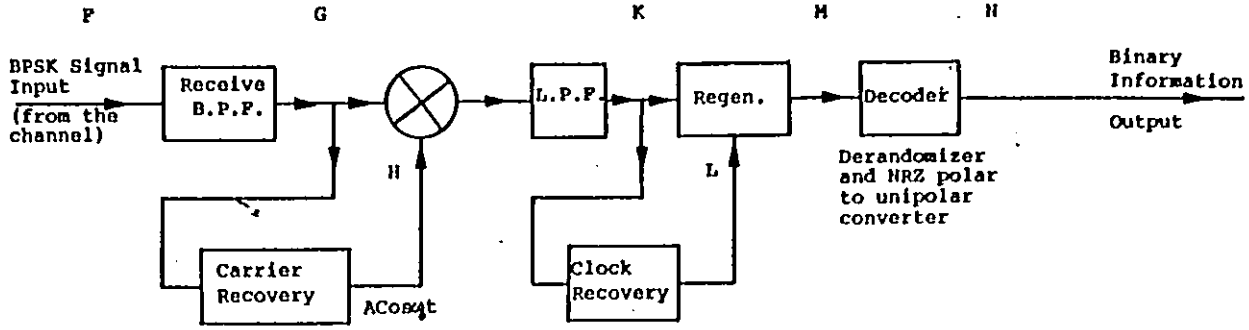

b) BPSK Demodulator

Figure 2.3 BPSK Modulation, Demodulation Block Diagrams

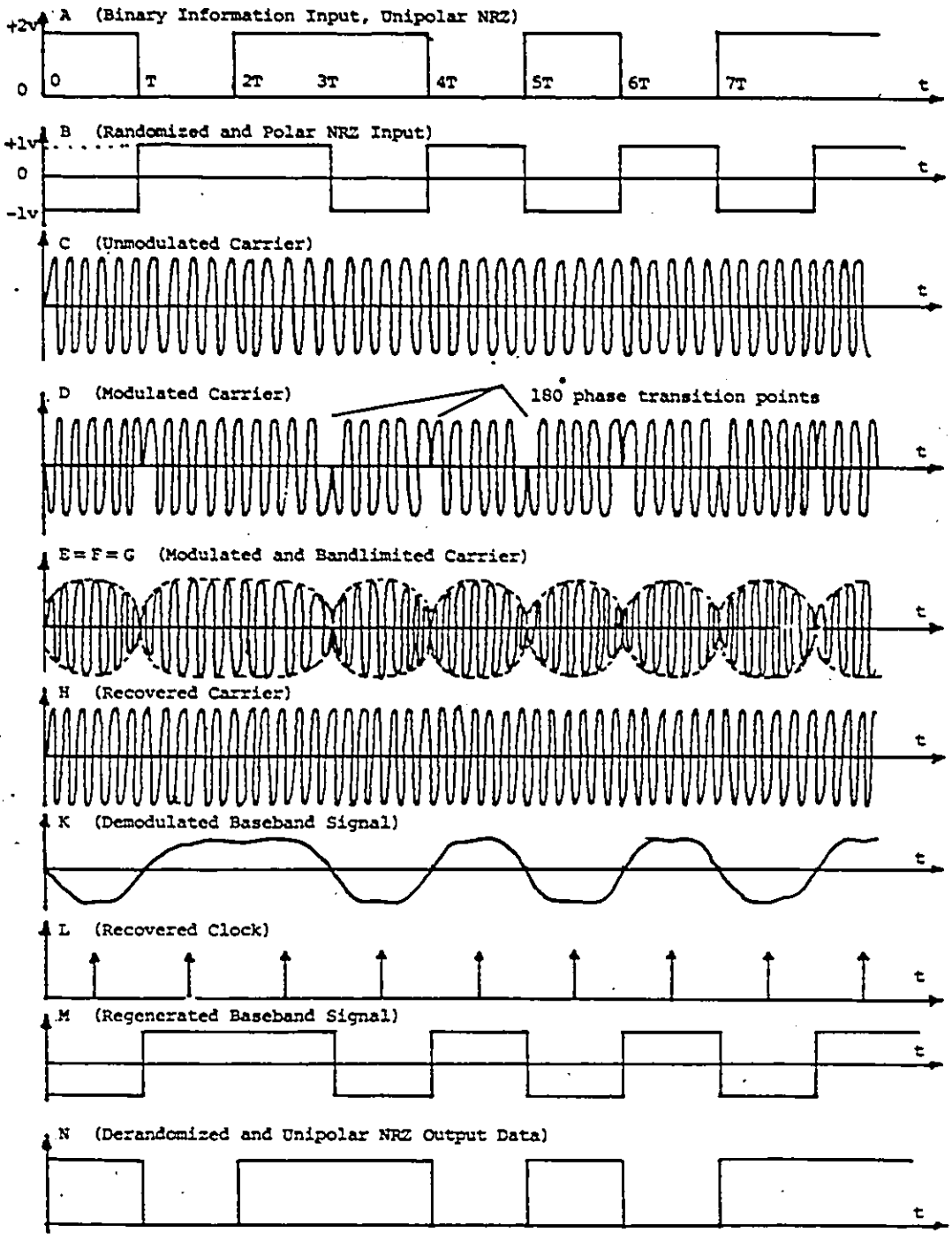

Figure 2.4 Time Domain Representation of the BPSK Modem Signals

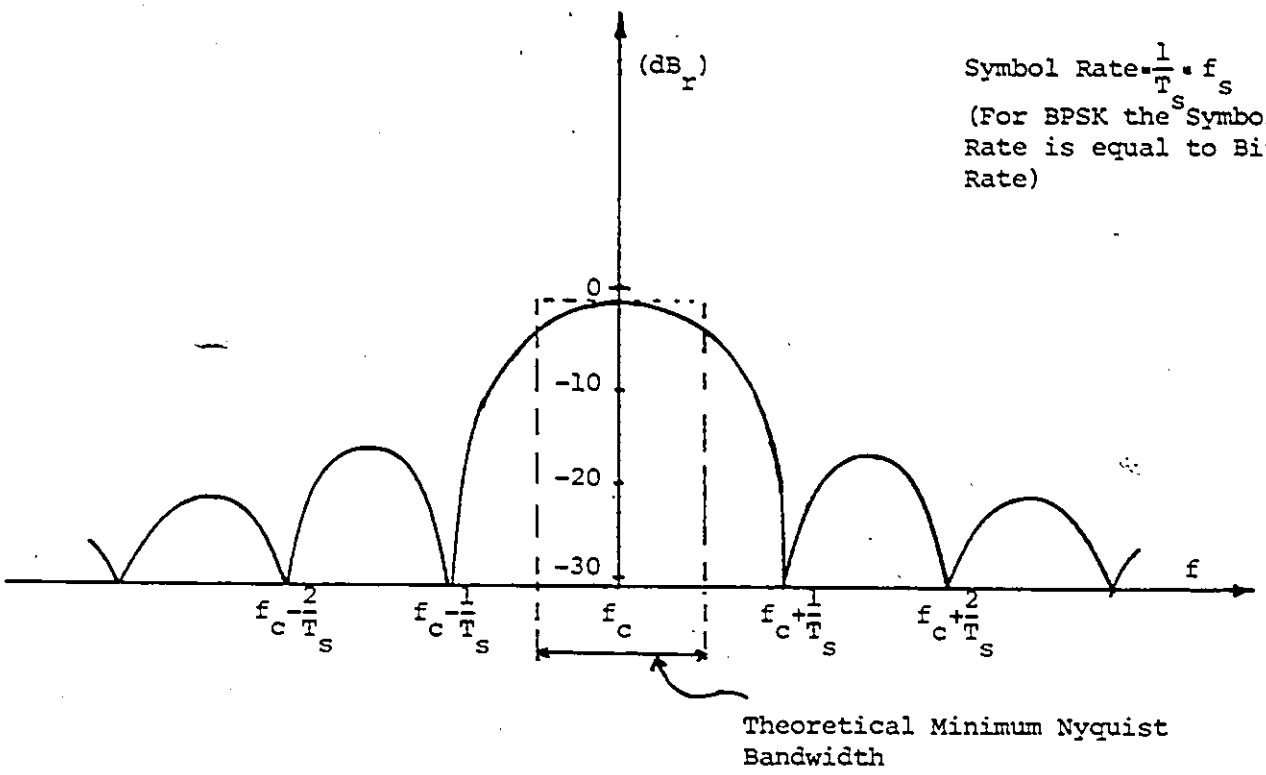

Figure 2.5 The Power Spectrum Density of a BPSK Signal

where the complementary error function erfc(x) is given by:

$$\text{erfc}(x) = 1 - \text{erf}(x) = \frac{2}{\sqrt{\pi}} \int_x^\infty e^{-x^2} dx \qquad (2.6)$$

The ideal channel is taken to be a Nyquist channel or a linear all-pass channel, corrupted only by Additive White Gaussian Noise (AWGN) with a constant (one-sided) power spectral density of N_o W/Hz. The ratio $\frac{E_b}{N_o}$, energy per bit (E_b)-to-noise density (N_o) is of particular interest. It is used as the figure of merit at a specified P_e in digital communication systems.

It can be shown that optimum receivers for binary signals in such channels call for matched filters with perfect phase reference available at the receiver [9]. For such coherent receivers, which base their bit decisions on observation of the signal over T_s seconds, there exists a class of signals, of which BPSK is one, which turns out to be optimum in the sense of requiring the minimum amount of E_b/N_o for a specified P_e. This optimum class of signals is called "antipodal", i.e., the two signals denoting the two possible information symbols have exactly the same shape but opposite polarity.

2.4 QPSK System

The optimum E_b/N_o performance available with BPSK led to a search for a PSK modulation scheme with a higher bandwidth efficiency than BPSK, but the same E_b/N_o performance. Such a

modulation scheme, increasing the bandwidth efficiency of BPSK system by two, is known as QPSK.

If the sequence of phases $\{\phi_k\}$ in (2.1) takes four values, i.e., $\phi_k = \pm 45^o$ or $\pm 135^o$, a QPSK signal is obtained, that is

$$m(t) = Ai(t)Cos\omega_c t + Aq(t)Sin\omega_c t \qquad (2.7)$$

where

$$i(t) = \sum_{k=-\infty}^{+\infty} a_k w(t-kT_s), \quad a_k = Cos\phi_k = \pm \frac{\sqrt{2}}{2} \qquad (2.8)$$

and

$$q(t) = \sum_{k=-\infty}^{+\infty} b_k w(t-kT_s), \quad b_k = Sin\phi_k = \pm\frac{\sqrt{2}}{2} \qquad (2.9)$$

The two terms in (2.7) represent two BPSK signals which can be detected independently due to the orthogonality of $Cos\omega_c t$, and $Sin\omega_c t$; therefore, the P_e performance or E_b/N_o performance of a QPSK will be essentially the same as for BPSK systems. While the spectral shape of the QPSK signal is identical to the spectral shape of the individual BPSK signals, the bandwidth efficiency of QPSK will be twice of that of the BPSK system.

The block diagram of a coherent QPSK system is shown in Figure 2.6. The serial input data stream to the modulator arrives at the rate of $1/T_s$ bps and is converted into two streams, i(t) and q(t), with the rate of $1/2T_s$; thus the

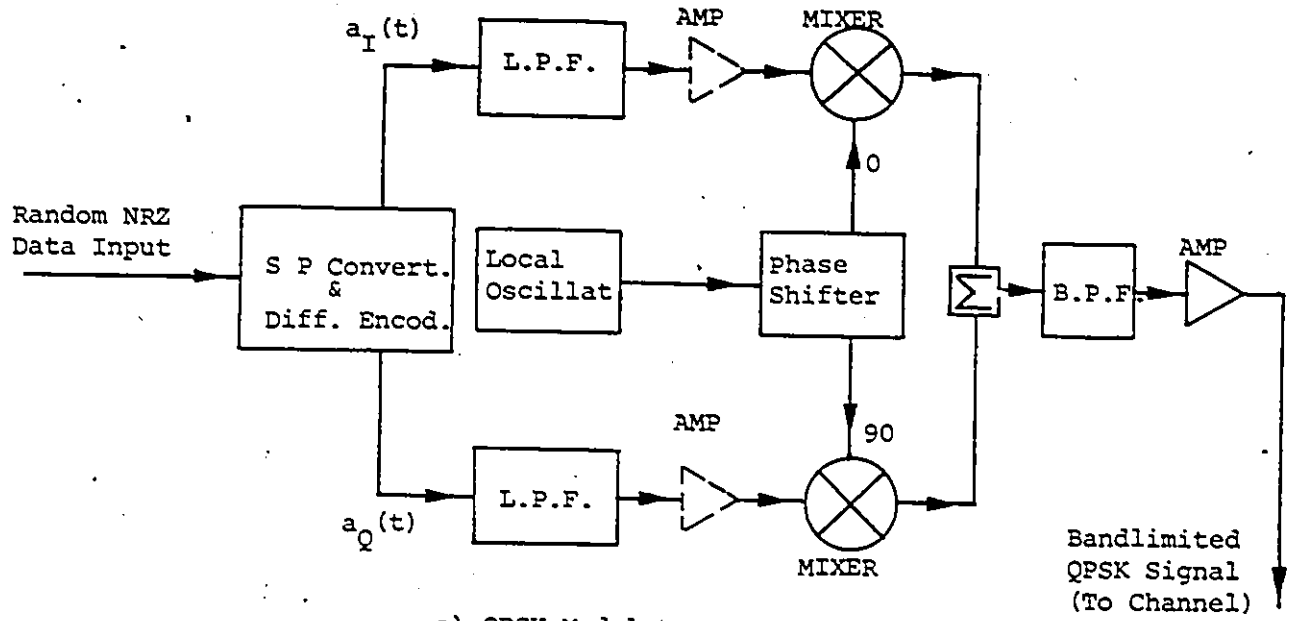

a) QPSK Modulator

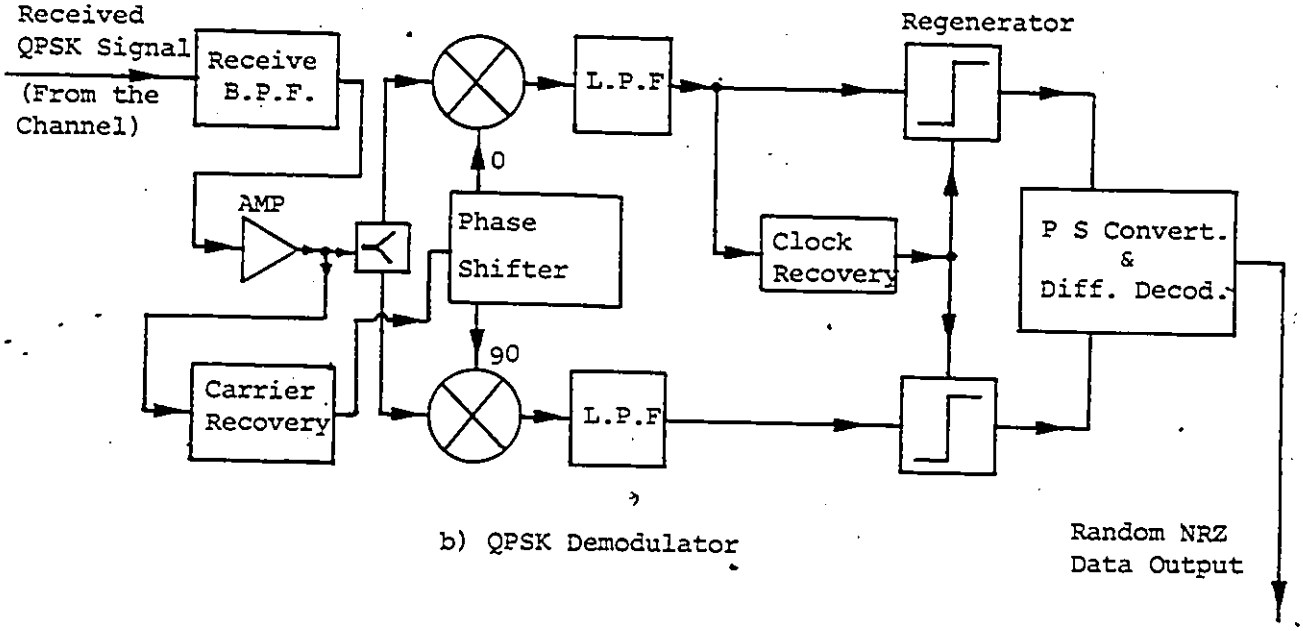

b) QPSK Demodulator

Figure 2.6 Model of Coherent QPSK Modulation, Demodulation

spectrum of the parallel streams is reduced to one-half of the serial input data. The two parallel data streams then modulate the inphase and quadrature components of the carrier. After linear addition of the corresponding inphase and quadrature modulated carriers, the QPSK signal is obtained.

The demodulator shown in Figure 2.6(b) performs the inverse functions to those of the modulator.

2.5 Bandlimitation in PSK Systems

In explaining the P_e performance of the BPSK and QPSK systems in the previous sections, ideal conditions of infinite bandwidth channel corrupted only by AWGN was considered. In practical communication systems, however, the available bandwidth is in many cases severely restricted and the channels are often surrounded by various types of interferences (in addition to AWGN).

To effectively utilize the spectrum and also to avoid interference into adjacent channels, stringent filtering at the transmitter is required. To reduce both noise and interference (from other systems) at the receiver, a certain amount of filtering is essential.

The introduction of filters between transmitter and receiver, however, causes waveform distortion and bit spreading. The waveform distortion is seen as fluctuations in the envelope of the modulated carrier, while bit spreading refers to

a data pulse not being confined to the signalling interval T_s, but lasting longer to interfere with adjacent bits causing intersymbol interference (ISI).

The envelope fluctuations induced in the modulated signal become very important when the signal is further passed through a nonlinear element such as a TWT, which can cause spectral spreading and additional distortion.

In many situations where the AWGN is small, the ISI, which is determined by the composite transmitter, channel, and receiver filter characteristics, could be a predominant cause of P_e performance degradation of digital systems [10, 11, 12, 13].

In linear channels, however, the ISI is minimized if a class of Nyquist pulse shaping filter characteristics called "raised cosine" is used as the overall system filtering characteristics [7, 8].

While Nyquist's criteria hold in the linear channel, they are no longer applicable in the nonlinear case. Nyquist shaping is meant to reduce ISI at the sampling instants. However, at all other times, the signal waveform amplitude is dependent upon pulse pattern and its oscillations. A saturating TWT amplifier output is dependent upon the data sequence and therefore the assumption of the message comprising a sequence of identical overlapping pulses, as required by a receiver (matched filter detector) for minimizing the ISI,

is no longer valid.

The selection of filters in the nonlinear channels will then be based upon optimum performance in consideration of channel constraints such as adjacent channel interference, degree of distortion introduced by the nonlinearities, noise, and the practicalities and economics of the filter structure. This is usually done by computer simulation as no analytical optimization is possible.

CHAPTER THREE

EFFECTS OF CHANNEL NONLINEARITIES ON THE POWER SPECTRUM DENSITY OF BANDLIMITED PSK SIGNALS

3.1 Introduction

Elements such as up-converters, limiters, and high power RF amplifiers when operated in a nonlinear mode close to saturation to achieve a higher power efficiency, constitute a potential source of signal distortion in digital radio systems. These nonlinear elements can usually be modeled as band-pass nonlinearities [14], that is, by defining their input-output characteristics in terms of AM/AM and AM/PM conversions. The nonlinear distortion in the output signal depends on the envelope fluctuations of the input signal.

Nonlinear distortion in a PSK signal arises, for example, if an IF modulator, followed by a filter and by nonlinear elements like an IF/RF converter or an RF amplifier is used.

The undesirable consequences of such distortion in PSK signals are P_e performance degradation and spectral spreading. The latter effect is known to be a critical factor in PSK transmitter design, because it is likely to produce harmful interference in adjacent radio channels.

The presence of spectral spreading phenomena may therefore require additional RF filtering after the last nonlinear element, and feasibility problems may arise if the RF filter bandwidth to center frequency ratio is rather small and/or

frequency agility is required.

Considerable research efforts [2, 5, 15] have been undertaken to overcome these problems, in the following fields:

1) Linear and quasi-linear RF devices
2) Digital modulation techniques with low envelope fluctuations, and therefore with low sensitivity to nonlinear distortion.

Considering the second topic, it has been shown that if the phase transitions in a QPSK signal occur in a controlled manner, the envelope fluctuations due to filtering are greatly reduced, and hence the effects of nonlinear distortion are reduced.

In this chapter, the spectral spreading of BPSK, QPSK, and controlled phase transition QPSK, i.e., offset QPSK (O-QPSK) modulation techniques due to channel nonlinearities will be at first analyzed by evaluating the envelope fluctuations that such signals exhibit after being filtered. In particular, it will be shown that if the smooth phase transition of a PSK signal is achieved by filtering, then the spectral spreading of such signal (at the output of a nonlinear device) will be drastically reduced.

3.2 Envelope Fluctuation of Filtered PSK Signals

The phase-state vector diagrams of PSK modulation are shown in Figure 3.1. The conventional BPSK modulator produces 0° and 180° phases.

In order to change from one of these states to the other, the phase vector traverses the straight solid line from 1 to 2, passing through zero amplitude along the way. The phase transition is instantaneous and occurs as the phase vector passes through zero amplitude.

A QPSK modulator can have any one of the four phase states at increments of 90°. Phase transitions of 90°, 180°, and 270° are allowed in standard QPSK. A phase transition from state 1 to 3 can be accomplished by reducing the amplitude of the 0° vector and by increasing the 90° vector to full amplitude. If these two operations are performed simultaneously, the phase vector will traverse the dotted line from state 1 to 3. This phase vector does not pass through zero amplitude, and indeed suffers a maximum drop in amplitude of only 3 dB, during the transition. During a 180° phase shift, however, the phase vector does pass through zero amplitude, just as in BPSK modulation.

In QPSK modulation, if one of the binary data stream delayed with respect to the other by an amount equal to $T_s/2$ (T_s being the symbol duration), the instantaneous phase transitions can then occur only in 90° increments. This form

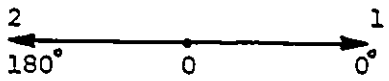

BPSK

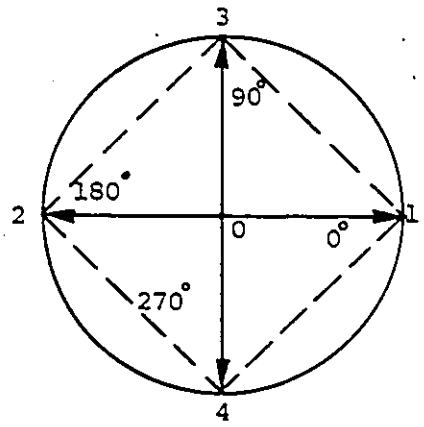

QPSK, O-QPSK

Figure 3.1 Phase Vector Diagrams of PSK Modulators

of QPSK,which is called offset QPSK or O-QPSK modulation [2, 16], avoids the zero vector amplitude problem of the standard QPSK modulation. The block diagram of an O-QPSK modulator is shown in Figure 3.2.

In an infinite bandwidth environment (no filtering), the above-mentioned PSK signals have a time invariant constant envelope, i.e., the instantaneous phase transitions, and hence the phase vector amplitude variations do not affect the envelope of the modulated signals.

Filtering of such signals, however, causes spurious envelope fluctuations and intersymbol interference [19, 20].

BPSK or QPSK signals with 180° phase reversals, after filtering,exhibit maximum envelope fluctuations from zero to maximum steady state value, as shown in Figure 3.3 [1]. This is because bandlimiting of a digital waveform results in rounding and widening of each individual pulse. Thus, adjacent BPSK or QPSK symbols are smeared into each other, causing intersymbol interference. As an example,in conventional QPSK when both binary components of the QPSK change state such as to yield the 180° phase shift, the two consecutive symbols can be thought of as having identical phases but opposite polarities for their magnitudes (As in BPSK modulation). Hence the smearing of two such pulses into each other (because of filtering) results in destructive interference. At any point at which symbols of opposite polarity overlap, the

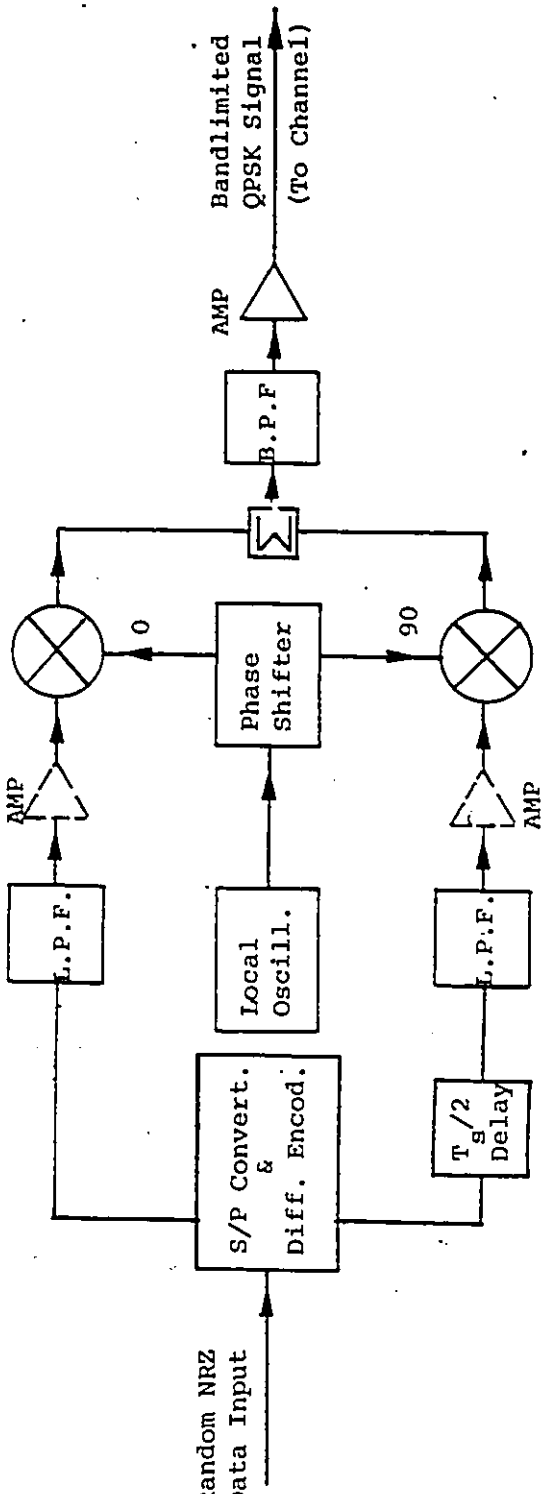

Figure 3.2 Block Diagram of an Offset QPSK Modulator

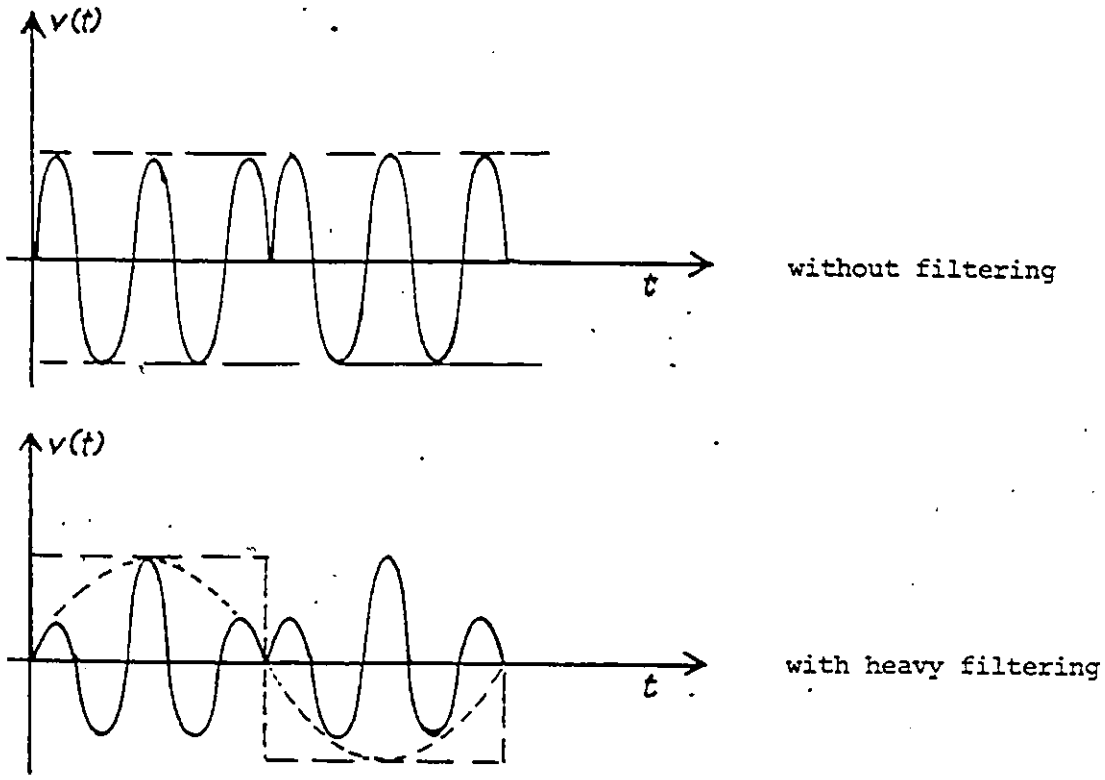

Figure 3.3 Effect of Filtering on the Envelope of BPSK or QPSK Signals with 180° Phase Reversals

envelope of the signal will be given by the difference in magnitude of the two contributions. Consequently, the signal envelope will be reduced in the transition region between the two symbol slots. About midway between the centers of the symbols, the magnitudes of the two contributions are equal and cancel because of their opposite polarities. Thus the envelope goes to zero at this point. Since the phase of the composite signal resulting from the two components of opposite polarity is equal to that of the larger component, there will be an instantaneous phase transition of 180° at the point at which the envelope vanishes.

The bandlimited O-QPSK signal on the other hand does not have any envelope zeros. Since the O-QPSK modulator allows only one binary modulation component to change state at any transition point, an instantaneous polarity change is avoided. For phase shifts of $\pm 90^{\circ}$, the intersymbol interference created by bandlimiting is not destructive but is vectorially additive. That is, the envelope of the signal at the region of 90° transition is equal to the sum of the RMS values of the magnitudes of each contribution.

Consider the O-QPSK modulator of Figure 3.2. The output signal can be represented as:

$$m_0(t) = x(t)\mathrm{Cox}\omega_c t + y(t)\mathrm{Sin}\omega_c t \qquad (3.1)$$

where

$x(t) = \sum_{k=-\infty}^{+\infty} a_k p(t-kT_s)$ is the envelope of the in-phase modulated signal

$y(t) = \sum_{k=-\infty}^{+\infty} b_k p(t-kT_s - \frac{T_s}{2})$ is the envelope of the quadrature modulated signal

$p(t) = g(t)*f(t)$ is the bandlimited symbol shape

$f(t)$ is the impulse response of the modulator's equivalent low-pass filter characteristics for each channel

$g(t)$ is the rectangular baseband symbol shape

a_k and b_k are sequences of random numbers having values of + 10r - 1 with equal probability

Using trigonometry, (3.1) can be written in the form of:

$$m_0(t) = s(t)\text{Cos}(\omega_c t + \phi(t)) \qquad (3.2)$$

where

$$s(t) = \sqrt{x^2(t) + y^2(t)} \qquad (3.3)$$

and $$\phi(t) = \tan^{-1} \frac{y(t)}{x(t)} \qquad (3.4)$$

In (3.2), $s(t)$, representing the envelope of the bandlimited O-QPSK signal, may droop slightly in the region of 90° phase transition. Indeed the minimum value of the envelope for reasonable filtering can be shown to be no less than 0.707 of its steady state value [18].

$\phi(t)$ in (3.2) represents the phase of bandlimited O-QPSK at any time t. With the envelopes $x(t)$ and $y(t)$ smeared into

each other by filtering, $\phi(t)$ will shift fairly smoothly from one state to the other in 90^0 increments. In Figure 3.4 the phase transition and also the envelope fluctuations of bandlimited QPSK and O-QPSK signals are shown.

The nature of phase transitions and associated envelope fluctuations of such bandlimited PSK signals play tant role on their spectral behaviour, when transmitted through a nonlinear channel.

3.3 Effects of Channel Nonlinearities on the Spectral Behaviour of Bandlimited BPSK, QPSK, and O-QPSK Signals

In this section, the spectral behaviour of these bandlimited PSK signals, when passed through an ideal hard-limiter, will first be investigated. (An ideal hardlimiter is a nonlinear device having the characteristic shown in Figure 3.5. Such a device removes the envelope fluctuations of its input signal without affecting the phase [9], and has been used as an extreme model of the AM/AM characteristics of a saturated TWT [21, 22, 23].) Then the effect of a more realistic AM/AM characteristic of a TWT amplifier, often encountered in satellite channels, will be considered.

3.3.1 Effects of Hardlimiter on Spectral Spreading

The instantaneous 180^o phase transitions of bandlimited BPSK and QPSK signals produce high frequencies that are

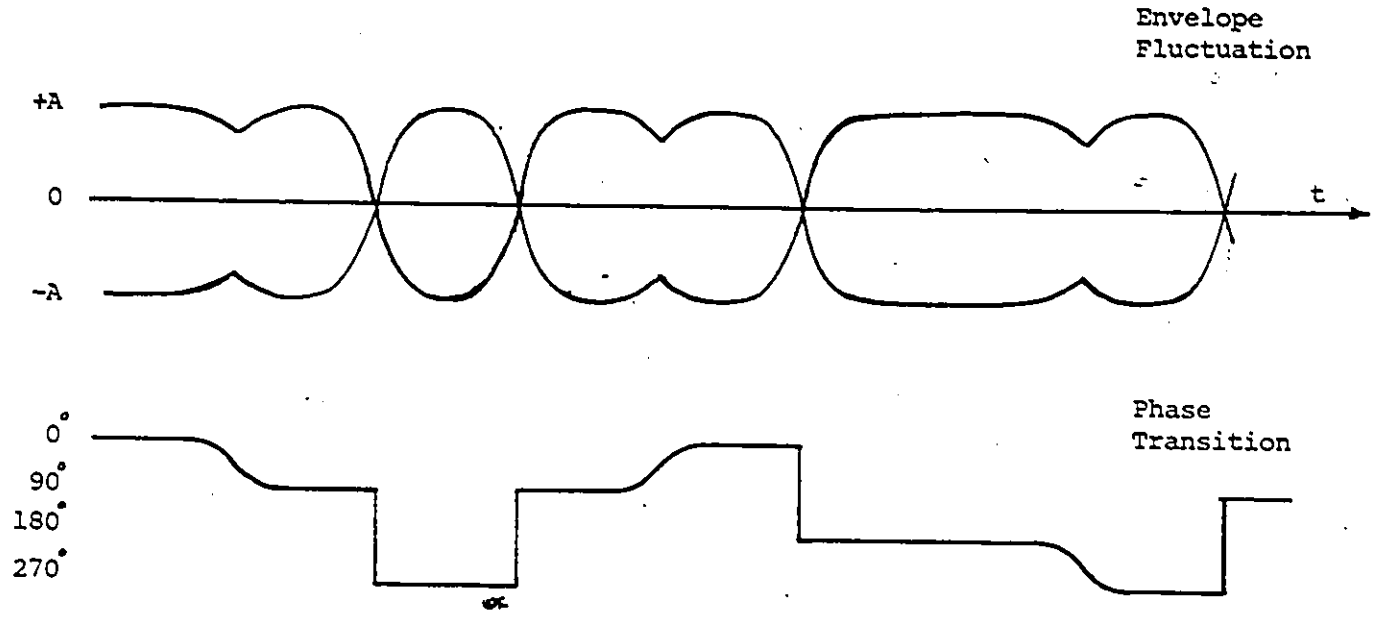

a) QPSK Signal

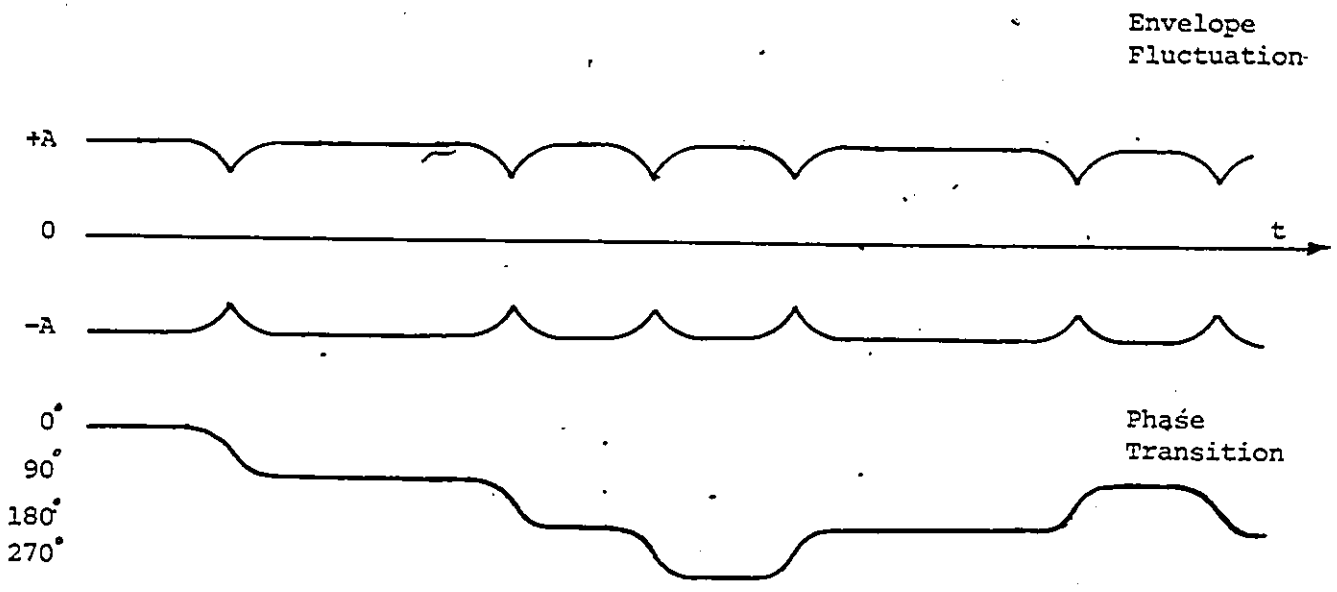

b) Offset QPSK Signal

Figure 3.4 Envelope Fluctuation and Phase Transitions of Filtered QPSK and Offset QPSK Signals

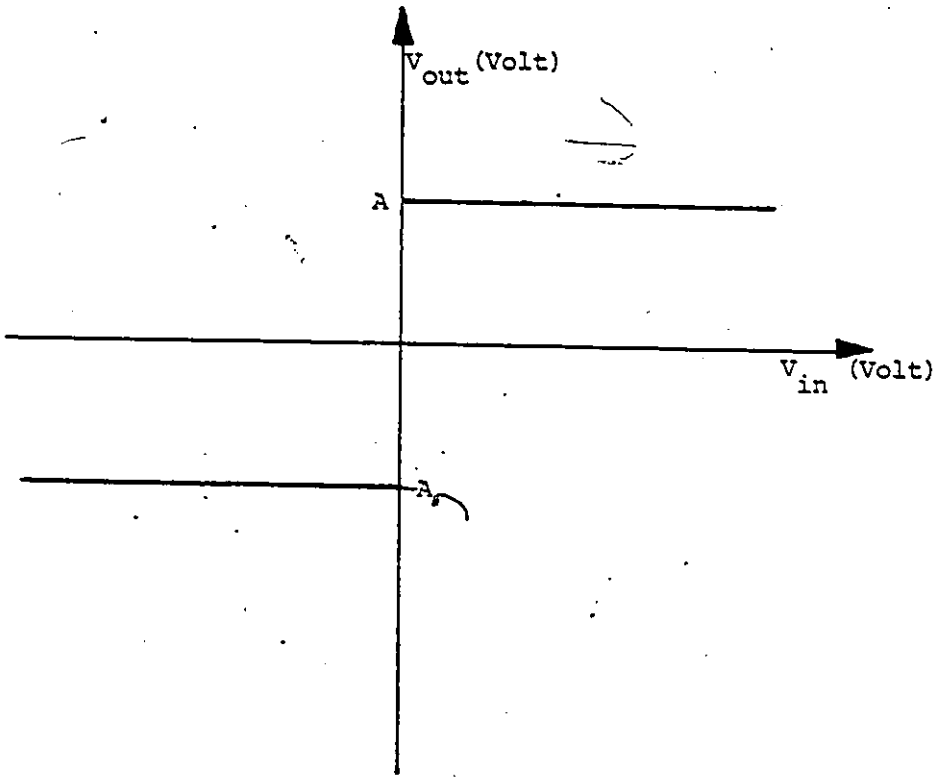

Figure 3.5 The Input-Output Characteristic of an Ideal Hardlimiter.

outside of the desired transmission band. Because of envelope zeros (at the 180° phase transition points), however, there is very little power associated with the high frequency content, as would be expected for such filtered signals. Hardlimiting of such signals, however, removes the envelope zeros and restores a constant envelope, and thus the instantaneous 180° phase transition results in a large amount of out-of-band spectrum. In fact, the restoration of a flat envelope by hardlimiting yields a rectangular waveform with an instantaneous 180° phase shift, which is identical to the waveform prior to filtering. Consequently, the hardlimiting of such bandlimited signals with instantaneous 180° phase transitions completely removes the effect of filtering, as shown in Figure 3.6.

Note that in PSK modulation the instantaneous frequency of the modulated signal is proportional to its rate of change of phase, i.e.,

$$f = \frac{1}{2\pi} \frac{d\phi(t)}{dt} \qquad (3.5)$$

Out-of-band interference can be suppressed by either avoiding instantaneous phase transitions and their associated high frequencies, or by causing the envelope to vanish in regions of large phase slopes. This latter technique, of a vanishing envelope, was shown to take place for bandlimited QPSK (as

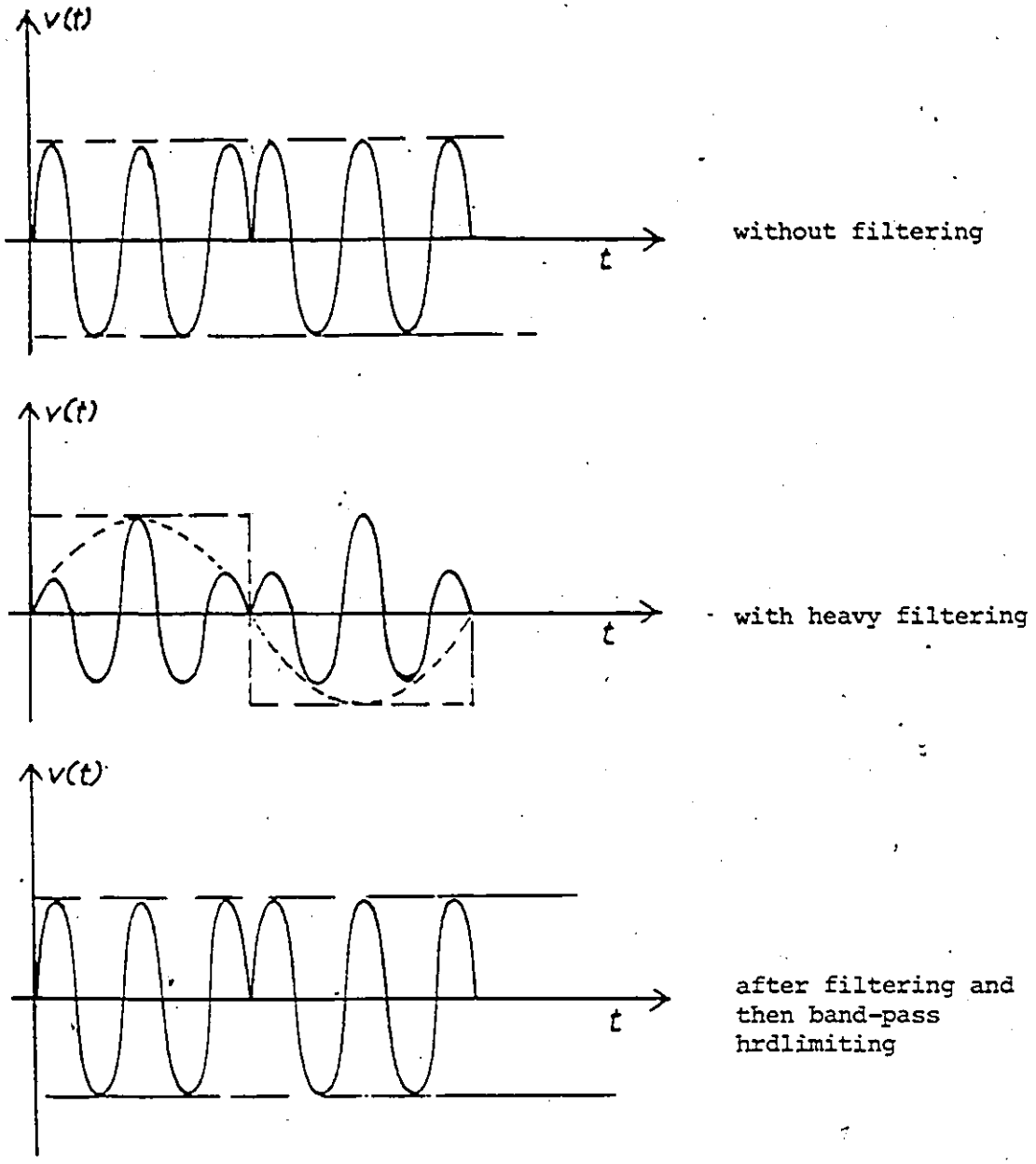

Figure 3.6 Effect of Filtering and Hardlimiting on BPSK or QPSK Signal with 180 Phase Reversals.

well as BPSK) signals. The effect of this form of bandlimiting obviously disappears if the signal is passed through a hardlimiter.

In O-QPSK modulation, due to smooth phase transition of bandlimited signal, the slope $d\phi/dt$ of the phase will be small at all points, and the transition region will not produce high frequencies.

If the bandlimited O-QPSK signal is passed through a hardlimiter the small envelope fluctuation is removed, but the smooth phase transitions which reflect the effect of filtering are preserved. In other words, the O-QPSK signal in (3.2), after hardlimiting can be represented as:

$$m_0'(t) = \text{Cos}(\omega_c t + \phi(t)) \qquad (3.6)$$

Using trigonometry, (3.6) can be written in the following form:

$$m_0'(t) = x'(t)\text{Cos}\omega_c t + y'(t)\text{Sin}\omega_c t \qquad (3.7)$$

where

$$x'(t) = \frac{x(t)}{s(t)} \text{ and } y'(t) = \frac{y(t)}{s(t)}$$

Comparing (3.7) with (3.1), and also considering $s(t)$ in (3.3), which has almost a constant value (very low and smooth fluctuation), it is evident that $x'(t)$ and $y'(t)$, which reflect the effect of filtering after hardlimiting, have almost the same shape as those of $x(t)$ and $y(t)$ respectively. The small modification of $x(t)$ and $y(t)$ due to hardlimiting corresponds

to a very low spectral spreading. A graphical example of this modification is shown in Figure 3.7.

3.3.2 Effects of TWT Nonlinearities

Consider the block diagram of Figure 3.8, where a PSK signal is fed to a band-pass filter followed by a nonlinear TWT amplifier. Such a scheme may refer to a satellite transponder, earth station, or other system configuration [24].

Many authors have used this simplified model and evaluated the spectral behaviour of filtered PSK signals at the output of the TWT, by means of computer simulations [20, 25, 26, 27, 28].

As an example, the results obtained in [26] for the power spectrum density of BPSK, QPSK, and O-QPSK signals at the output of a typical TWT (see Figure 1.3) are shown in Figures 3.9, 3.10, and 3.11.

In this simulation, the data input rates of 60 Mbs for QPSK and O-QPSK and 30 Mbs for BPSK are used, and in all modulation cases a 36 MHz band-pass filter with a square root raised cosine characteristic is employed.

Since the spectrum is approximately symmetric about the carrier frequency, only half of the spread PSK spectrum is displayed. Included with each figure are the integrated powers over the wanted and adjacent RF channels.

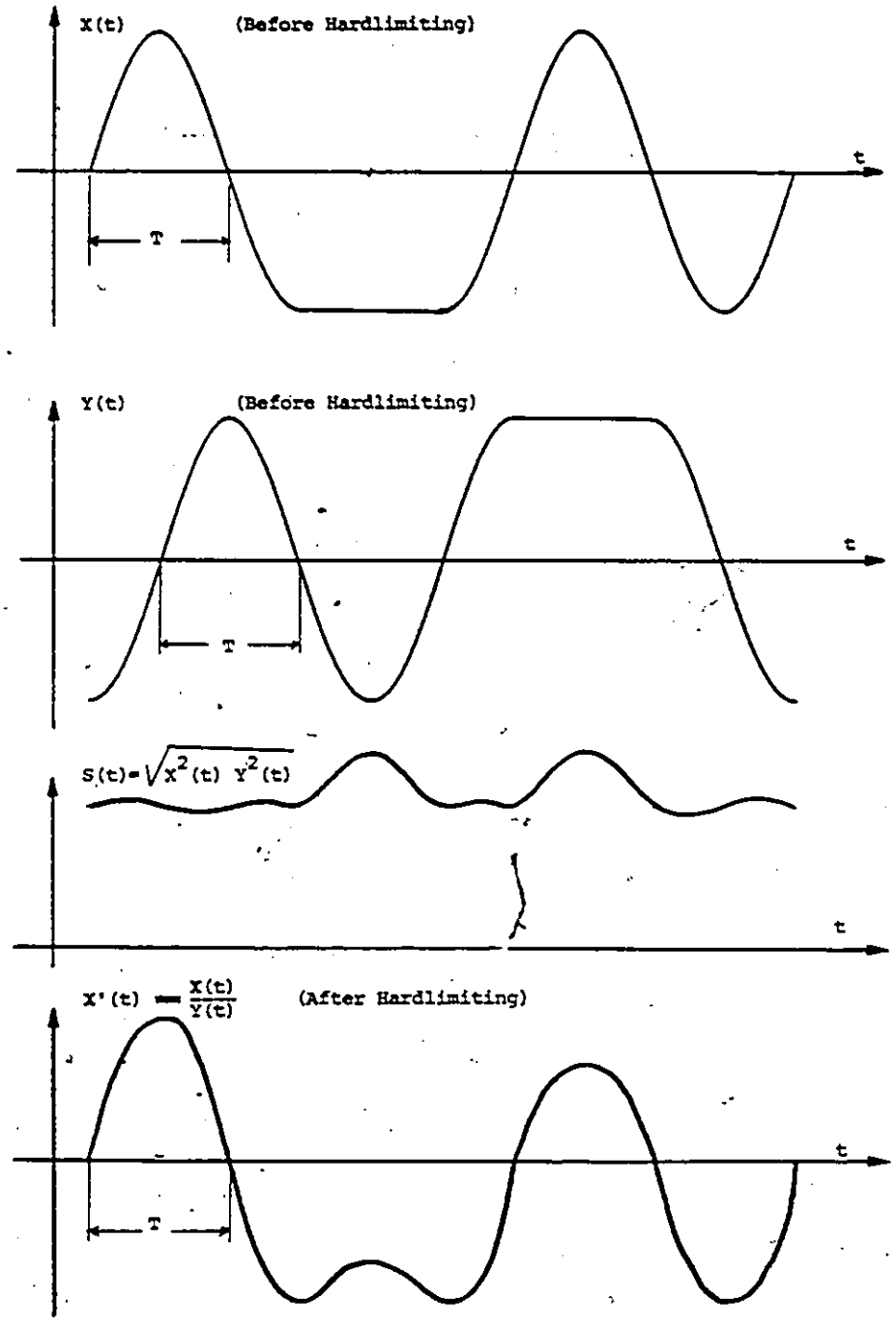

Figure 3.7 Reflection of the Effect of Filtering on the O-QPSK Baseband Signals Amplitude, before and after Hardlimiting

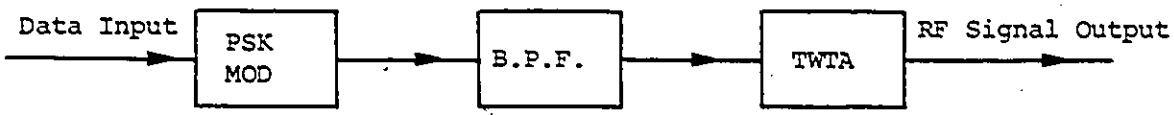

Figure 3.8 A General Model of a Nonlinear Radio Communication Channel.

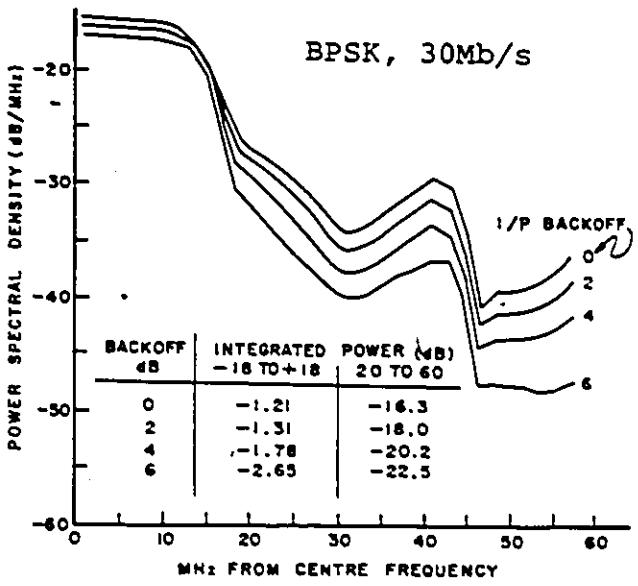

Fig. 3.9 Spectral Spreading of a Filtered BPSK Signal Caused by a Nonlinear TWT. (fromRef.[26])

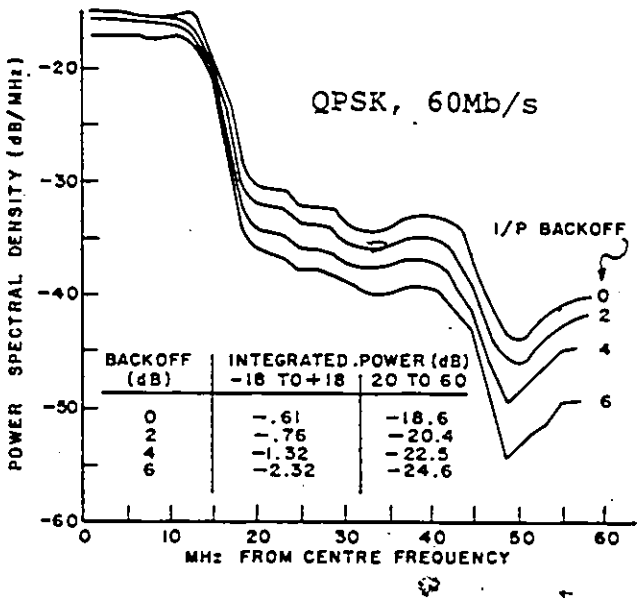

Fig. 3.10 Spectral Spreading of a Filtered QPSK signal Caused by a Nonlinear TWT. (from Ref.[26])

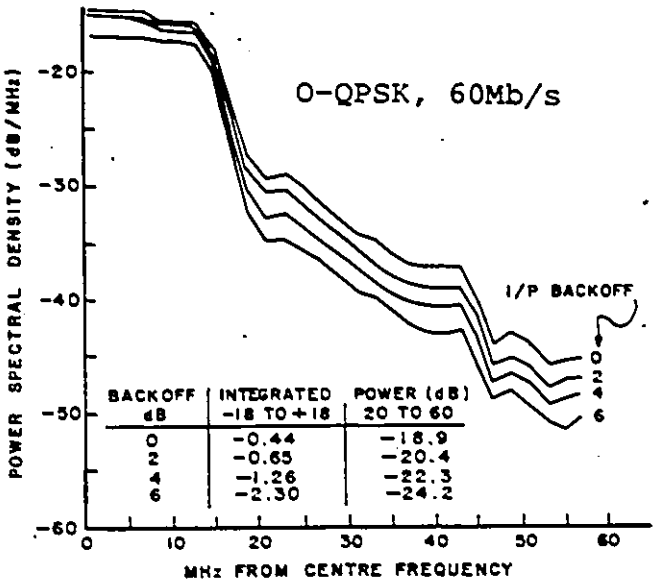

Fig. 3,11 Spectral Spreading of a Filtered O-QPSK Signal Caused by a Non-linear TWT. (from Ref.[26])

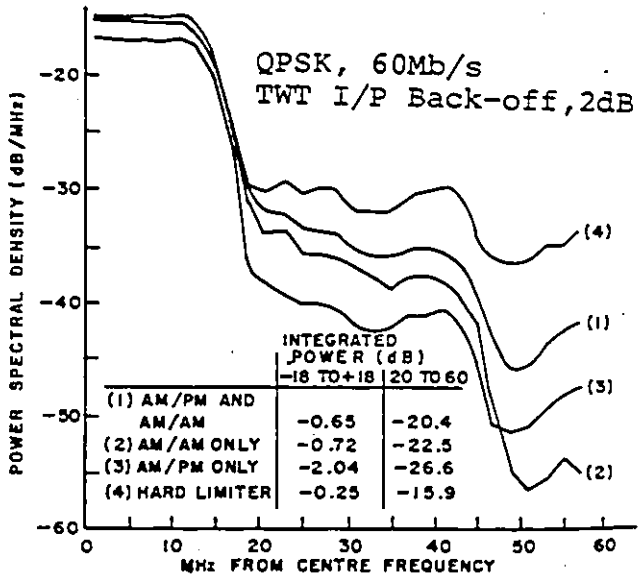

Fig. 3.12 Comparison of QPSK signal power spectrum density at the output of a TWT with 2dB input power back-off, when the TWT AM/AM and AM/PM conversions are applied simultaneously and individually. (from Ref.[26])

These graphs demonstrate the variation in the TWT output spectrum with input back-off and modulation type. As can be seen, the spectral spreading of the O-QPSK signal is much less than those of BPSK and QPSK signals. This is merely because of the lower envelope fluctuations of the O-QPSK signal at the input of the TWT.

Furthermore, Figure 3.12 compares the spectum of the 60 Mb/s QPSK signal at the TWT output, when the AM/AM and AM/PM conversion of TWT are applied simultaneously and individually. From this figure, it can be seen that the spectral spreading is caused primarily by AM/AM conversion, while AM/PM conversion accounts for most of the in-band distortion and corresponding degradation in P_e performance of the system [25]. Another case which has been considered in Figure 3.12 is the hardlimiter with no AM/PM conversion (a limiter prior to the satellite TWT has been proposed to provide gain control and reduce AM/PM degradation in PSK TDMA system). As would be expected, it results in a substantial increase in spectral spreading.

CHAPTER FOUR

GENERATION OF A CONSTANT ENVELOPE BANDLIMITED BPSK SIGNAL

4.1 Introduction

In Chapter Three, it was shown that the spectral spreading of a bandlimited O-QPSK signal due to channel nonlinearity is much less than those of bandlimited BPSK and QPSK signals. This is because the O-QPSK signal, by avoiding the instantaneous 180° phase transitions of QPSK signal after bandlimiting, achieves smooth phase transition and hence low envelope fluctuations.

In this chapter it will be shown that the same benefit gained in the O-QPSK modulation can be obtained for BPSK modulation, if instantaneous 180° phase transitions are avoided. A modified BPSK modulation technique using premodulation filtering is introduced, and its spectral characteristics are analysed. The modified BPSK (MBPSK) modulator achieves a smooth phase transition from 0° to 180° by going through an intermediate value of 90°. The resultant PSK signal has a very low AM component, and hence is less sensitive to channel nonlinearities.

4.2 Modified BPSK (MBPSK) Modulation

As in the case of O-QPSK modulation, smooth phase transitions can be achieved in BPSK modulation with premodulation

filtering if the phase vector is designed so as to rotate with a constant amplitude through the 90° phase state to 180°. This implies that a source of 90° shifted component is necessary to achieve the desired phase transition path. The transition path which is shown by the dotted line in Figure 4.1, can be expressed by the following equation [29]:

$$x^2(t) + y^2(t) = A^2 = \text{constant} \qquad (4.1)$$

where $x(t)$ is the amplitude of the filtered input data to the modulator, $y(t)$ is the amplitude of the auxiliary 90° phase vector component, which is hereafter called the phase smoothing signal, and A is the peak amplitude of $|x(t)|$.

From (4.1), the phase smoothing signal $y(t)$ can be obtained in terms of $x(t)$, that is:

$$y(t)=\sqrt{A^2 - x^2(t)} \qquad (4.2)$$

When $x(t)$ in (4.2) takes the peak value, i.e., $x(t) = \pm A$, then $y(t) = 0$. In other words, when we are in the zero and 180° phase states, we do not need the 90° phase component. During data transitions (which correspond to 180° phase reversals), as $x(t)$ becomes zero, $y(t)$ becomes A, creating a phase vector rotation passing through 90°.

The block diagram of this modified BPSK modulator is shown in Figure 4.2. The output can be written as:

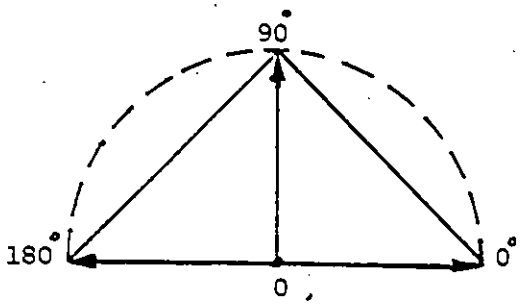

Figure 4.1 The Phase Transition Path of an Ideal Modified BPSK Modulator.

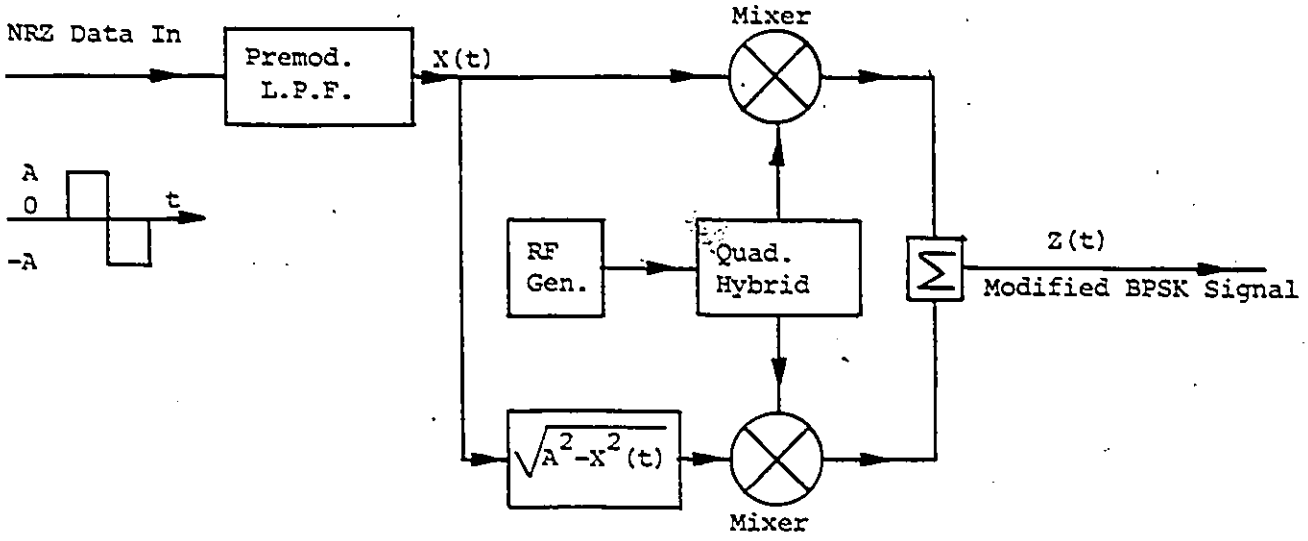

Figure 4.2 Block Diagram of the Modified BPSK Modulator

$$z(t) = x(t)\cos\omega_c t + y(t)\sin\omega_c t \tag{4.3}$$

or $$z(t) = b(t)\cos(\omega_c t + \phi(t)) \tag{4.4}$$

where

$$b(t) = \sqrt{x^2(t) + y^2(t)} = \sqrt{x^2(t) + A^2 - x^2(t)} \tag{4.5}$$

$$= A = \text{Constant}$$

and $$\phi(t) = \tan^{-1}\frac{y(t)}{x(t)} = \tan^{-1}\frac{\sqrt{A^2-x^2(t)}}{x(t)} \tag{4.6}$$

From (4.5) and (4.6) it is evident that z(t) having a constant envelope now preserves the full effect of premodulation filtering in its phase function $\phi(t)$. This signal can be transmitted through a highly nonlinear channel with a minimum spectral spreading.

An example of phase transition of such a MBPSK signal is shown in Figure 4.3. For comparison, the phase transition of a conventional bandlimited BPSK signal is given in the same figure. Note from Figure 4.3 that the phase transitions of MBPSK signal are now smooth and resemble the filtered data input.

4.3 Realization of an MBPSK Modulator

Referring to Figure 4.2, the realization accuracy of a MBPSK modulator depends on how successfully equation (4.2), which is a nonlinear function of x(t), can be implemented with minimum circuit complexity.

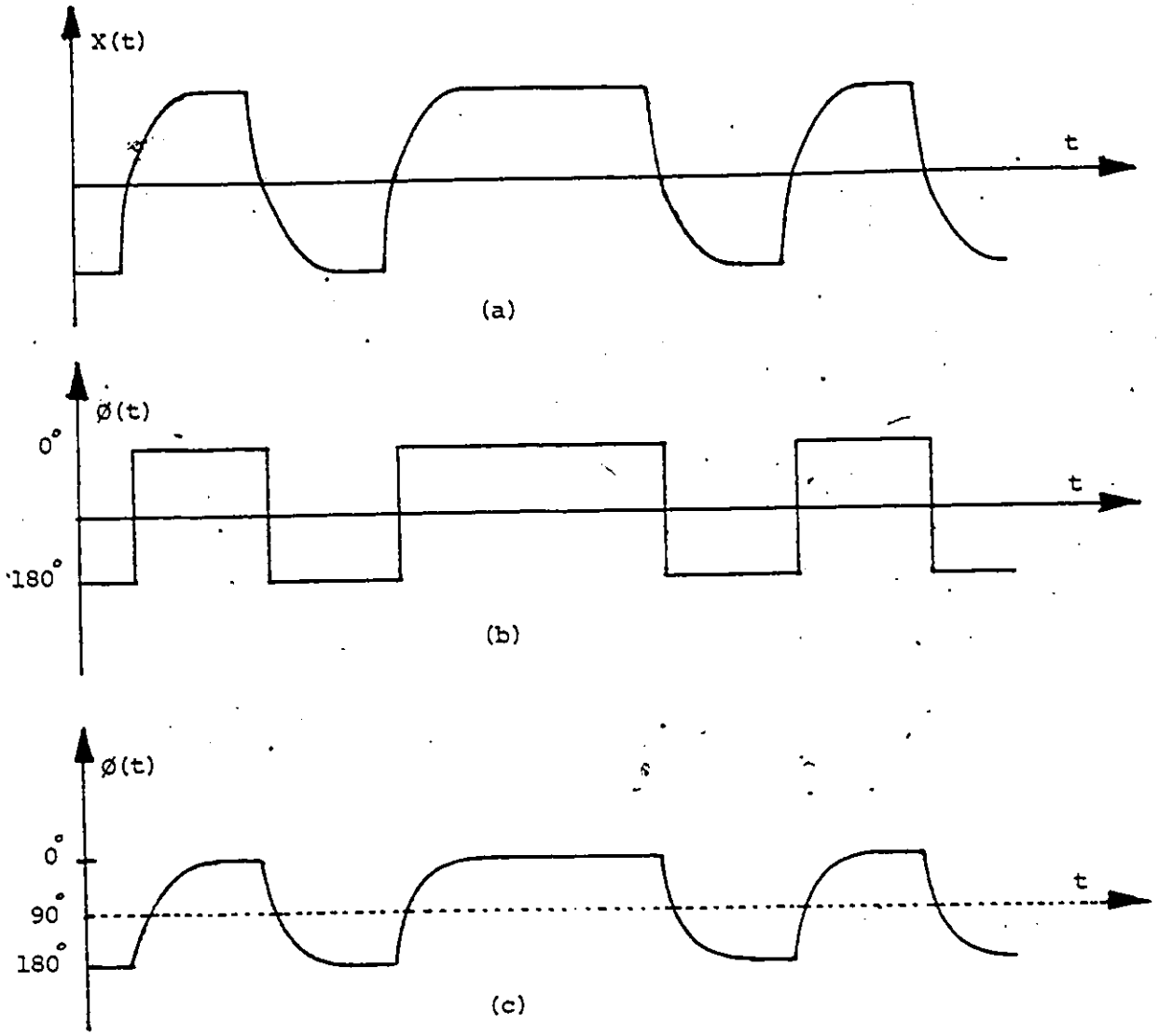

Figure 4.3 a) Bandlimited Digital Data
b) Phase Transition of the Conventional BPSK Signal
c) Phase Transition of the Modified BPSK Signal

One of the easiest methods is the simplification of (4.2) to a simple realizable form. Indeed, if the ideal phase transition path of MBPSK signal, which is shown by a dotted arc in Figure 4.1, is approximated to chord (solid lines), then (4.2) can be simplified to the following form [30]:

$$y(t) = A - |x(t)| \tag{4.7}$$

Now (4.7) can be implemented by a very simple circuit. The design and analysis of this circuit will be discussed in the next chapter.

The block diagram of this MBPSK modulator is shown in Figure 4.4. The MBPSK signal now can be represented as:

$$z(t) = x(t)\cos\omega_c t + [A-|x(t)|]\sin\omega_c t \tag{4.8}$$

which can be written in the form of

$$z(t) = b(t)\cos(\omega_c t + \phi(t)) \tag{4.9}$$

where

$$b(t) = \sqrt{A^2 + 2x^2(t) - 2A|x(t)|} \tag{4.10}$$

and

$$\phi(t) = \tan^{-1}\frac{A-|x(t)|}{x(t)} \tag{4.11}$$

The resultant MBPSK signal now exhibits some envelope fluctuations, as shown in (4.10). However, the minimum value of $b(t)$ is not less than 0.707 of its peak value.

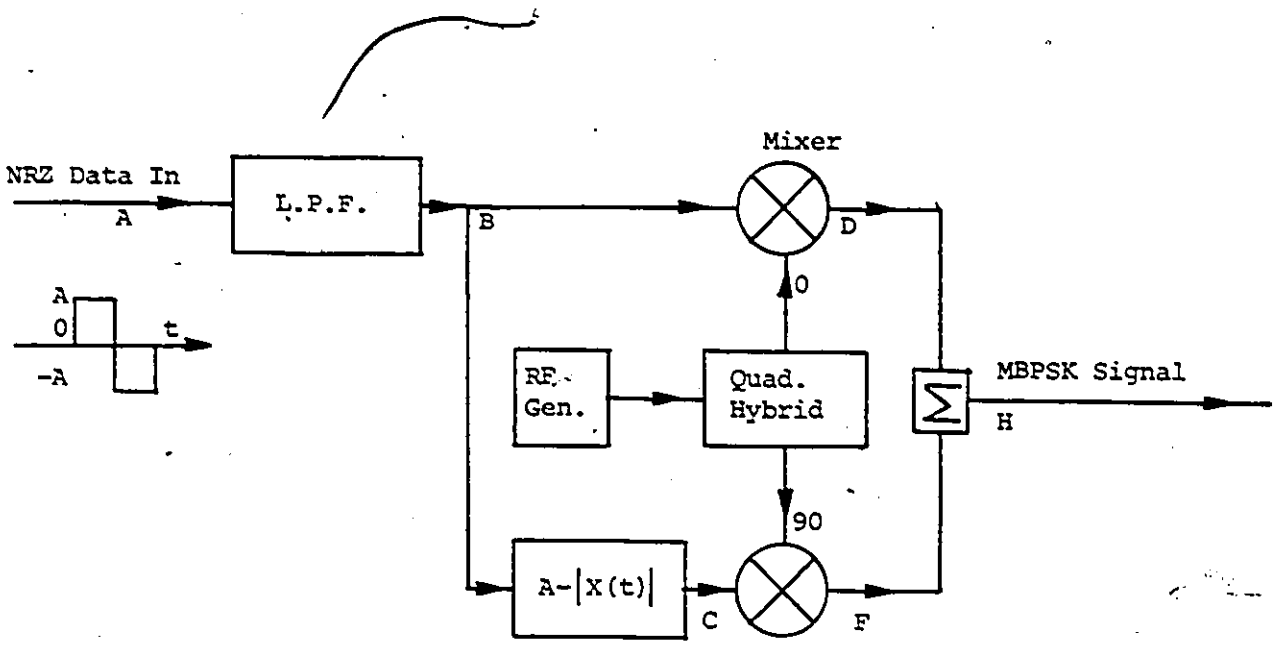

Figure 4.4 Premodulation Filtered Modified BPSK Modulator Block Diagram.

The predicted waveforms at different points of this MBPSK modulator are shown in Figure 4.5. Line a of Figure 4.5 shows the polar input data to the modulator (block diagram of Figure 4.4). Line b is the input signal after filtering, i.e., the x(t) signal. Line c shows the y(t) signal created by a circuit which performs A-|x(t)|. Line d shows the in-phase channel RF amplitude, which has the 180° phase transitions shown in line e. Line f gives the quadrature channel RF signal which has the 90° phase shown in line g. The algebraic sum of lines d and f is shown in line h, which is the output of the RF combiner. Note that a small envelope variation remains, which results from the chord approximation of the desired arc. Note also that the phase transitions shown in line i are now smooth, and resemble the filtered data.

4.4 Spectral Characteristics of the MBPSK Signal

The derivation of the power spectrum density of the modulated signal z(t) is fairly complex, as evidenced by the correlation between the signals x(t) and y(t). In order to have some insight into the shape of the spectrum, the power spectra of the baseband signals x(t) and y(t) are first calculated. From these spectra, the power spectrum of the output signal z(t) can be estimated.

a – The polar input data

b – The filtered input data, x(t)

c – The signal y(t) = A – |x(t)|

d – I-channel RF signal amplitude

e – I-channel RF signal phase

f – Q-channel RF signal amplitude

g – Q-channel RF signal phase

h – Modified BPSK signal amplitude, z(t).

i – Modified BPSK signal phase

j – Modified BPSK signal amplitude after hardlimiting(without changing the phase)

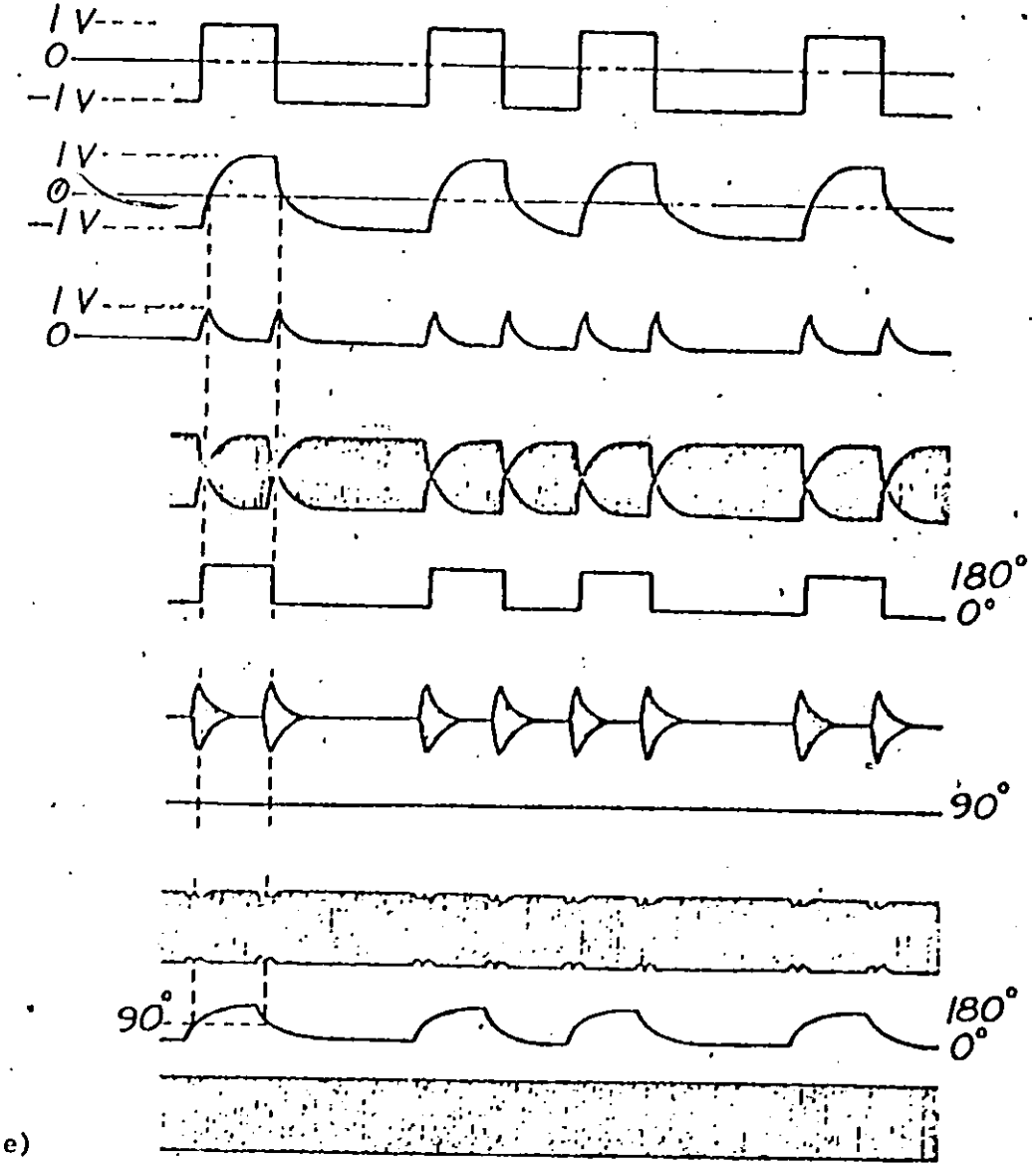

Figure 4.5 Reduced Spectrum BPSK Waveform

The Power Spectral Density of the Baseband Signal x(t)

Assume that the input signal (see Figure 4.4) is random and is described by

$$S(t) = \sum_{n=-\infty}^{+\infty} a_n g(t-nT_s) \qquad \frac{(2n-1)T_s}{2} < t < \frac{(2n+1)T_s}{2} \tag{4.12}$$

where

$$a_n = \begin{cases} +1 \text{ with prob. } 1/2 \\ -1 \text{ with prob. } 1/2 \end{cases}$$

and $g(t)$ is a rectangular pulse of duration T_s.

The power spectrum of this signal is given by [7]

$$S_s(f) = 2f_s|G(f)^2|^2 = \frac{2}{f_s}\left|\frac{A\sin\pi f/f_s}{\pi f/f_s}\right|^2 \tag{4.13}$$

where $S_s(f)$ is the power spectrum of $S(t)$, $G(f)$ is the Fourier transform of $g(t)$, and $f_s = \frac{1}{T_s}$ is the signaling frequency. The power of $x(t)$ is related to $S_s(f)$ by

$$S_x(f) = |H(f)|^2 S_s(f) \tag{4.14}$$

$$S_x(f) = \frac{2}{f_s}|H(f)|^2\left|\frac{A\sin\pi f/f_s}{\pi f/f_s}\right|^2 \tag{4.15}$$

where $H(f)$ is the transfer function of the premodulation low-pass filter.

As (4.15) manifests, $S_x(f)$ has spectral nulls at the signaling frequency and its integral multiples.

B) The Power Spectral Density of the Baseband Signal y(t)

Referring to Figure 4.4, the baseband signal for the Q-channel is given by

$$y(t) = A - |x(t)| \quad |x(t)| \leq A. \tag{4.16}$$

Considering (4.12), the signal x(t) can be expressed as

$$x(t) = \sum_{n=-\infty}^{+\infty} a_n r(t-nT_s) \tag{4.17}$$

where

$$r(t) = g(t)*h(t) \qquad \text{for} \qquad 0 \leq t < T_s \tag{4.18}$$

h(t) is the impulse response of the premodulation low-pass filter, r(t) is the response of this filter to a rectangular pulse shape g(t), and the symbol * denotes convolution. To simplify the calculation, it is assumed that the premodulation filter rounds off the edges of the pulse shape g(t) to a sine shape, i.e.,

$$r(t) = \begin{cases} A \sin \dfrac{\pi t}{2aT_s} & \text{for } 0 < t < aT_s \\ A & \text{for } aT_s < t < (1-a)T_s \\ A \sin \dfrac{\pi(T_s-t)}{2aT_s} & \text{for } (1-a)T_s < t < T_s \end{cases} \tag{4.19}$$

$$(0 < a < 1/2)$$

Then using (4.16), (4.17), and (4.18), y(t) can be represented by

$$y(t) = \sum_{n=-\infty}^{+\infty} y_n(t) \tag{4.20}$$

Where for the interval $(2n-1)T_s/2 < t < (2n+1)T_s/2$

$$y_n(t) = \begin{cases} p(t-nT_s) = A - |r(t-nT_s)| & \text{with prob. } q \\ 0 & \text{with prob. } 1-q \end{cases} \tag{4.21}$$

and

$$p(t) = \begin{cases} 0 & \text{for } -T_s/2 < t < -aT_s \\ A(1+\text{Sin } \frac{\pi t}{2aT_s}) & \text{for } -aT_s < t < 0 \\ A(1-\text{Sin } \frac{\pi t}{2aT_s}) & \text{for } 0 < t < aT_s \\ 0 & \text{for } aT_s < t < T_s/2 \end{cases} \tag{4.22}$$

An example of the signal y(t) is shown in Figure 4.6.

The power spectrum of y(t) can be written as [7]

$$S_Y(f) = 2f_s q(1-q)|P(f)|^2 + q^2 f_s^2 [P(0)]^2 \delta(f) + 2q^2 f_s^2 \sum_{m=1}^{\infty} |P(mf_s)|^2 \delta(f-mf_s) \tag{4.23}$$

where P(f) is the Fourier transform of p(t) and is given by

$$P(f) = \int_{-\infty}^{+\infty} p(t) e^{-j2\pi ft} dt = \int_{-aT_s}^{0} A(1+\text{Sin } \frac{\pi t}{2aT_s}) e^{-j2\pi ft} dt$$

$$+ \int_{0}^{aT_s} A(1-\text{Sin } \frac{\pi t}{2aT_s}) e^{-j2\pi ft} dt = \frac{A \frac{\pi f_s}{2a}}{(\frac{\pi f_s}{2a})^2 - (2\pi f)^2}$$

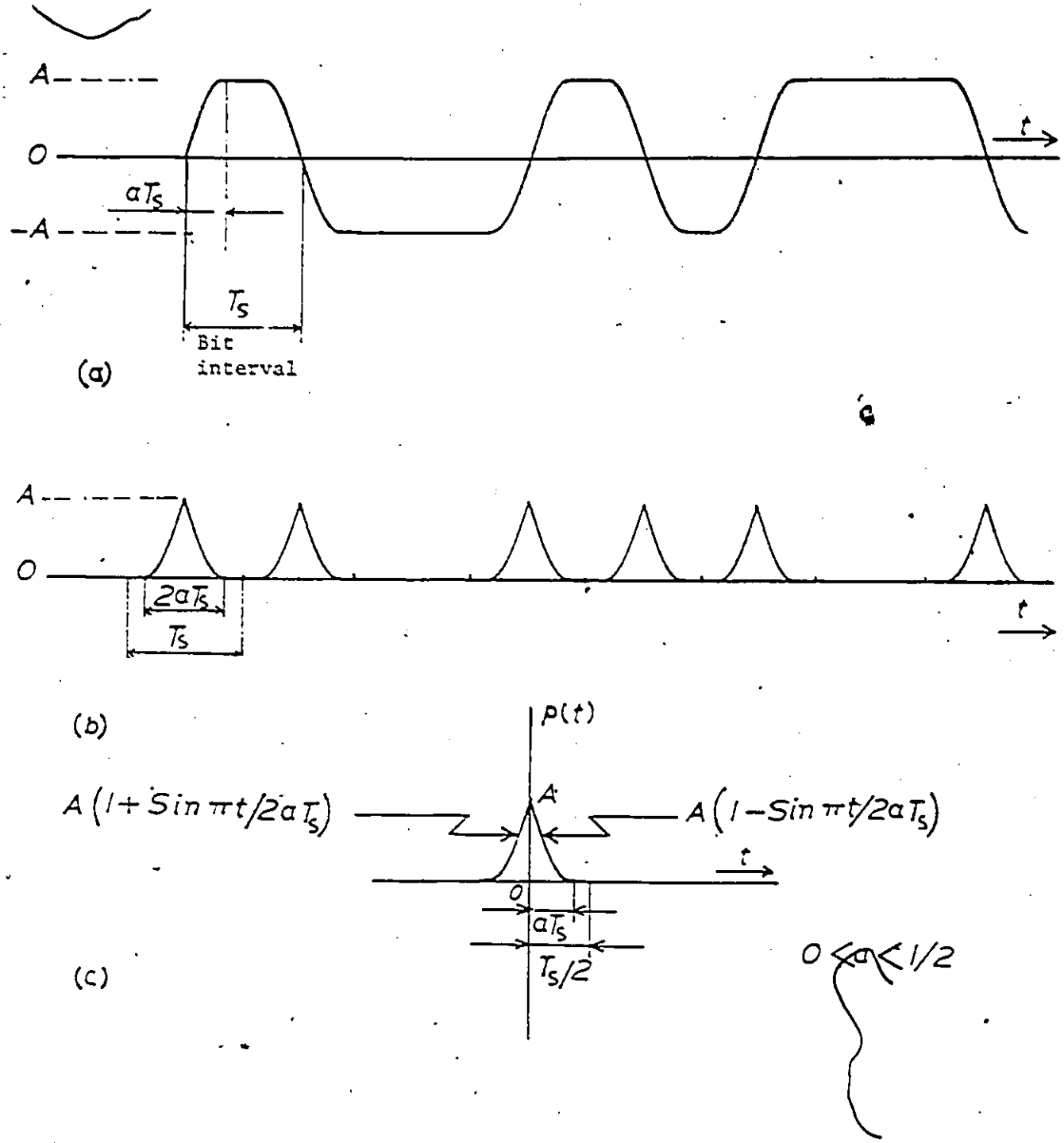

Figure 4.6 An Example of Baseband Signals, X(t) and Y(t)
a) X(t) Signal
b) Y(t) Signal
c) A single Pulse Shape of the Baseband Signal Y(t)

$$\cdot \left[\pi \frac{\operatorname{Sin}\frac{2a\pi f}{f_s}}{\frac{2a\pi f}{f_s}} - 2\right] \qquad (4.24)$$

Substituting (4.24) into (4.23) gives the power spectrum of the signal y(t) at point c in Figure 4.4.

$$S_y(f) = \{2f_s q(1-q)\left[\frac{A\frac{\pi f_s}{2a}}{(\frac{\pi f_s}{2a})^2 - (2\pi f)^2}\right]^2 \cdot \left|\pi \frac{\operatorname{Sin}\frac{2a\pi f}{f_s}}{\frac{2a\pi f}{f_s}} - 2\right|^2\}$$

$$+ \{q^2(2aA\,\frac{\pi-2}{\pi})^2\delta(f) + 8q^2(\frac{aA}{\pi})^2 \cdot \sum_{m=1}^{\infty}\left[\frac{1}{1+(4am)^2}\right]^2$$

$$\cdot \left|\frac{\operatorname{Sin}2a\pi m}{2a\pi m} - 2\right|^2 \delta(f-mf_s)\} \qquad (4.25)$$

The first bracket in (4.25) indicates the continuous part of the spectrum, while the second bracket gives the discrete part, which consists of spectral lines at zero and integral multiples of the signalling frequency. A plot of (4.25) is given in Figure 4.7.

C) The Power Spectra of the MBPSK Signal

The MBPSK signal was given by:

$$z(t) = \underset{\left(\begin{smallmatrix}\text{I-channel RF}\\ \text{signal}\end{smallmatrix}\right)}{x(t)\ \operatorname{Cos}2\pi f_c t} + \underset{\left(\begin{smallmatrix}\text{Q-channel RF}\\ \text{signal}\end{smallmatrix}\right)}{y(t)\cdot \operatorname{Sin}2\pi f_c t}$$

The power spectra of the signal z(t) can be expressed by

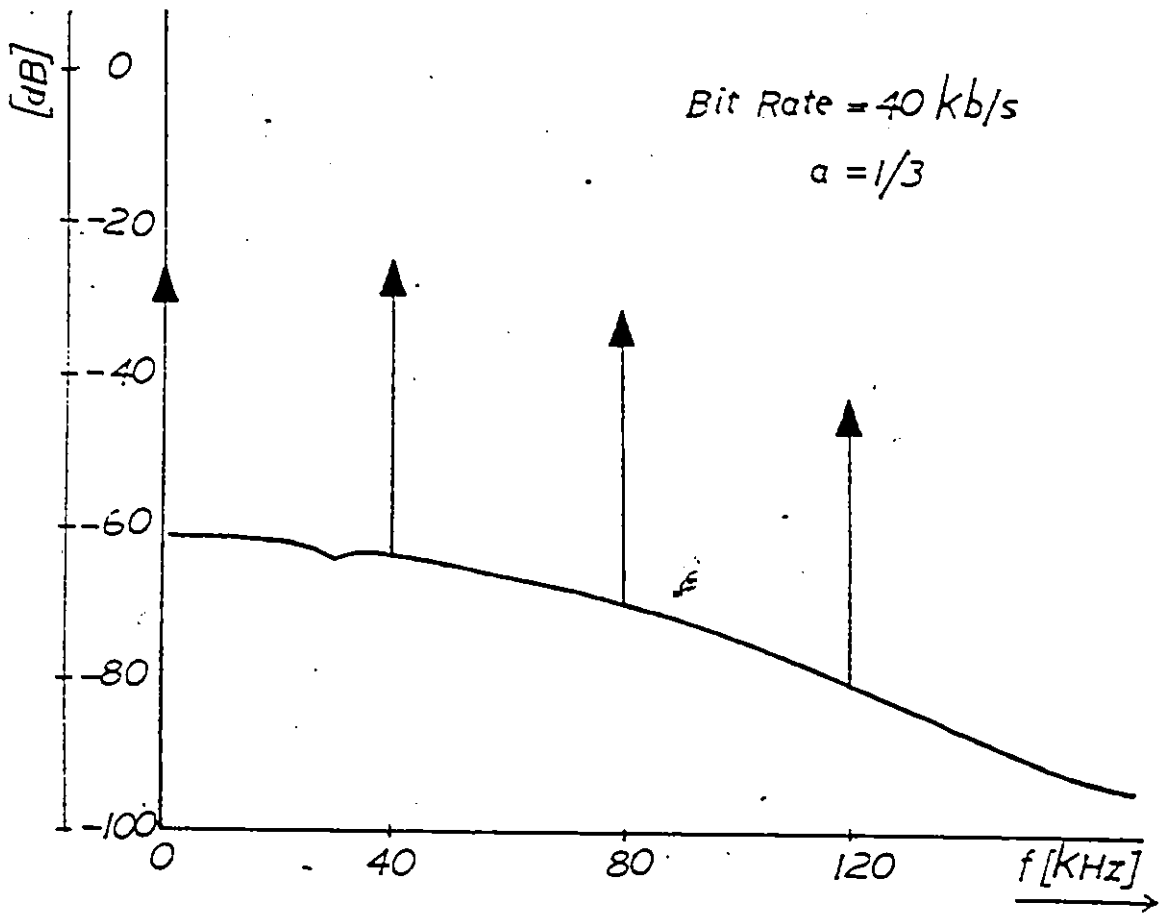

Figure 4.7 The Computed Power Spectrum of the Y(t) Signal

$$S_z(f) = S_x(f+f_c) + S_y(f+f_c) + \begin{matrix}\text{cross power spectra} \\ \text{of I and Q channels}\end{matrix} \quad (4.26)$$

The first term in (4.26) denotes the useful energy which contains the information, and the last two terms indicate the energy required (much less than $S_x(f+f_c)$ because of the low power contribution of the Q-channel) for smoothing the 180^o phase transitions of the I-channel RF signal.

The overall shape of the output power spectra $S_z(t)$ is much the same as the shape of $S_x(f+f_c)$, which is modified by $S_y(f+f_c)$ and the cross power spectra of the I and Q channels. One drawback of this modification is that the resultant power spectra $S_z(f)$, in addition to having a continuous part, also contains discrete spectral lines at f_c and $f_c + mf_s$ ($m = \pm 1, 2, \ldots$).

The spectral line at the carrier frequency f_c is due to the DC component of the y(t) signal. As indicated in (4.16), the y(t) signal can have only positive values during any transition of the x(t) signal; hence, it has a positive DC average component. The DC component can be removed by letting the y(t) signal alternate between positive and negative values during the transitions of the x(t) signal from positive to negative, and vice-versa, i.e.,

$$y(t) = \begin{cases} [A-|x(t)|] & \text{in the transition region when } x(t) \text{ changes from positive to negative polarity} \\ 0 & \text{If there is no transition in } x(t) \\ -[A-|x(t)|] & \text{in the transition region when } x(t) \text{ changes from negative to positive polarity} \end{cases} \quad (4.27)$$

In this case, the DC component of the signal y(t) would be zero, and therefore no discrete line would appear at the zero frequency in $S_y(f)$, as well as at the carrier frequency f_c in $S_z(f)$. However, in this case, as indicated in (4.27), the y(t) signal is a three-level signal, and therefore its power spectum has a null at the zero frequency that will slightly change the shape of the composite power spectum $S_z(f)$.

The spectral lines at $f_c + mf_s (m = 1, 2, \ldots)$ in $S_z(f)$, after polarity alternation of the y(t) signal, are still present. The out-of-band spectral lines could be suppressed simply by passing the signal Z(t) through an appropriate band-pass filter. The spike at $f_c + f_s$ might be useful in linear processing of the received signal at the receiver, to extract timing signals [31].

CHAPTER FIVE

AN EXPERIMENTAL MODIFIED BPSK SYSTEM

5.1 Introduction

This chapter presents the design and evaluation of an experimental MBPSK/BPSK system. Following the circuit description of the experimental system, the measurement techniques used are briefly described. The evaluation starts with the spectral characteristics of the experimental modulator. Then the measured power spectral densities of conventional BPSK and MBPSK signals, after being passed through a nonlinear element (hardlimiter), are presented and compared.

The probability of error performance of the MBPSK system in an additive White-Gaussian Noise environment is measured. Performance is first evaluated in a linear channel, and then where the channel is nonlinear (hardlimited channel). In both cases the measured results will be compared with those of conventional BPSK systems.

5.2 The MBPSK/BPSK Modulator

The block diagram of an experimental MBPSK modulator, which is designed to transmit 40 Kb/s of binary data, using a 920 kHz RF carrier frequency, is shown in Figure 5.1.

The input unipolar NRZ to polar NRZ converter (UP/P CONV), which also act as a buffer amplifier, was realized by using an

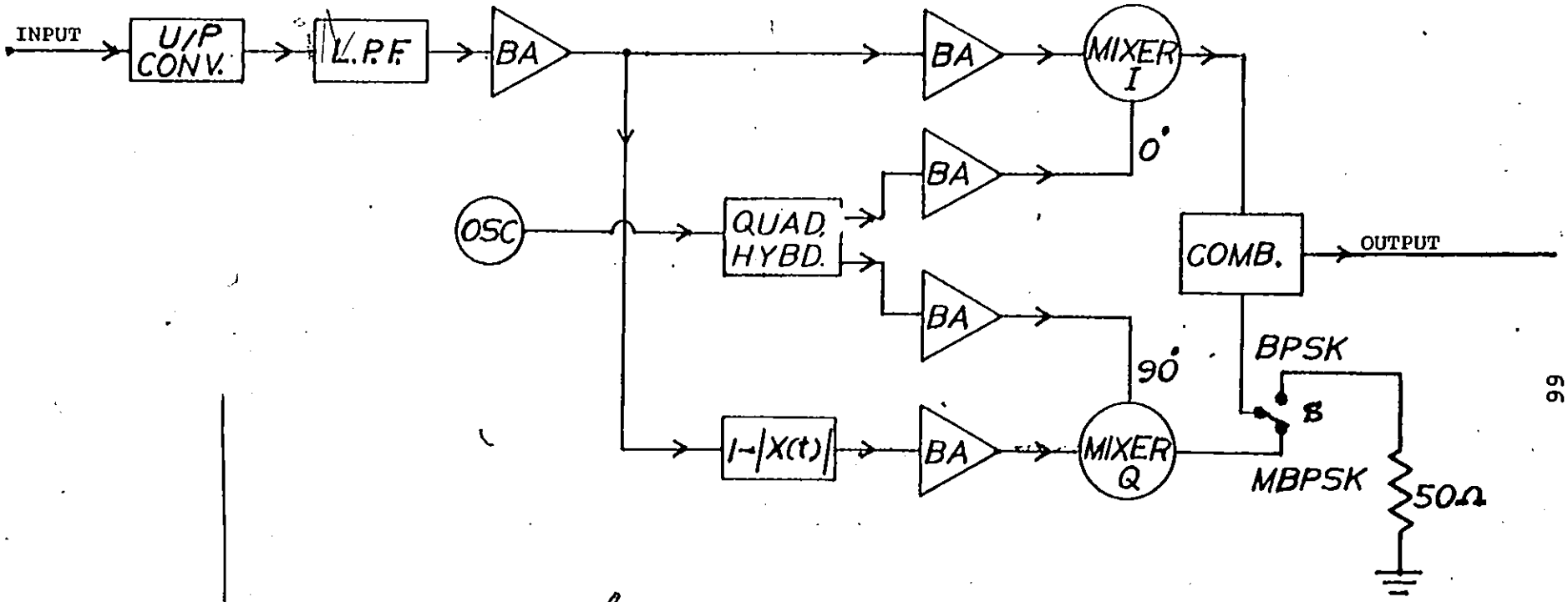

Figure 5.1 Block Diagram of an Experimental MBPSK Modulator

operational amplifier with a variable negative voltage input. The circuit diagram is shown in Figure 5.2.

The signal from the UP/P CONV. is fed to a low-pass filter which provides spectrum shaping (reduction) by slowing down the data transitions. A three-pole Butterworth passive low-pass filter having a corner frequency (3 dB point) of 30 kHz was designed. The circuit diagram of the low-pass filter followed by a buffer amplifier (B.A.), along with its frequency response, is shown in Figure 5.3.

The output of the low-pass filter buffer, x(t), is directed along two paths; one for the modulation of the in-phase RF carrier, and the other to provide the auxiliary signal y(t) for the modulation of the quadrature RF carrier.

The auxiliary signal $y(t) = A - |x(t)|$ is easily generated by means of the circuit diagram of Figure 5.4. In this circuit, transistors T_1 and T_2 (which are selected to be as closely matched as possible) form a so-called current mirror. That is, the collector current of transistor T_2 is equal to the base current of transistor T_1, which in turn is proportional to the filtered data input voltage, x(t). When the filtered data input signal is at a maximum positive amplitude, that is +A volts, the collector voltage of transistor T_2 will be approximately zero volts. The output voltage, y(t), therefore is approximately zero (transistor T_3 acts as an emitter follower). When the filtered data input signal is zero volts, the collector current in transistor T_2 will be zero; hence

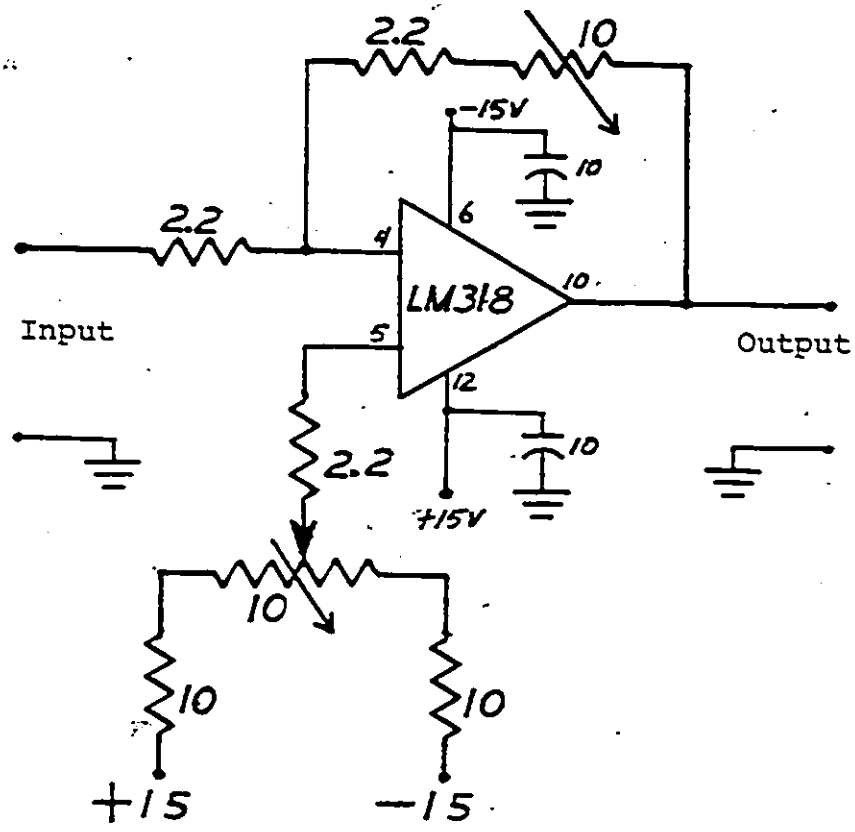

Figure 5.2 Input Buffer and Unipolar to Polar NRZ Converter

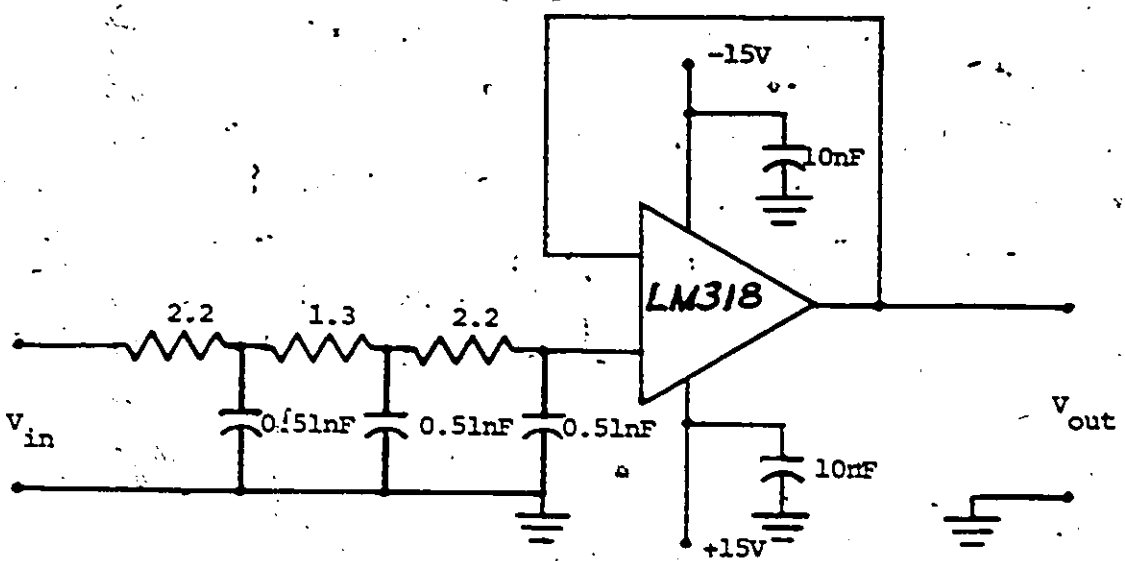

(a)

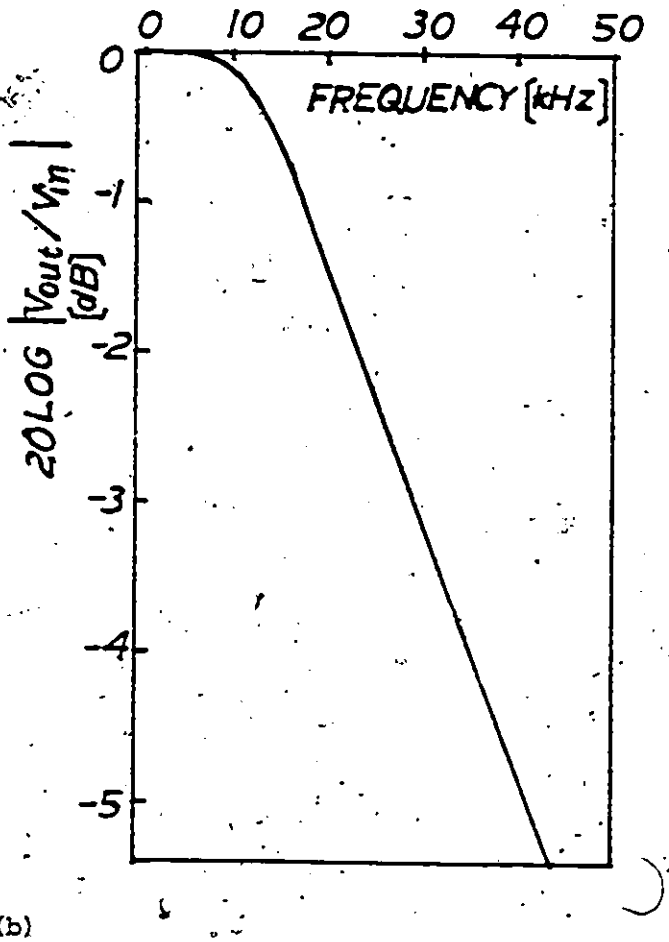

(b)

Figure 5.3 a) Schematic Diagram of a Three-pole Butterworth Passive Low-Pass Filter followed by a Buffer Stage
b) The Frequency Response of the Filter

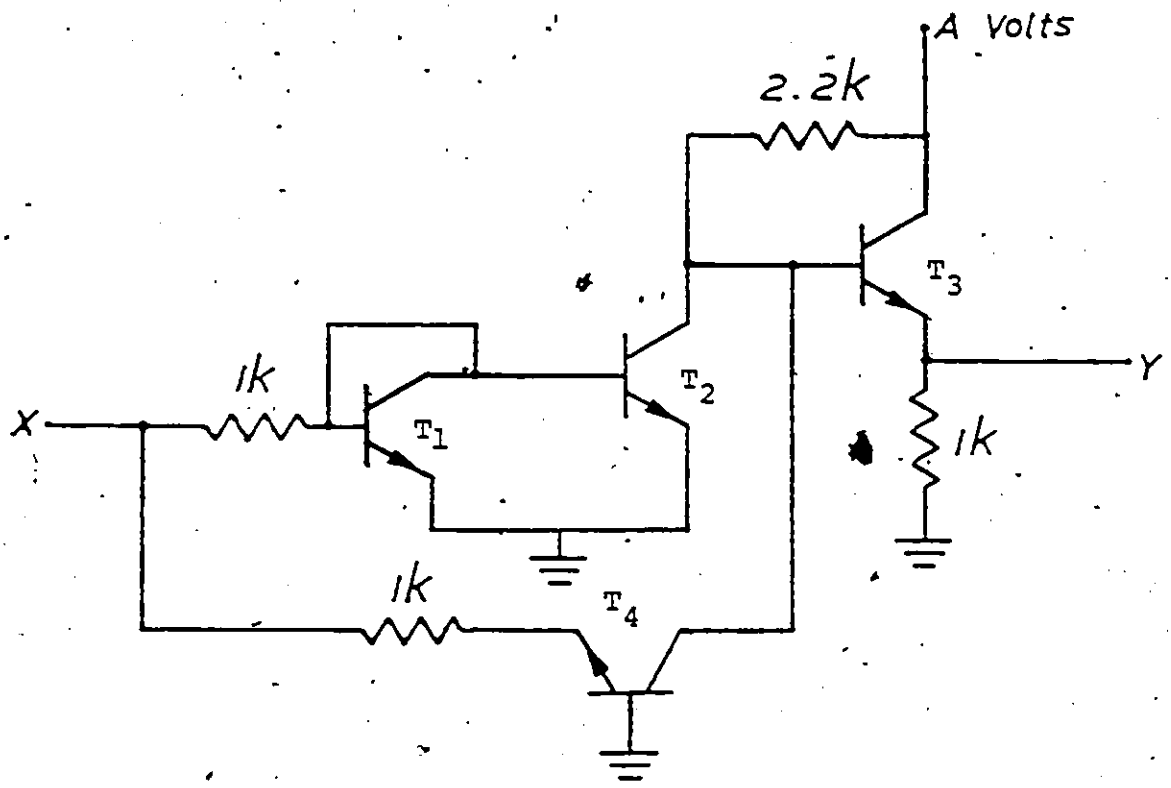

Figure 5.4 A Circuit which performs the Function Y(t)= A- X(t)

its collector voltage will be approximately +A volts. When the amplitude of x(t) signal goes from zero to +A volts, the output voltage y(t) at the emitter of transistor T_3 will vary linearly with the input voltage x(t), but inverted in sense and referenced to the +A volts source. For negative input voltages the transistor T_1 and T_2 will be in the cut-off mode and transistor T_4 will control the output voltage y(t). When the input signal amplitude is at -A volts, transistor T_4 will be in saturation mode, causing transistor T_3 to go to the cut-off mode, which corresponds to zero output voltage. When the amplitude of the input signal is zero volts, transistors T_1, T_2 and T_4 will all be in the cut-off mode and the output voltage will be at its maximum value of +A volts.

As an RF generator, an ordinary sine wave generator (HP 3312 A) was used. The quadrature hybrid circuit used is shown in Figure 5.5. The outputs of the quadrature hydrid are taken at the points marked V_1 and V_2. The phases of these two signals differ by 90° (at the carrier frequency of 920 kHz). The outputs are applied to two double-balanced mixers (Mini Circuits SRA-1) via buffers which also act as current drivers.

The two modulated outputs are added using a 2-way 0° power combiner (Mini Circuits MCL PSC2-1), resulting in a modified BPSK (MBPSK) signal.

The complete circuit diagram and also the measured waveforms at the different points of the MBPSK modulator are given in Figure 5.6 and Figure 5.7 respectively. Note that the mode

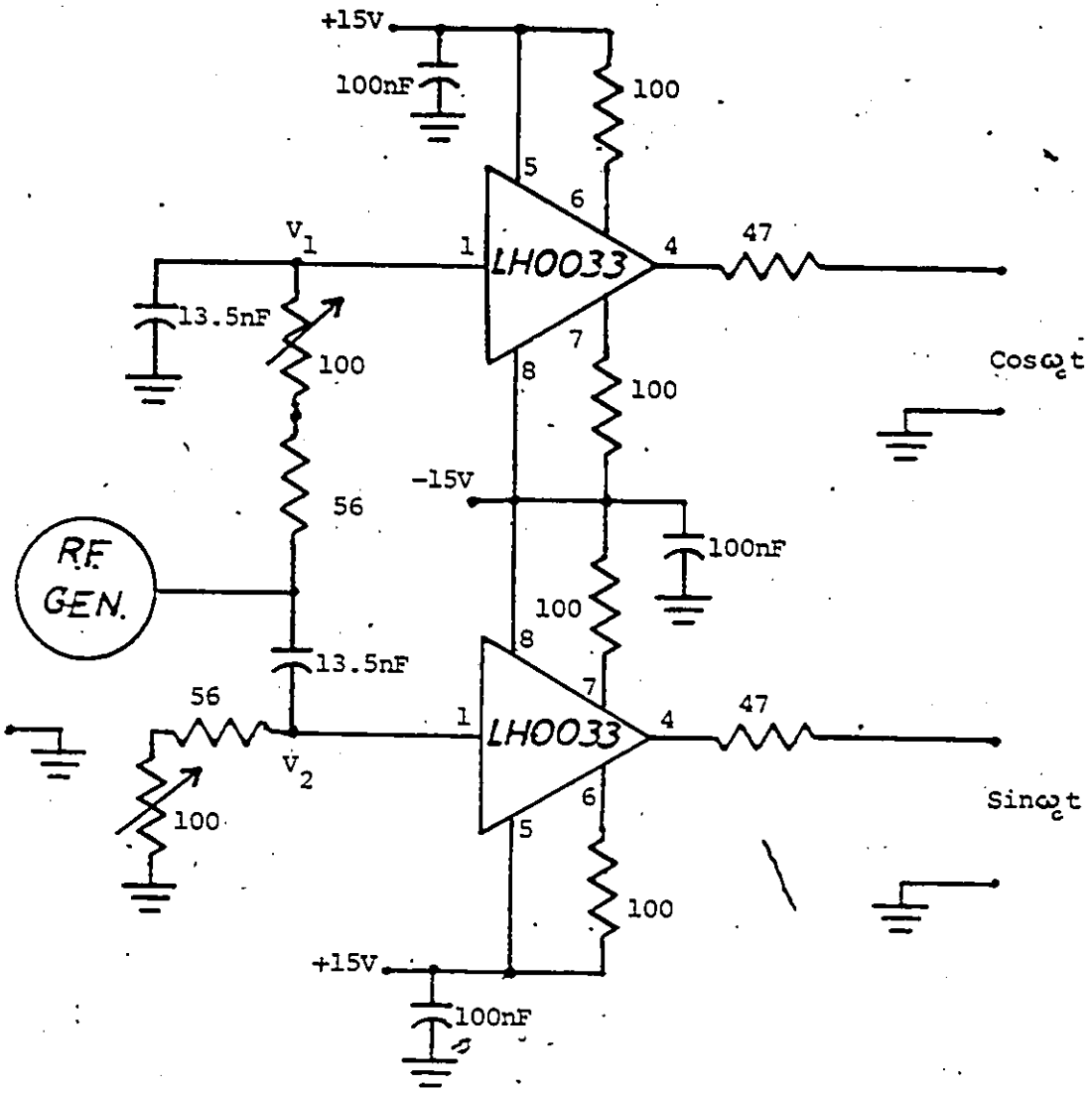

Resistors in Ohm

Figure 5.5 Schematic Diagram of the Quadrature Hybrid followed by Current Drivers

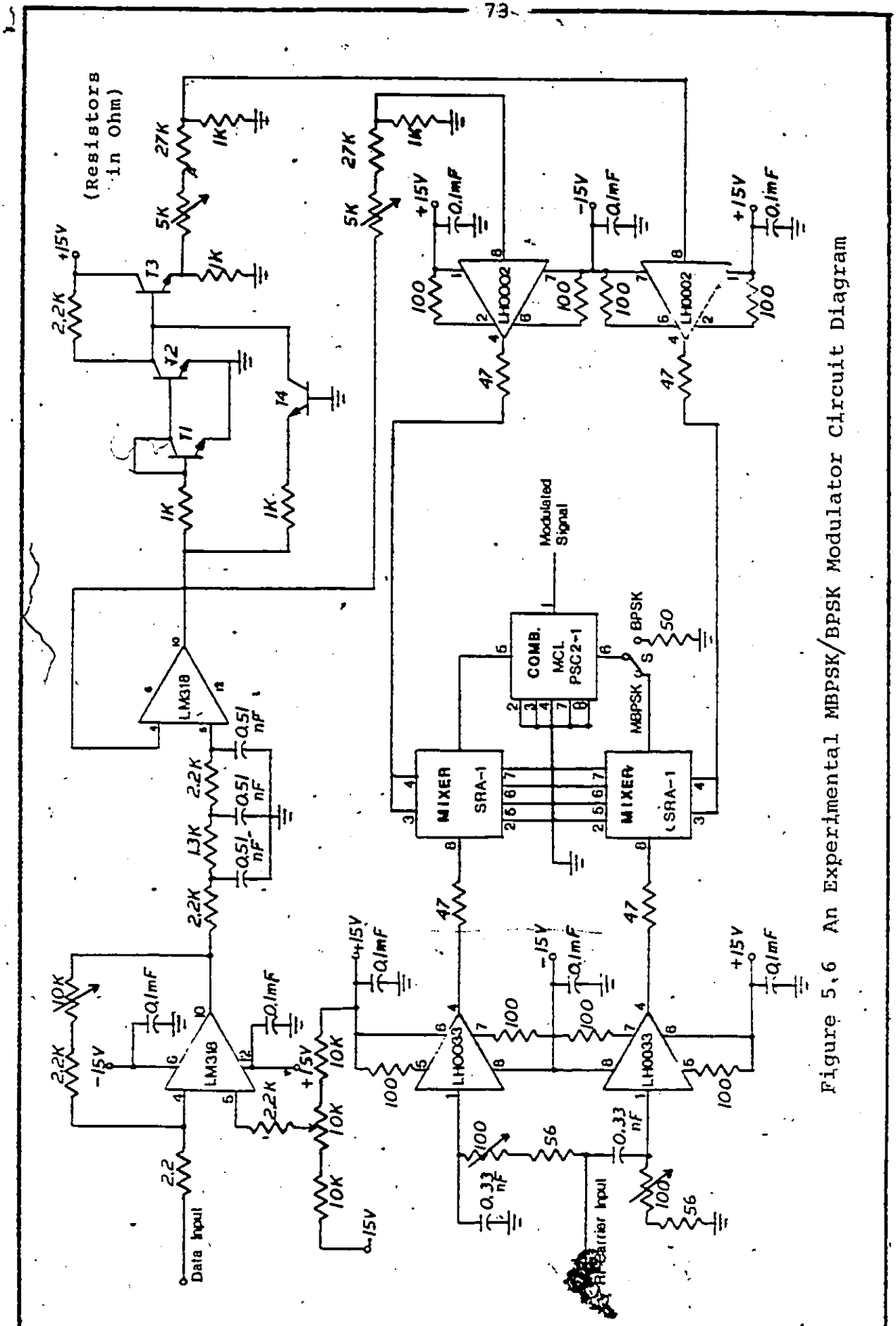

Figure 5.6 An Experimental MBPSK/BPSK Modulator Circuit Diagram

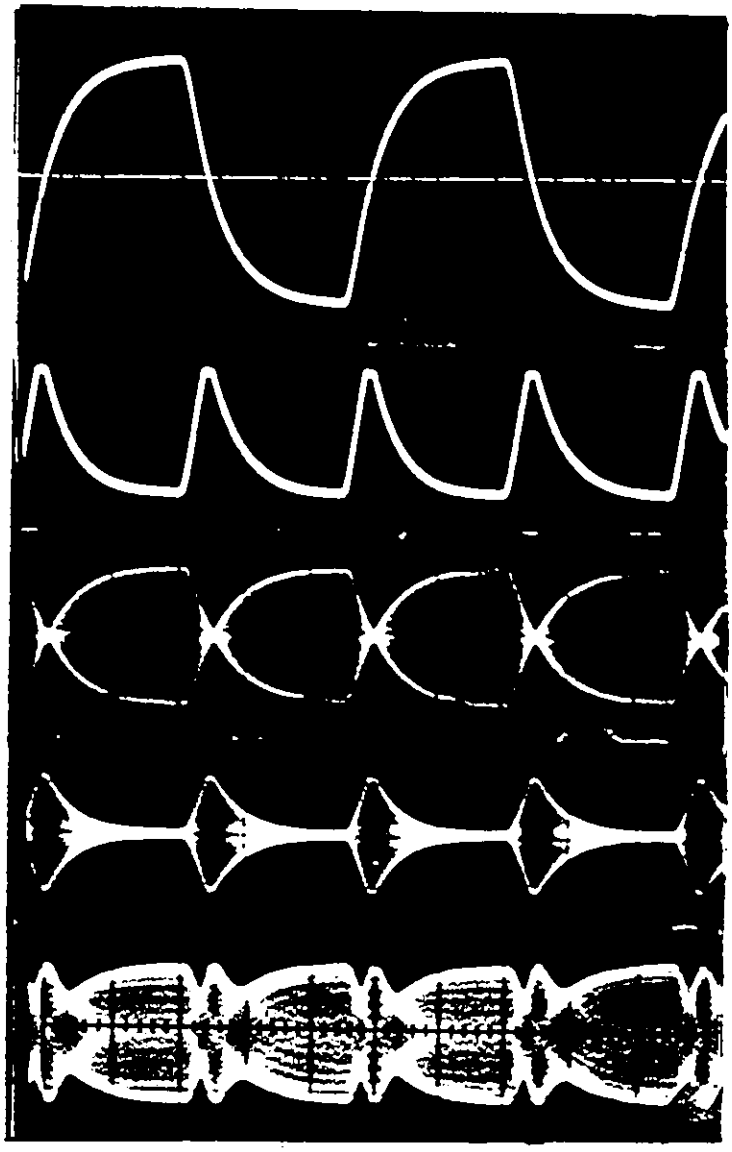

Filtered Binary input signal, x(t)

Quadrature channel input signal A - |x(t)|

Modulated Binary channel

Modulated Quad. channel

Modified BPSK signal

Figure 5.7 Measured Waveforms at Different Points of the Modified BPSK Modulator

select switch S in Figure 5.6, is provided to allow the change from MBPSK to conventional BPSK modulation.

5.3 The Demodulator

The MBPSK signal can be demodulated with a conventional BPSK demodulator. The block diagram of the experimental BPSK demodulator is shown in Figure 5.8.

The received signal is applied to a bandpass filter preceded by an RF amplifier. An active bandpass filter having a 3 dB bandwidth of 80 kHz (BT=2, where B is the bandwidth and T is the bit duration) was designed. The BT=2 introduced only negligible intersymbol interference and it was chosen because the main purpose of the demodulator design was to compare the P_e performance of the MBPSK system with that of a conventional BPSK system under ideal conditions of an only-AWGN environment. The circuit diagram of the bandpass filter along with its frequency response is shown in Figure 5.9.

The output of the bandpass filter is fed to a double balanced mixer (WJ-M1C) via a buffer acting also as a current driver. The other input of the mixer is fed with a coherent carrier signal. For test purposes in the laboratory the carrier was taken ("hardwired") from the in-phase carrier of the modulator. This avoids the trouble of carrier recovery and synchronization.

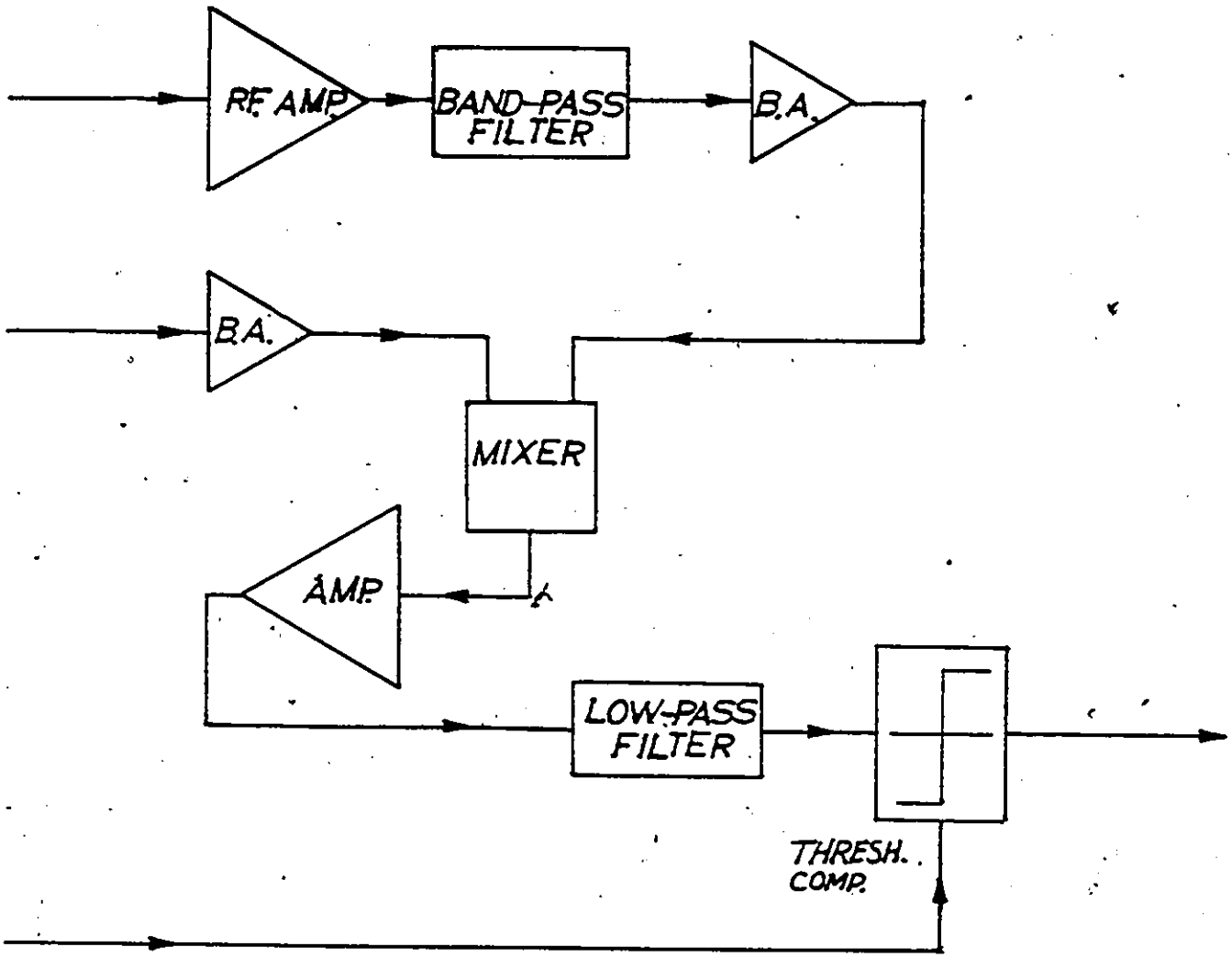

Figure 5.8 Block Diagram of the Experimental BPSK Demodulator

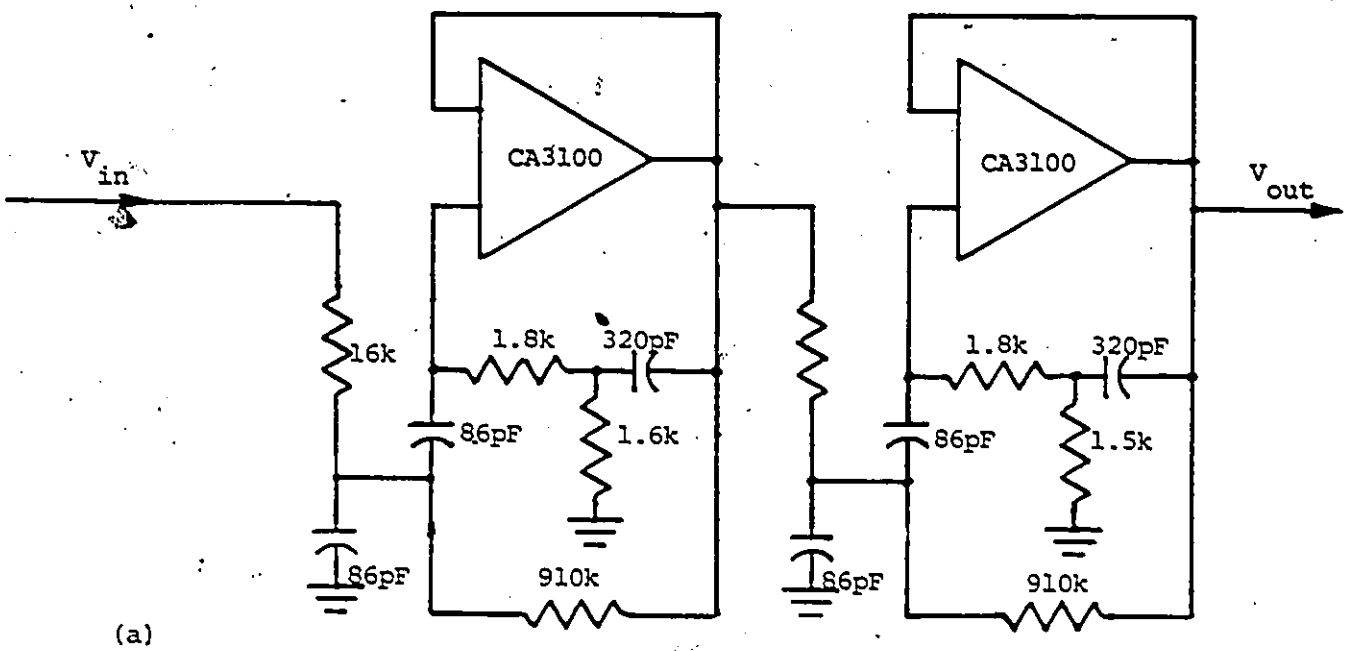

(a)

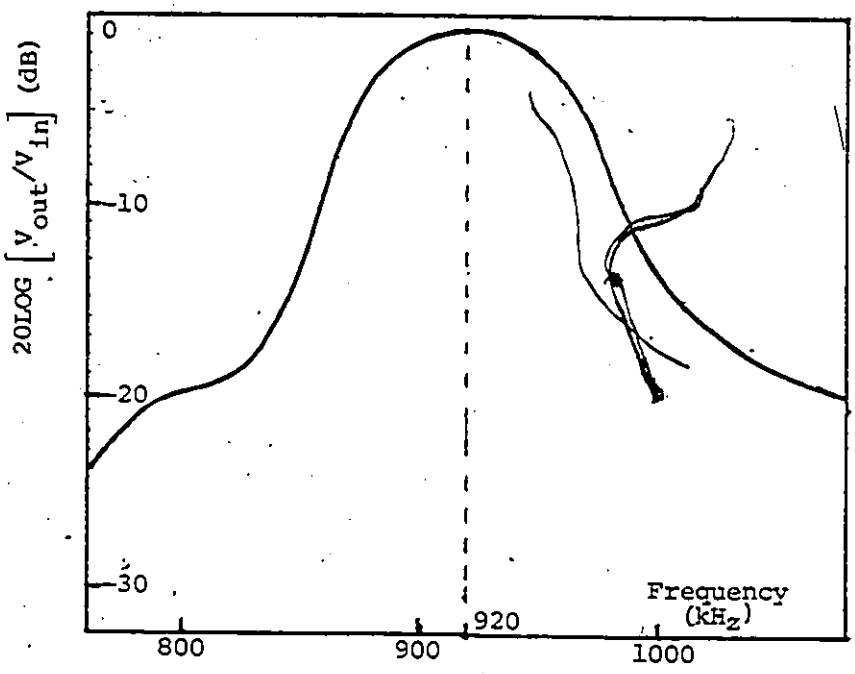

(b)

Figure 5.9 a) Demodulator Band-Pass Filter Circuit Diagram
b) The Frequency Response of the Filter

The output of the mixer is then passed through a low-pass filter preceded by an amplifier. A fourth-order Butterworth active low-pass filter having a 3 dB bandwidth of 40 kHz (twice the required minimum Nyquist bandwidth) is used to recover the raw data. This bandwidth was chosen to ensure freedom from the excessive intersymbol-interference, with a simple unequalized filter. The circuit diagram and also the frequency characteristic of this filter are shown in Figure 5.10. At the output of this filter a bandlimited approximation of the original (transmitted) data is obtained. To clean the bandlimited data and reconstitute the distortion-free binary data, the signal is then passed through a threshold comparator which is sampled at the data rate. Since no sampling clock recovery circuitry was used in the demodulator, the sampling clock (with an adjustable delay) was taken from the modulator, that is a hard wire clocking approach was used. The circuit diagram of the threshold comparator and the complete circuit diagram of the demodulator are given in Figure 5.11 and Figure 5.12 respectively.

5.4 Measurement and Test Results

This section describes the measurement techniques used in evaluating the MBPSK system. The test set-ups are described and the measured results are presented and discussed.

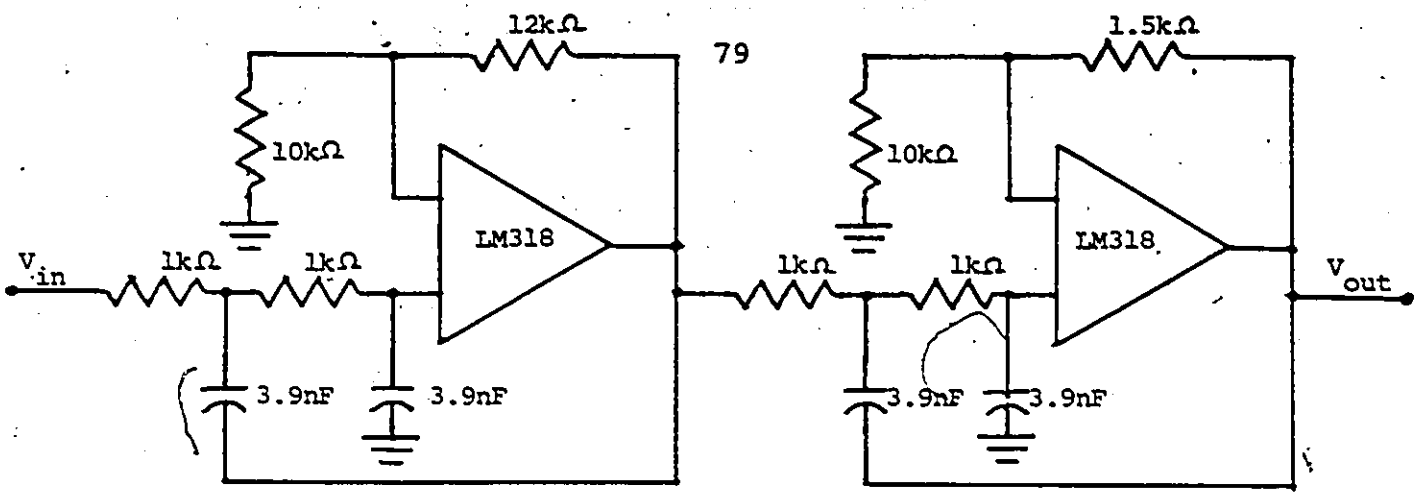

(a)

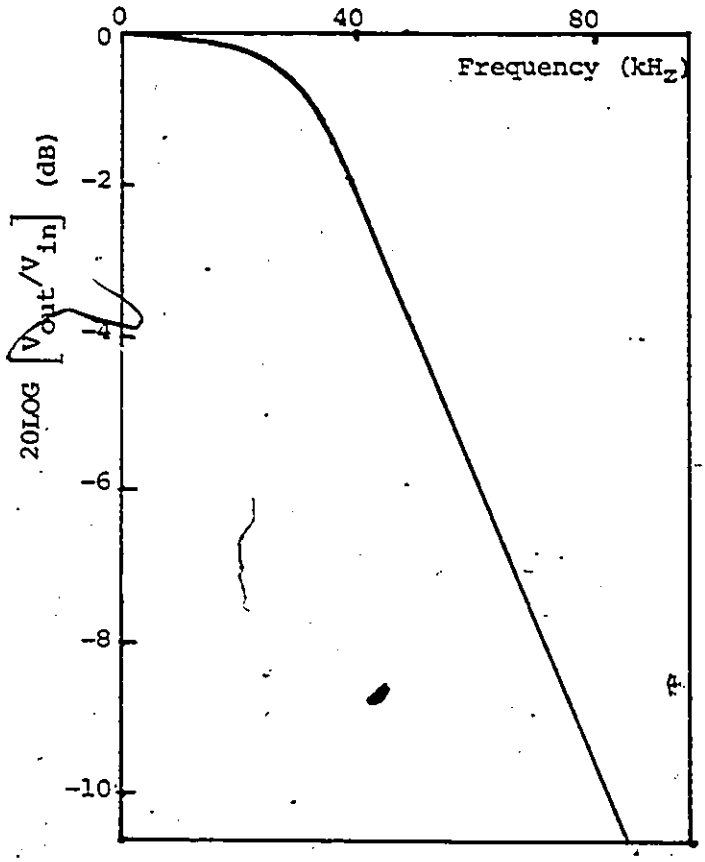

(b)

Figure 5.10 a) Demodulator Low-Pass Filter Circuit Diagram
b) The Frequency Response of the Filter

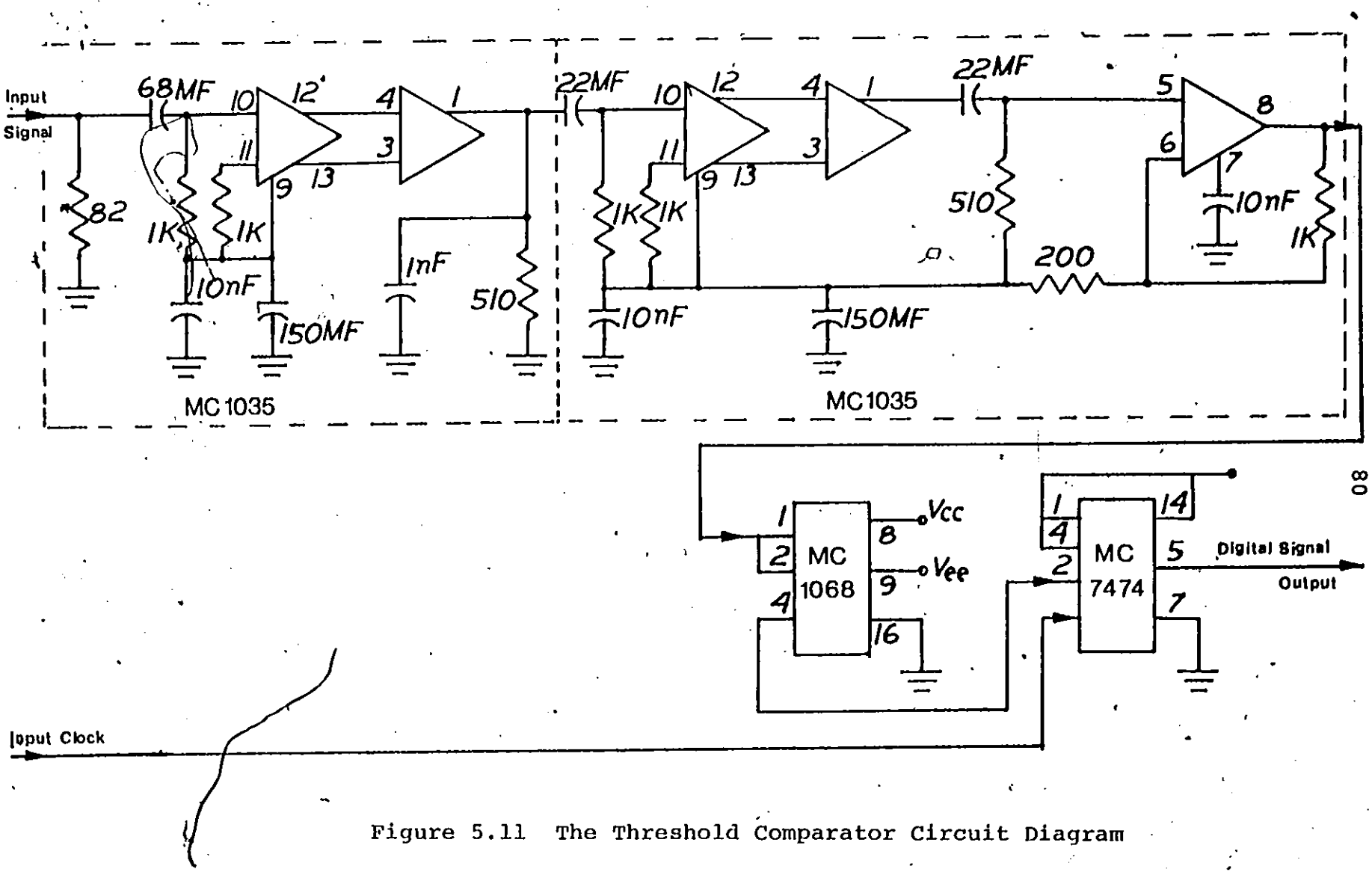

Figure 5.11 The Threshold Comparator Circuit Diagram

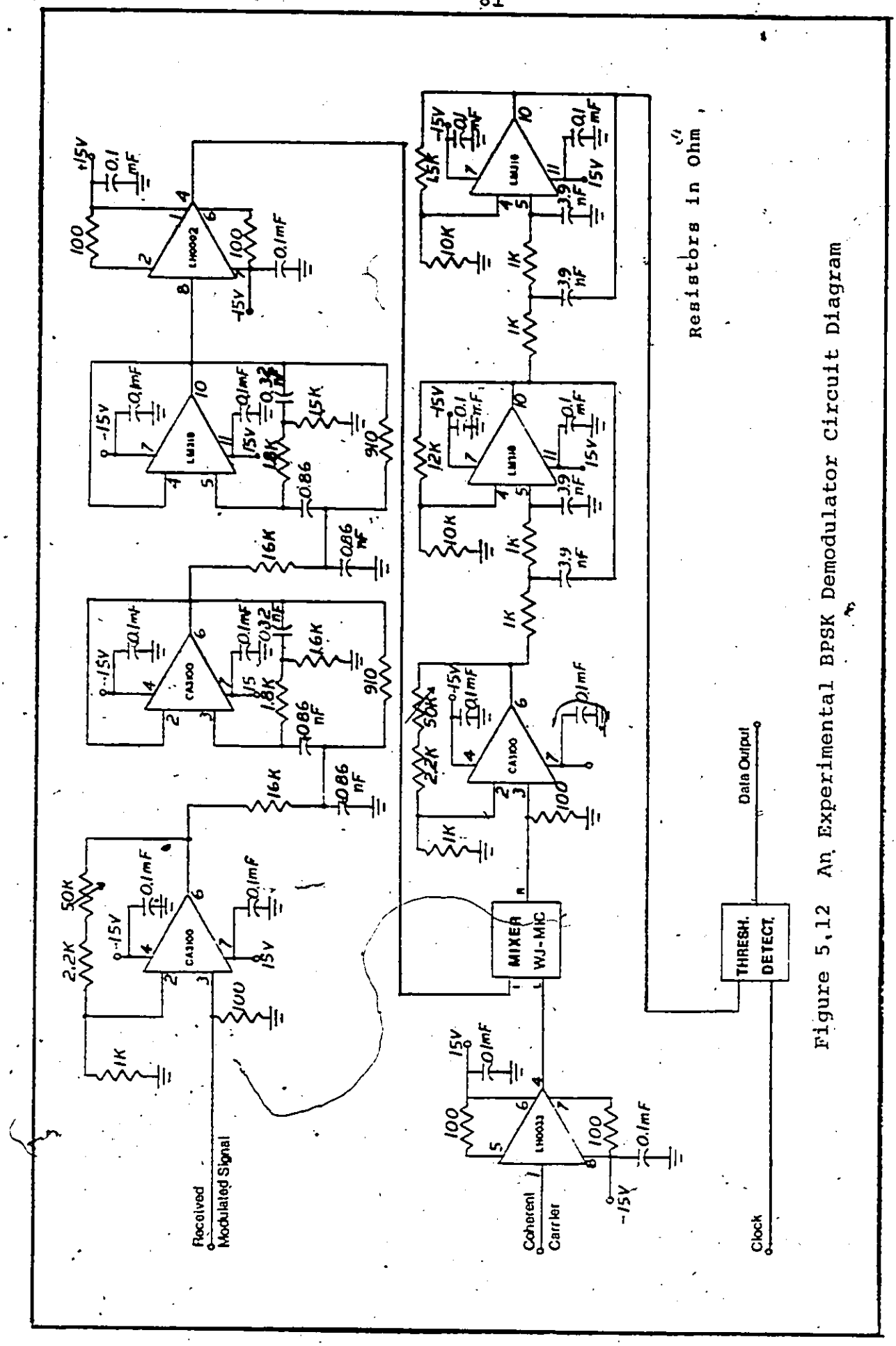

Figure 5.12 An Experimental BPSK Demodulator Circuit Diagram

5.4.1 Spectral Characteristics

To evaluate the spectral characteristic, which is one of the most important features of the MBPSK modulator, a laboratory set-up as shown in Figure 5.13 was arranged. The HP 3310 A function generator, set at 40 kHz, was used to clock the Hewlett Packard HP 3760 A pseudo-random binary sequence (PRBS) generator. The latter provides a 40 kb/s NRZ data input to the modulator. Another HP 3310 A function generator provides the 920 kHz sinusoidal RF input signal to the modulator. To measure the power spectral density, a Hewlett-Packard spectrum analyzer with a HP 141 T display unit and a HP 8553 B RF-section plug-in unit were used. An x-y plotter was used to record the spectra.

Figure 5.14 shows the measured power spectra of the x(t) and y(t) signals. The shapes of the computed and measured power spectra of the y(t) signal, as shown in Figures 4.7 and 5.14(a), respectively, are in a good agreement. The relative heights of the measured spectral lines are 30 dB lower than those of the computed ones. This is because the spectrum analyzer was set to a 1 kHz IF bandwidth; thus the displayed continuous spectral power was 10 log 1000 = 30 dB higher than the computed (1 Hz bandwidth) continuous density.

Figure 5.15 represents the measured bandlimited spectra of the MBPSK signal (Composite Signal $S_z(f)$), with that of the conventional BPSK also shown for comparison.

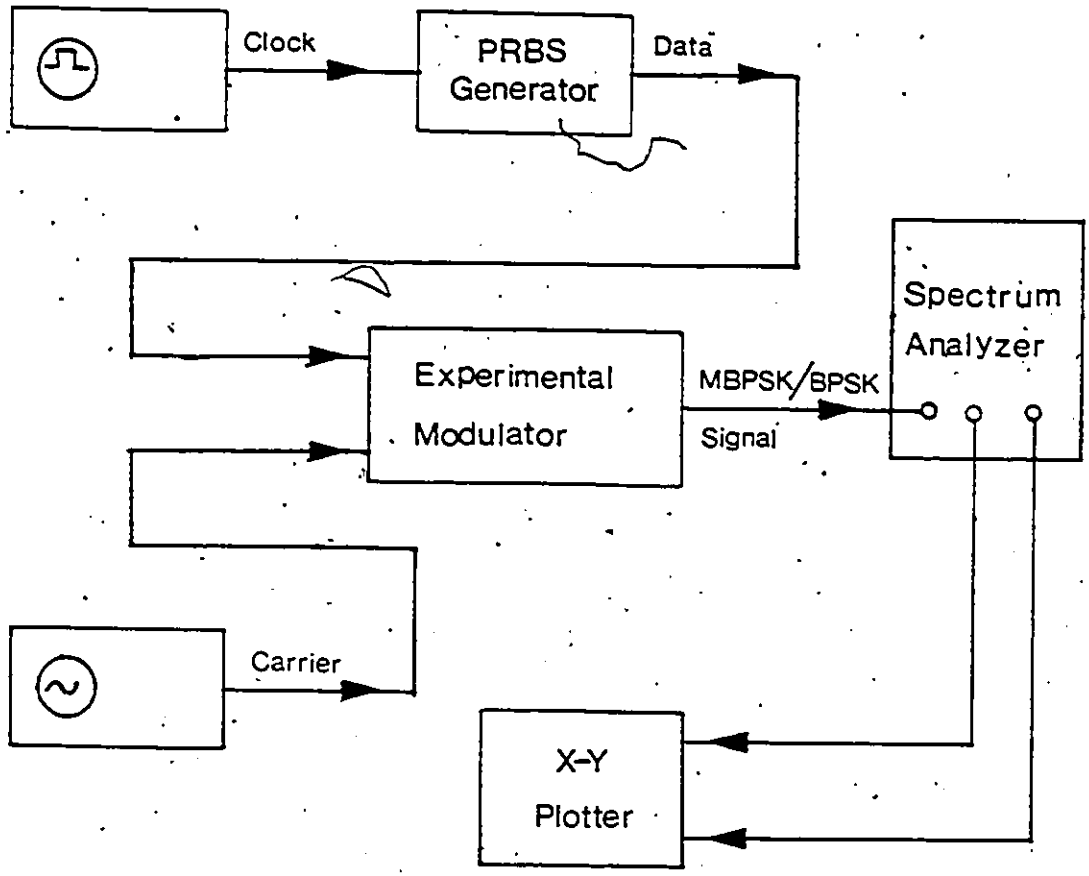

Figure 5.13 Laboratory set-up for measurement of the Power Spectrum Density

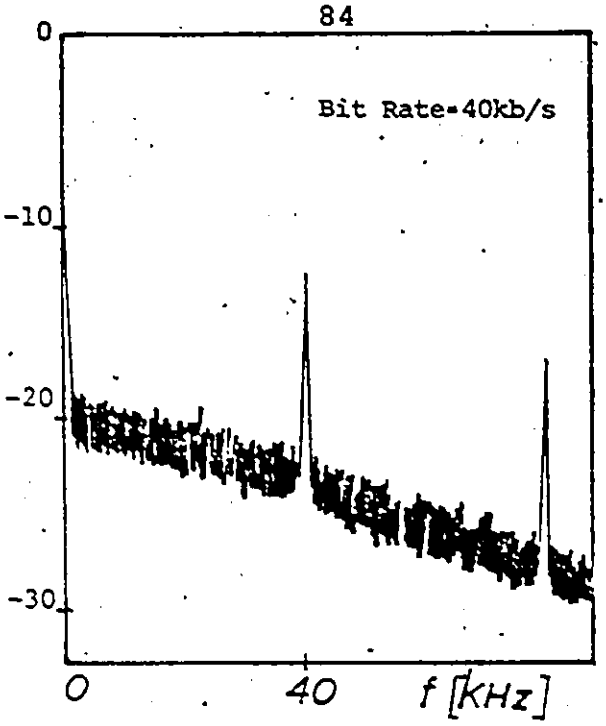

(a)

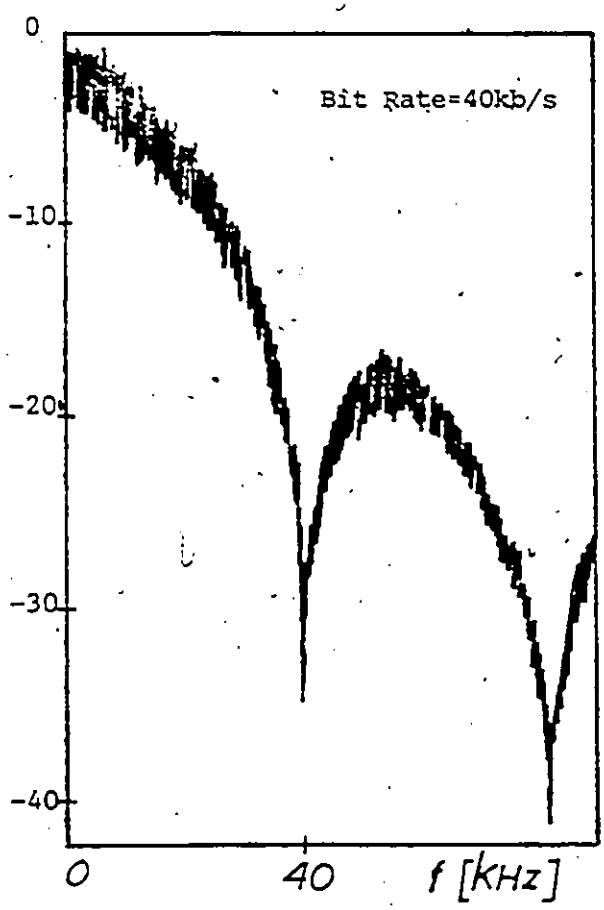

(b)

Figure 5.14 The Measured Power Spectrum of :
a) The Y(t) Signal
b) The X(t) Signal

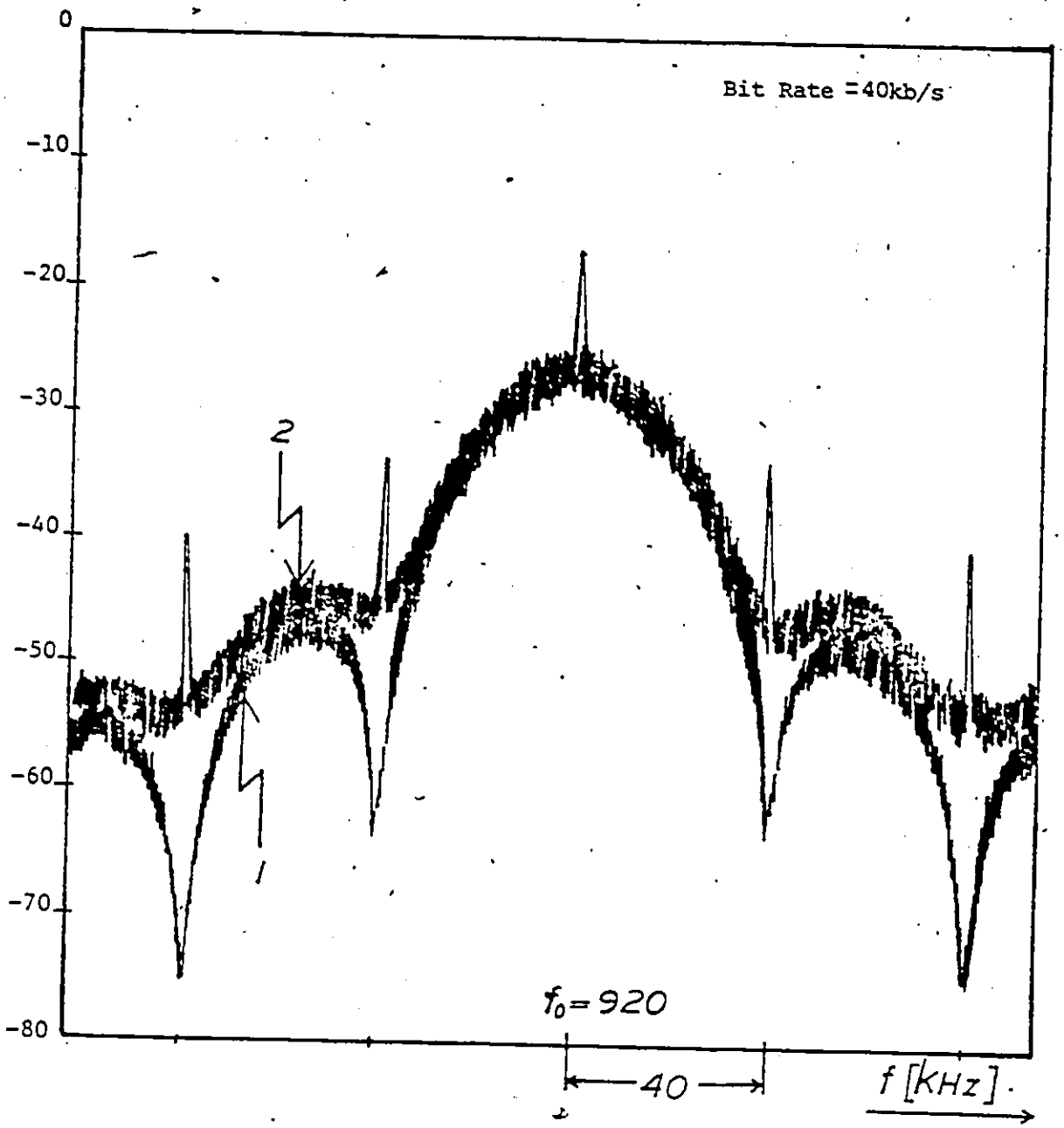

Figure 5.15 1) The Measured Power Spectrum of the Conventional BPSK Signal

2) The Measured Power Spectrum of the Modified BPSK Signal, $S_z(f)$

Afterwards the z(t) signal (MBPSK signal) was passed through a nonlinear element. An MC1035 threshold comparator acting as a hardlimiter was used as a nonlinear element. The output spectrum of the hardlimiter is shown in Figure 5.16. For comparison, the output spectra of the hardlimiter due to unfiltered and filtered conventional BPSK signals are also indicated. As can be seen, the hardlimiter removes the effect of filtering on a BPSK signal, but it has a minimal effect on the MBPSK signal. Figure 5.17 is the same as Figure 5.16, but with a different frequency scale.

5.4.2 Probability of Error, P_e, Performance

For data transmission systems one of the most important criteria of performance is the probability of error P_e. The detailed laboratory set-up for the measurement is depicted in Figure 5.18. The set-up up to the modulator output is exactly the same as is described in the previous section. The linear channel was simulated by an attenuator in the signal path and a linear adder which adds noise. To simulate a nonlinear channel, a hardlimiter was added in the signal path before the attenuator. The resistive adder has the resistors chosen such that the input and output terminals have 50 ohms impedance. The white noise was generated by a General Radio GR 1383 instrument which has a 20 Hz to 20 MHz bandwidth. The composite signal (MBPSK or BPSK signal plus noise) was

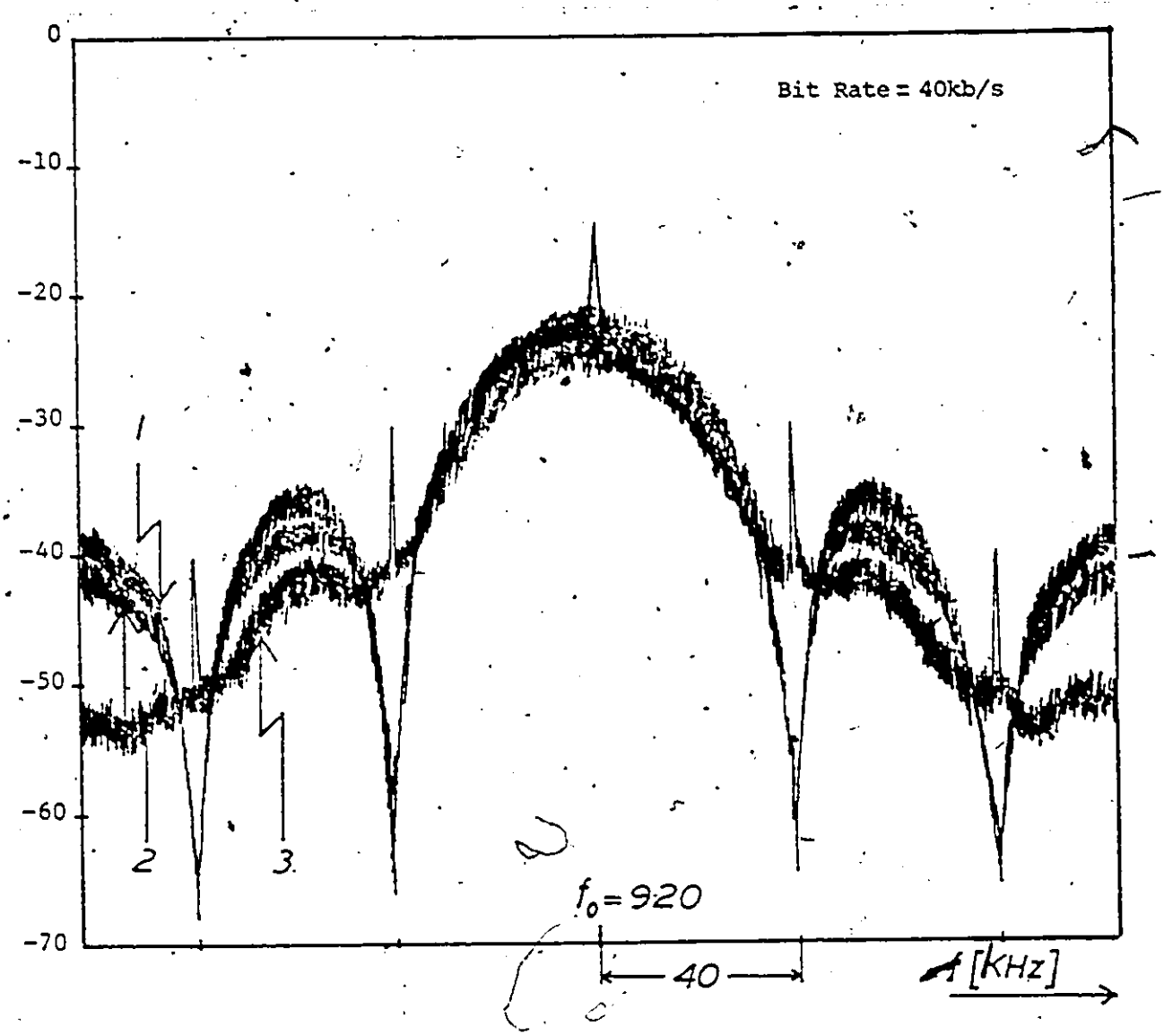

Figure 5.16 The Measured Output Power Spectra of a Hardlimiter having one of the following Inputs:

1) Unfiltered Conventional BPSK Signal
2) Filtered " " "
3) Modified BPSK Signal

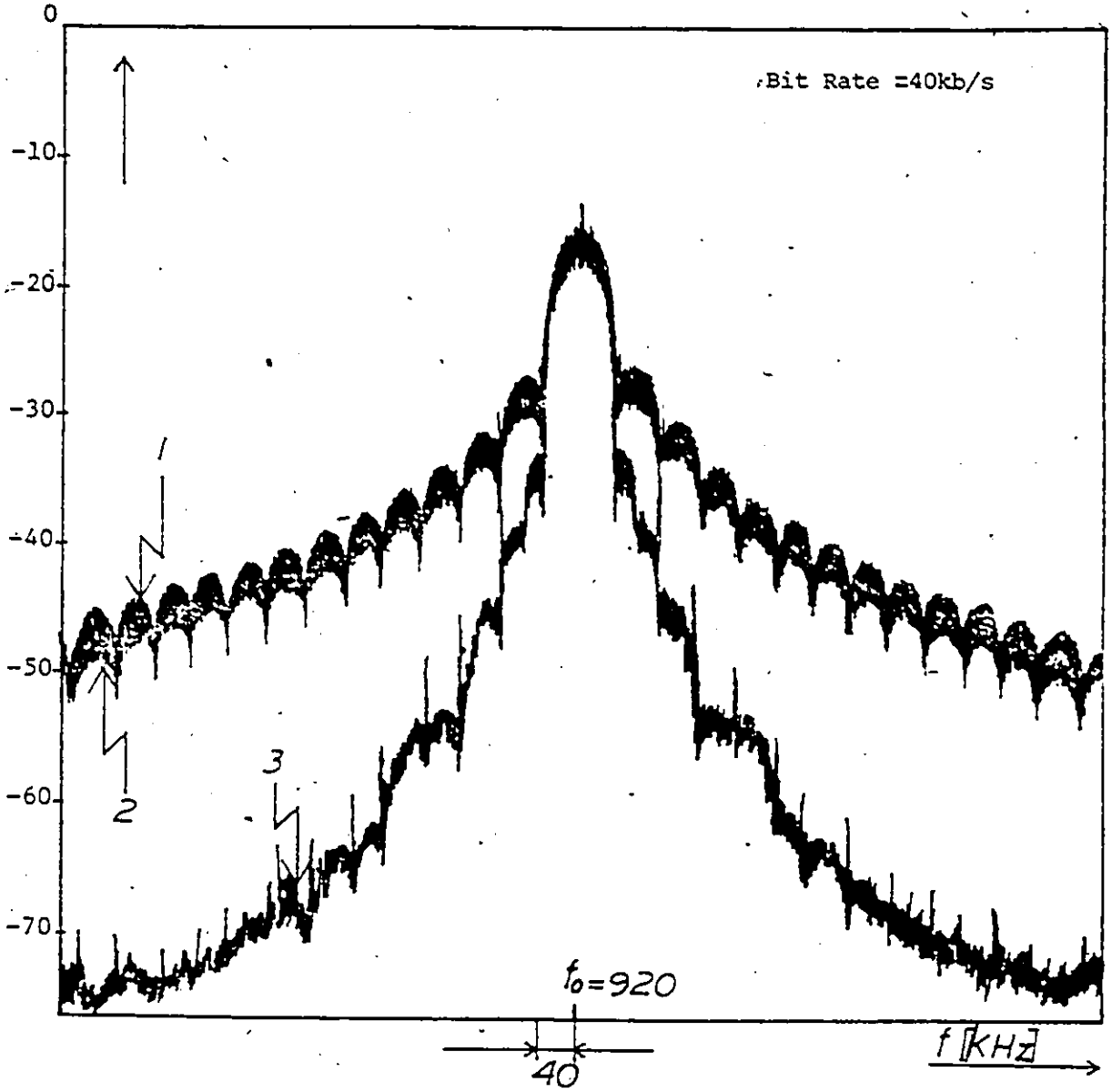

Figure 5.17 The Measured Output Power Spectra of a Hardlimiter having one of the following Inputs :
1) An Unfiltered Conventional BPSK Signal
2) A Filtered " " "
3) A Modified BPSK Signal

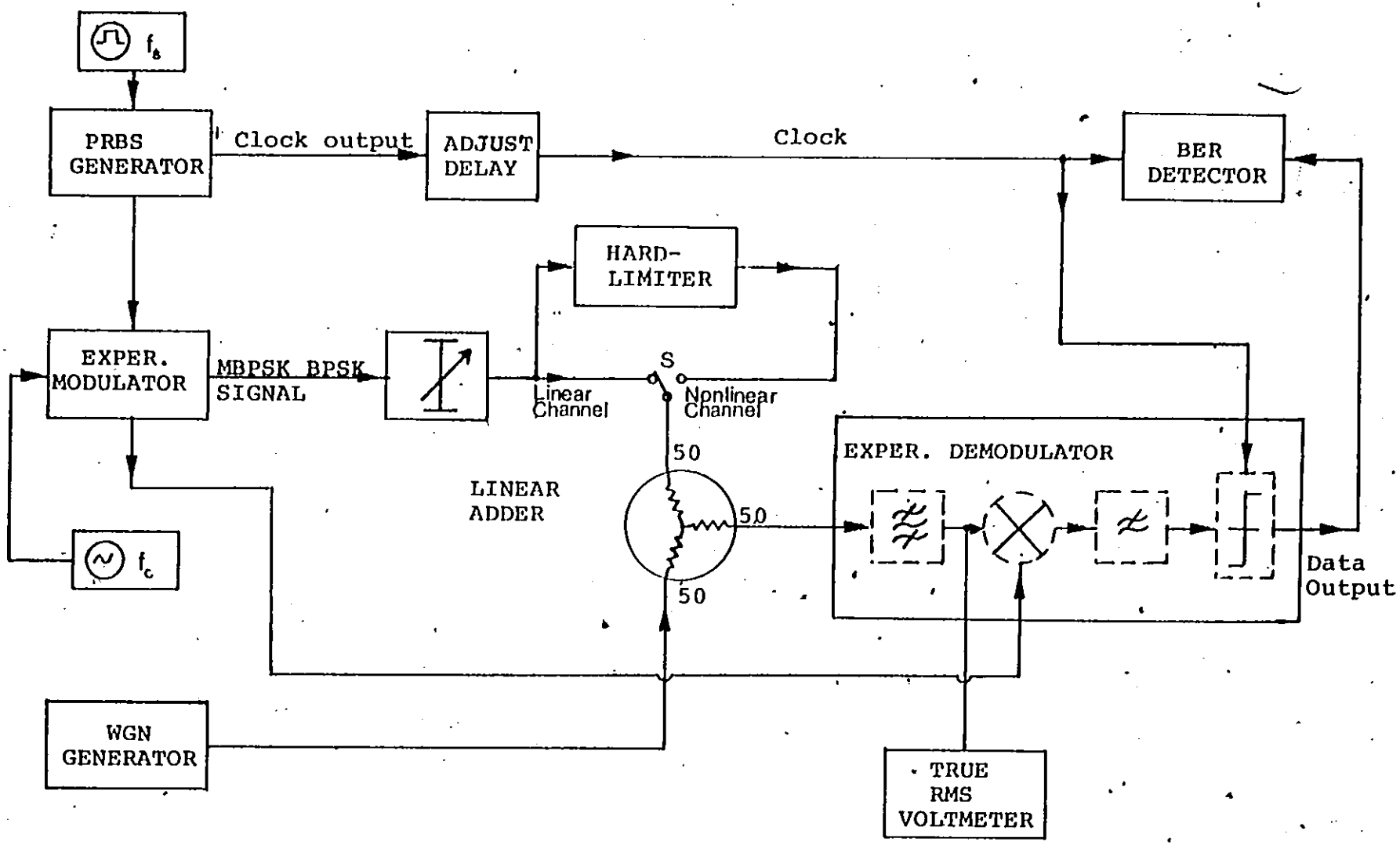

Figure 5.18 Laboratory set-up for measurement of the Probability of Error.

then applied to the demodulator input. The coherent carrier to the demodulator was hardwired from the in-phase carrier of the modulator, and also the bit timing signal (clock) with an adjustable delay was hardwired from the PRBS generator to the threshold comparator (regenerator). The regenerated data at the output of the demodulator (some of which are in error because of the corruption by noise etc.) are fed into the error detector, HP3761A, where they are compared bit by bit with a copy of the original transmitted data. The number of disagreements gives an indication of the bit error rate or probability of error. Throughout the measurements no path was disconnected, in order to maintain stable impedance characteristics.

A true rms voltmeter, HP3403C, was used at the output of the demodulator band-pass filter (or the demodulator mixer input) to measure the modulated carrier (or simply, carrier) signal and the noise rms voltage. To measure the carrier signal, the noise path was attenuated by at least 60 dB. To measure the noise, the carrier was also attenuated by at least 60 dB.

The probability of error is affected by the sampling instant in the regenerator. To experimentally optimize the P_e, the clock delay was adjusted so as to sample at the centre of the eye diagram observed at the input of the

regenerator, and hence obtain the best P_e possible.

In the following, the measured P_e performances of the experimental BPSK and MBPSK systems are given versus energy per bit to noise density ratio (E_b/N_o). The E_b/N_o enables a system comparison which is independent of the system bandwidth.

The E_b/N_o is related to the carrier power-to-noise power ratio, C/N by:

$$E_b/N_o = \frac{C}{N} - \frac{BR}{NB} \qquad \text{(in dB)} \qquad (5.1)$$

where BR is the system symbol rate (in this case, bit rate) and NB is the noise bandwidth of the demodulator band-pass filter.

NB can be calculated by [32]:

$$NB = \frac{1}{|G(f_c)|^2} \int_{-\infty}^{+\infty} |G(f)|^2 df \qquad (5.2)$$

where G(f) is the frequency characteristic of the band-pass filter, centered at f_c Hz. For the experimental system the calculated noise bandwidth of the demodulator band-pass filter was 87.07 kHz, and therefore:

$$\frac{E_b}{N_o} = \frac{C}{N} - 10 \log \frac{40}{87.07} = \frac{C}{N} + 3.4 \text{ [dB]}$$

In Figure 5.19 the performance of the experimental MBPSK and the conventional BPSK systems over a linear channel and

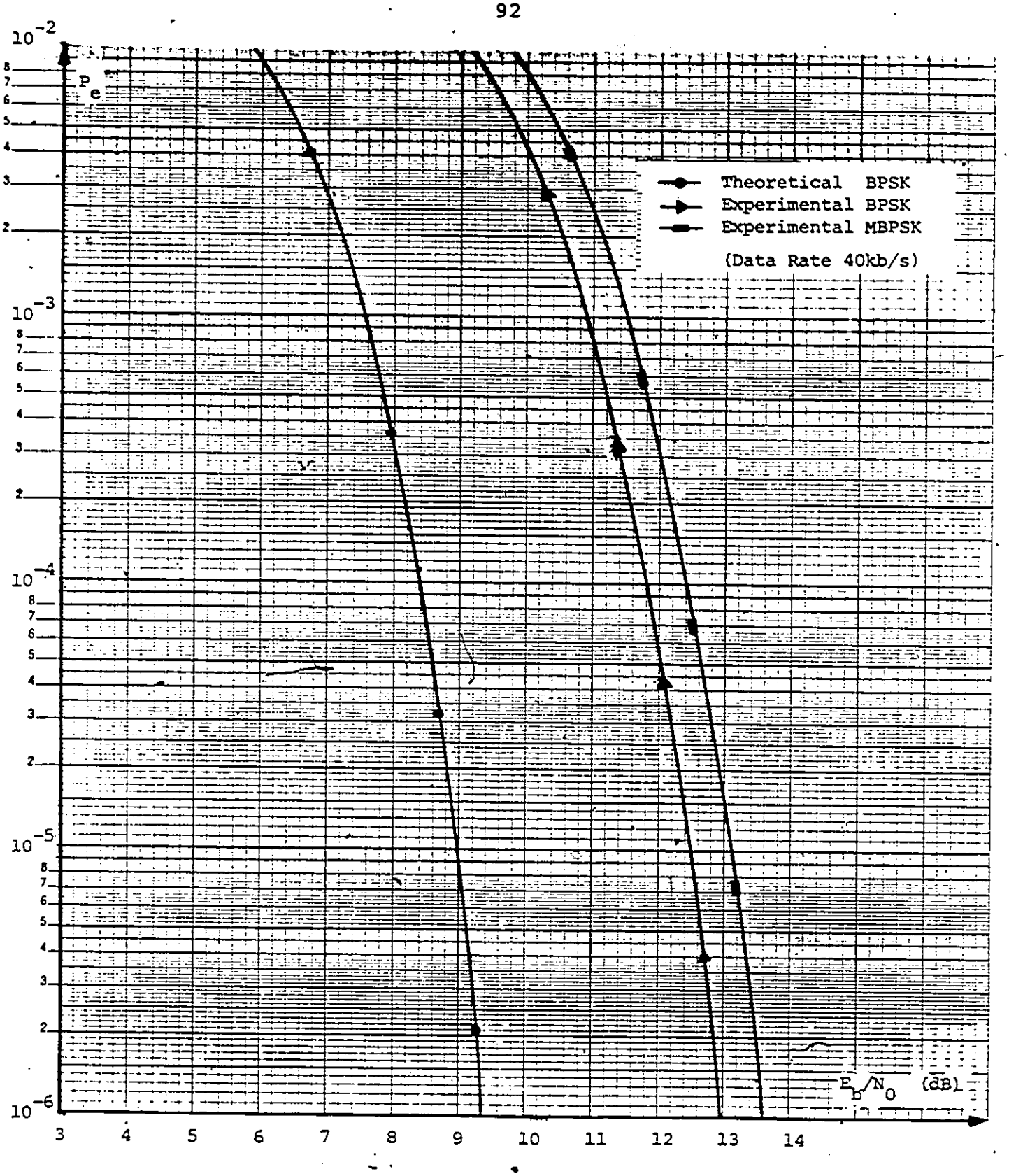

Figure 5.19 P_e Performance of the Experimental MBPSK and BPSK Systems in a White Gaussian Noise Environment (Linear Channel)

in the presence of white Gaussian noise are shown together with the theoretical performance of the conventional BPSK system. The experimental curve for the conventional BPSK system (which is used as a reference for comparing the performance of the experimental MBPSK system) is seen to differ from the theoretical one by about 3.4 dB. This is mainly due to the use of a post-demodulation low-pass filter with 3 dB bandwidth of 40,kHz which is twice the theoretical minimum bandwidth (minimum bandwidth for 40 kb/s data is 20 kHz).

The performance of the experimental MBPSK system is about 0.6 dB off (degraded) from that of the experimental BPSK system. This is because, for transmitting the same information, MBPSK modulator requires additional power for transmitting the auxiliary y(t) signal (which does not carry any information), as compared to the conventional BPSK system.

In a more realistic MBPSK system, where the coherent carrier must be recovered from the received MBPSK signal, however, slightly more degradation should be expected, since in such a case the transmission of the auxiliary signal y(t) would presumably enhance the phase noise in the carrier recovery loop at the demodulator [33].

Figure 5.20 presents the P_e performance of the experimental MBPSK and BPSK systems over a hardlimited channel, and in the presence of White Gaussian Noise. For comparison, the performance over a linear channel are also indicated.

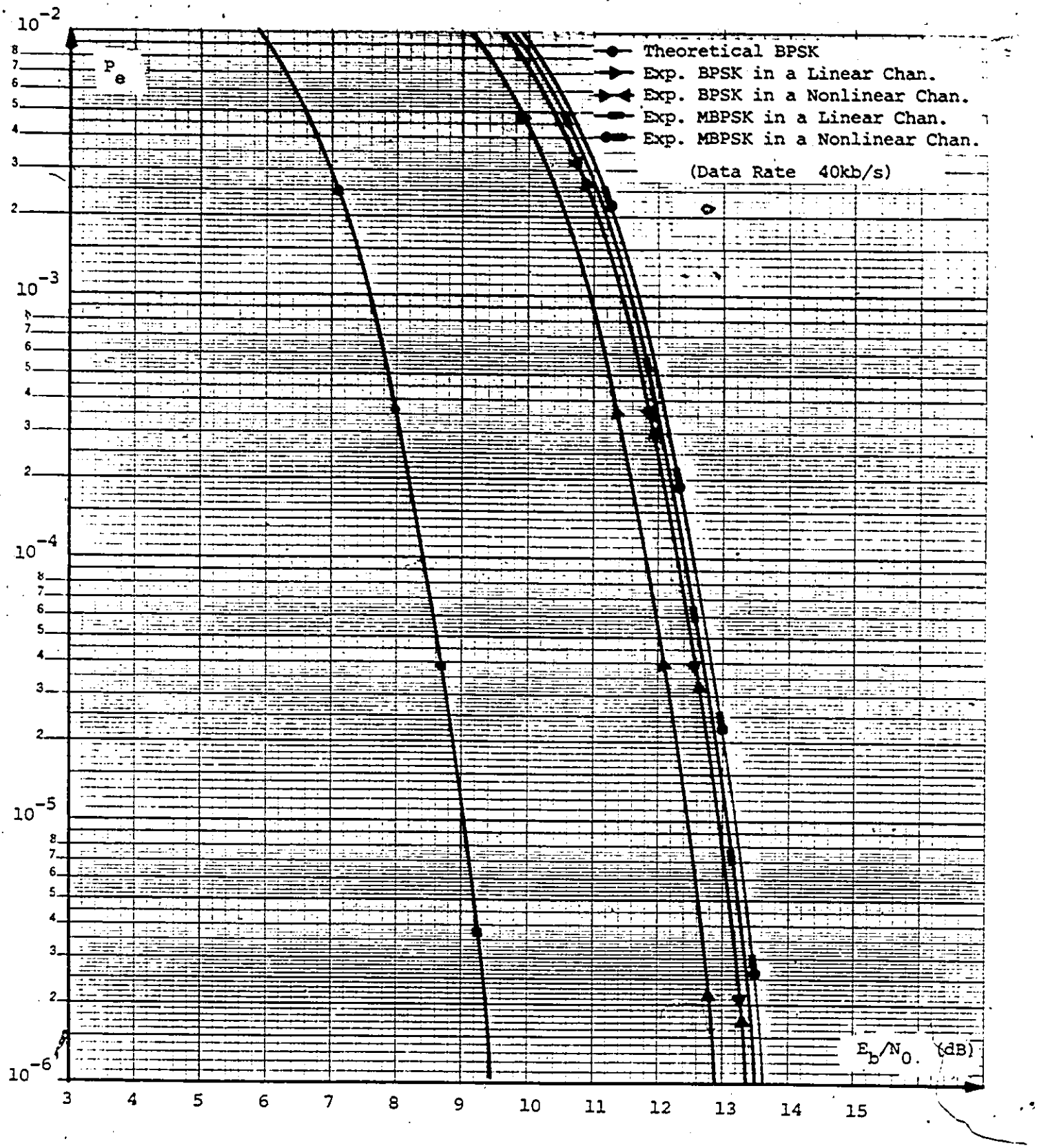

Figure 5.20 P_e Performance of the Experimental MBPSK and BPSK Systems in a Nonlinear Channel and in the presence of White Gaussian Noise

The performance of the hardlimited BPSK system is seen to be degraded by about 0.5 dB as compared to the linear case. This degradation could be due to the hardware limitation and hence non-ideal characteristics of the hardlimiter used. If the hardlimiter exhibits some AM/PM nonlinearity, it could cause the eye diagram of the demodulated data to be non-symetrical about the center of the eye and hence degrade the P_e performance.

The performance of the hardlimited MBPSK system, on the other hand, is almost the same as in the linear case (about 0.15 dB degraded as compared to the MBPSK performance in a linear channel). This is because the possible AM/PM nonlinearity of hardlimiter in this case has a minimal effect on the MBPSK signal (the MBPSK signal has a constant envelope).

CHAPTER SIX

CONCLUSION AND SUGGESTIONS FOR FUTURE RESEARCH

6.1 Conclusion

Phase-Shift-Keying is the most popular modulation technique, widely employed in digital satellite communication systems. An introduction of some practical constraints, such as power, bandwidth, etc, enabled us to demonstrate the spectral spreading problem associated with transmission of a bandlimited PSK signal through channels exhibiting a nonlinear characteristic of AM/AM conversion.

The spectral spreading which causes interference into adjacent channels, is primarily due to the envelope fluctuation of a bandlimited PSK signal at the input of the nonlinearity.

As a main objective, and presenting the mutual relationship between the phase transition and envelope fluctuation of a bandlimited PSK signal, a novel BPSK modulator, called modified BPSK or MBPSK modulator, was introduced. The MBPSK modulator, avoiding the instantaneous 180° phase transitions of the conventional BPSK modulator, was shown to produce a virtually constant envelope bandlimited BPSK signal, and that the channel nonlinearity (AM/AM conversion) has minimal effect on the spectral spreading of this signal.

An expression for the power spectrum density of the MBPSK signal was derived, and it was found that MBPSK modulator introduces spectral lines at f_c and $f_c + mf_s$ ($m = 1, 2, \ldots$). The spectral lines at $f_c + mf_s$ might be useful in linear processing of the received signal at the receiver, to extract timing signals.

An experimental MBPSK system was implemented and the test results were presented.

The test results show that the MBPSK signal, when passed through a hardlimiter, has a spectrum splatter much lower than the conventional BPSK signal, and hence it could be a good candidate for applications when the channel is nonlinear.

Finally, the P_e performance of the experimental MBPSK system in a random Gaussian noise environment was evaluated, and compared with that of conventional BPSK system. Even though, for the same P_e, the MBPSK system requires about 0.6 dB more E_b/N_o than BPSK system, however, its drastically reduced spectral spreading in a nonlinear channel is far superior than the conventional BPSK system.

6.2 Suggestions for Future Research

One of the possible extensions of this work could be the application of the same modification scheme (as applied to BPSK) to QPSK modulator for generating a constant envelope

bandlimited QPSK signal. The suggested block diagram of such a modified QPSK modulator could be as given in Figure 6.1. The output signal can be written as:

$$z(t) = x(t)\cos\omega_c t + [1-|y(t)|]\sin\omega_c t + y(t)\sin\omega_c t + [1-|x(t)|]\cos\omega_c t \quad (6.1)$$

or $$z(t) = b(t)\cos(\omega_c t + \phi(t)) \quad (6.2)$$

where

$$b(t) = [2(x^2(t) + y^2(t)+1)-2(|x(t)|+|y(t)|)]^{\frac{1}{2}} \quad (6.3)$$

and

$$\phi(t) = \tan^{-1}\frac{1+y(t) - |y(t)|}{1+x(t) - |x(t)|} \quad (6.4)$$

From (6.3), the envelope of the modified QPSK signal, b(t), can be shown to be virtually constant, that is, the minimum value of b(t) is not less than 0.707 of its peak value. However, more investigations on the spectral behaviour, demodulation process, and BER performance of such a modified QPSK signal are necessary before making any judgement about its advantage or disadvantage as compared to an O-QPSK signal.

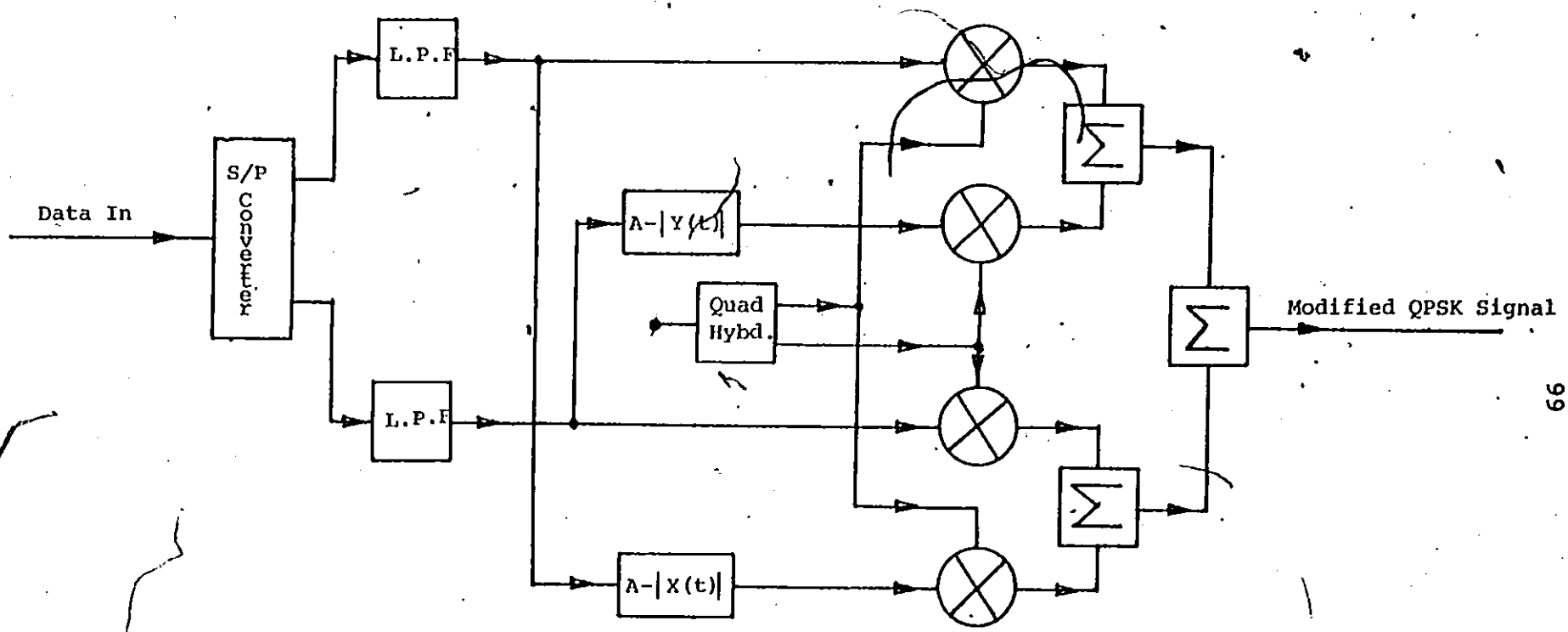

Figure 6.1 The Suggested Block Diagram of a Modified QPSK Modulator.

REFERENCES

[1] C. Woletsza, "State of the Art of PSK Modulation Technique". Second International Conference on Digital Communication. 1972 Paris, pp. 154-163.

[2] S.A. Rhodes, "Effects of Hardlimiting on Bandlimited Transmissions with Conventional and Offset QPSK Modulation". NTC 1972 Houston (Texas), pp. 20F, 20F7.

[3] J. Max, "Envelope Fluctuations in the Output of a Bandpass Limiter". IEEE Trans. Commun. Technol., 1970, COM-18, pp. 597-605.

[4] N. Ishida, "On the Waveform Distortion of Rectangular PSK Pulses". Rev. Elec. Commun. Lab., Japan, 1971, Vol. 19, pp. 1258-1274.

[5] P. Porzio Giusto, "L-PSK: A New Type of PSK Modulation". Alta Frequenza, Vol. XLIII, N. 12, Dec. 1974.

[6] W.A. Wood, "Modulation and Filtering Techniques for 3 bits/hertz Operation in the 6 GHz Frequency Band". IEEE ICC-77, pp. 5.3-97 - 5.3-101. Chicago, June 1977.

[7] W.R. Bennett and J.R. Davey, Data Transmission, McGraw-Hill Book Company, New York, 1965.

[8] R.W. Lucky, J. Salz, and E.J. Weldon, Jr., Principles of Data Communications, McGraw-Hill Book Company, New York, 1968.

[9] H. Taub, D. Schilling,"Principles of Communication Systems", McGraw-Hill Book Company, New York, 1971.

[10] S. Benedetto and E. Biglieri, "Performance of M-ary PSK Systems in the Presence of Intersymbol Interference and Additive Noise", Alta Frequenza, Vol. XLI, 1972, pp. 225-239.

[11] T.S. Koubanitsas and L.F. Turner, "Simple Bound on the Error Probability in Coherent Multi-phase Phase-Shift-Keyed Systems with Intersymbol Interference and Gaussian Noise", Proc. IEE, Vol. 120, pp. 725-732, July 1973.

[12] V.K. Pradhu, "Error Probability Performance of M-ary CPSK Systems with Intersymbol Interference". IEEE Trans. on Comm., Vol. COM-21, pp. 97-109, Feb. 1973.

[13] J.J. Jones, "Filter Distortion and Intersymbol Interference Effects on PSK Signals", IEEE Trans. on Comm., Vol. COM-19, No. 2, April 1971.

[14] N.M. Blachman, "Detectors, Bandpass Nonlinearities and their Optimization: Inversion of the Chebyshev Transform", IEEE Trans. Inform. Theory, Vol. IT-17, pp. 398-404, July 1971.

[15] H.R. Mathwhich, J.F. Bakewicz, and M. Hecht, "The Effect of Tandem Band and Amplitude Limiting on the E_b/N_o Performance of Minimum (Frequency) Shift Keying (MSK)", IEEE Trans. Comm., Vol. COM-22, pp. 1525-1450, Oct. 1974.

[16] K. Feher, "Digital Modulation Techniques in an Interference Environment", Vol. 9 of EMC Encyclopedia. Gainesville, Va: Don White Consultants Inc., 1977.

[17] J.J. Spilker, "Digital Communications by Satellite", Englewood Cliffs, N.J.: Prentice-Hall Inc., 1977.

[18] L.J. Greenstein and P.J. Fitzgerald, "Envelope Fluctuation Statistics of Filtered PSK and Other Digital Modulations", IEEE Trans. on Comm., Vol. COM-27, No. 4, April 1979.

[19] K. Feher, "Digital Communications: Microwave Applications", Englewood Cliffs, N.J.: Prentice-Hall Inc., 1981.

[20] C. Devieux, "Analysis of PSK Signal Power Spectrum Spread with a Markov Chain Model", COMSAT Tech. Rev., Vol. 5, Fall 1975.

[21] L.D. Davisson and L.B. Milstein, "On the Performance of Digital Communication Systems with Bandpass Limiters - Part I: One-Link System", and "Part II: Two Link System", IEEE Trans. on Comm., Vol. COM-20, pp. 972-980, October 1972.

[22] P.C. Jain and N.M. Blachman, "Detection of a PSK Signal Transmitted Through a Hardlimited Channel", IEEE Trans. Inform. Theory, Vol. IT-19, pp. 623-630, Sept. 1973.

[23] T. Mizuno, N. Morinaga, and T. Namekawa, "Transmission Characteristics of an M-ary Coherent PSK Signal Via a Cascade of N Bandpass Hardlimiters", IEEE Trans. on Comm., Vol. COM-24, pp. 540-545, May 1976.

[24] L. Moreno, "Sensitivity of PSK Modulation Technique to Nonlinear Distortion", IEEE Trans. on Comm., Vol. COM-27, pp. 806-812, May 1979.

[25] G. Robinson, O. Shimbo, and R. Fang", PSK Signal Power Spectrum Spread Produced by Memoryless Nonlinear TWTs", COMSAT Tech. Rev., Vol. 3, No. 2, Fall 1973.

[26] R.G. Lyons, "Effects of PSK Spectral Spreading in a Satellite Transponder", IEEE ICC-74, pp. 36B-1 - 36B-6. Minneapolis, June 1974.

[27] M.A. Marsan, E. Biglieri, "Power Spectra of Complex PSK for Satellite Communications", Alta Frequenza, Vol. XLVI-N.6, June 1977.

[28] M. El-Torky, K. Feher, "The Effects of Transmitter Power Amplifier Nonlinearity on QPSK and Offset QPSK Radio Transmission Over Severely Bandlimited Channels", IEEE Canadian Communications and Power Conference, Montreal, Oct. 1978.

[29] H. Yazdani, K. Feher, and W. Steenaart, "Constant Envelope Bandlimited BPSK Signal", IEEE Trans. on Comm., Vol. COM-28, pp. 889-897, June 1980.

[30] C. Andren, "PSK Sidebands Reduced by Premodulation Filtering", Microwave Journal, Vol. 21, No. 1, Jan. 1978.

[31] K. Feher, "Bit Timing Transmission and Spectral Shaping of Digital Signals", Canadian Elec. Eng. J., Vol. 3, 1978.

[32] Bell Telephone Laboratories, "Transmission Systems for Communications", Western Electric Company, Inc., Winston-Salem, North Carolina, 1971.

[33] K. Greene, W. Sones, M. Grossman, J. Jones, and N. Jacoubs, "Automatic Seismic Observatory Communications System", Comsat Technical Review, Vol. 10, No. 1, Spring 1980.